SCUOLA DOTTORALE IN SCIENZE MATEMATICHE E FISICHE
Dottorato di ricerca in fisica - XXX ciclo

FORM FACTORS OF THE $D \to \pi(K)\ell\nu$ SEMILEPTONIC DECAYS AND DETERMINATION OF THE CKM MATRIX ELEMENTS $|V_{cd}|$ AND $|V_{cs}|$ WITH $N_f = 2+1+1$ TWISTED MASS LATTICE QCD

PhD thesis in physics

BY

Giorgio Salerno

Dissertation Advisors:

Prof. Vittorio Lubicz

Prof. Silvano Simula

Program Coordinator:

Giuseppe Degrassi

Academic Year 2016/2017

Contents

Introduction

The Standard Model (SM) of Particle Physics describes in an extremely precise and elegant way the fundamental costituents of matter and their interactions. Over the last fifty years it has been extremely successful in providing very accurate theoretical predictions for most of the experimentally accessible phenomena. Furthermore, with the observation of the Higgs boson at the Large Hadron Collider (LHC) [1, 2], the entire set of fundamental particles predicted by the SM has been discovered. Nevertheless many questions remain opened and lead us to believe that the SM is not the final theory of particle interactions, but just a low-energy approximation of a more fundamental theory.

Probably the most evident limit of the SM is that it does not provide a quantum description of the gravity, which becomes relevant at the Plank scale $\Lambda_{\rm Pl} \approx 10^{19}\,\text{GeV}$. Moreover we do not have a viable dark matter candidate, as well as an explanation of the matter-antimatter asymmetry in the universe. Other problems are the lack of a complete unification of the fundamental forces, expected around the grand unification scale $\Lambda_{\rm GUT} \approx 10^{16}\,\text{GeV}$, and the fact that the SM does not provide a natural explanation for neutrino oscillations and their small masses.

A current fundamental issue is represented by the *hierarchy problem* between the electroweak and the NP scales, which is related to the instability of the Higgs mass to radiative corrections. In partcular the Higgs boson gets very large corrections proportional to the mass of virtual particles. Thus if we assume some New Physics (NP) at either the Plank or the GUT scale, we would expect the Higgs boson mass to be inevitably huge, i.e. comparable to the energy at which NP appears. This is true unless we consider an incredible fine-tuning cancellation between the radiative corrections and the bare Higgs mass, which is considered *unnatural* by many theorists. This problem leads physicists to believe that some NP around the TeV scale, able to provide a regularization of radiative corrections to the Higgs mass, should be there.

In this scenario, the flavor sector of the SM, the branch of particle physics that studies the transitions between different quarks and leptons, plays a fundamental role. The structure of flavor, as well as the hierarchical structure of either the mass spectrum and the Cabibbo-Kobayashi-Maskawa (CKM) matrix [3, 4], is very peculiar, although its origin has no explanation: Why are there exactly 3 families of quarks and leptons? Why the mass spectrum of quarks and leptons covers 5 orders of magnitude? And what gives rise to the pattern of quark mixing and the magnitude of CP violation? Flavor physics, because of its highly non trivial structure, is particularly sensitive to high-energy scales. This property allows us to search for NP in an indirect way by looking at the effects that it produces at low energies. Such effects should manifest themself as small corrections to

the SM predictions.

In particular the CKM matrix in the SM is unitary, so we have that $V_{\rm CKM} \times V_{\rm CKM}^{\dagger} = \mathbb{1}$. This gives rise to unitarity conditions between the elements of its rows and columns, that are represented by diagonal constraints and "unitarity triangles", whose investigation has been the focus of much of the experimental and theoretical efforts in Flavor Physics during the recent years. On one hand inconsistencies in the CKM-picture would indicate the presence of NP beyond the SM. On the other hand, if all the precision tests of the SM performed so far are in agreement with the CKM paradigm, the absence of deviations provides stringent constraints on non-standard phenomena and their energy scale. It is therefore important to determine all CKM matrix elements as precisely as possible by studying flavour-changing processes both experimentally and theoretically.

The golden modes for testing the unitarity of the second row of the CKM matrix, namely $|V_{cd}|^2 + |V_{cs}|^2 + |V_{cb}|^2 = 1$, are represented by the leptonic and semileptonic decays of charmed D and D_s mesons, which probe the $c \to d$ and $c \to s$ quark transitions, respectively. Combining experimental measurements of the branching fractions of these processes with theoretical calculations of the relevant hadronic matrix elements, i.e. the leptonic decay constants f_D and f_{D_s} and the semileptonic vector form factors $f_+^{D\to\pi}(q^2)$ and $f_+^{D\to K}(q^2)$, the CKM entries $|V_{cd}|$ and $|V_{cs}|$ can be determined. The CKM matrix element $|V_{cb}|$, being of the order $\mathcal{O}(10^{-2})$, is marginal for the second-row unitarity test at the current level of precision. The theoretical calculations of hadronic matrix elements based entirely on first principles can be properly carried out by simulating the fundamental theory of the strong interaction, QCD, on a lattice. Thanks to the remarkable progress in algorithms and computing machines, Lattice QCD (LQCD) has entered the precision era and the accuracy of numerical computations is becoming comparable to that of the experiments. For some relevant hadronic quantities in Flavour Physics the goal of the percent level of precision has been already achieved (see, e.g., the FLAG review [5]) and the precision will be improved in the future.

In this thesis we study the semileptonic decays $D \to \pi\ell\nu_\ell$ and $D \to K\ell\nu_\ell$, which are relevant for the extraction of the CKM matrix elements $|V_{cd}|$ and $|V_{cs}|$. Within the SM, the semileptonic $D \to P\ell\nu$ differential decay rate is given by

$$\frac{d\Gamma(D\to P\ell\nu)}{dq^2} = \frac{G_F^2|V_{cx}|^2}{24\pi^3}\frac{(q^2-m_\ell^2)^2|\vec{p}_P|}{q^4 M_D^2}\left[\left(1+\frac{m_\ell^2}{2q^2}\right)M_D^2|\vec{p}_P|^2|f_+^{DP}(q^2)|^2 + \right. \\ \left. + \frac{3m_\ell^2}{8q^2}(M_D^2-M_P^2)^2|f_0^{DP}(q^2)|^2\right], \tag{1}$$

where $x = d(s)$ is the daughter quark, $|\vec{p}_P|$ is the momentum of the daughter pseudoscalar meson $P = \pi(K)$ in the D-meson rest frame and $q = (p_D - p_P)$ is the 4-momentum of the outgoing lepton pair. Since in Eq. (1) the contribution of the scalar form factor $f_0(q^2)$ is proportional to m_ℓ^2, in the case of $\ell = e(\mu)$ the differential decay rate can be simplified to

$$\frac{d\Gamma(D\to Pe(\mu)\nu)}{dq^2} = \frac{G_F^2\,|V_{cx}|^2}{24\pi^3}\,|\vec{p}_P|^3\left|f_+^{DP}(q^2)\right|^2 \ . \tag{2}$$

Each experiment provides results for the product $|V_{cx}|f_+^{DP}(q^2)$ in various q^2-bins. On the other hand the LQCD calculations performed so far provide the value of the vector

form factors at zero 4-momentum transfer, $f_+^{D\pi(K)}(q^2=0)$. These can be used to extract the relevant CKM entries adopting experimental averages of the products $|V_{cd}|f_+^{D\to\pi}(0)$ and $|V_{cs}|f_+^{D\to K}(0)$, like the ones determined by the Heavy Flavor Averaging Group (HFAG) in Ref. [15]. However, the analyses of the experimental data from BELLE [6], BABAR [7, 8], CLEO [9] and BESIII [10] on the $D\to\pi(K)e(\mu)\nu$ decays, which compose the HFAG average, are based on a variety of parameterizations for the shape of the vector form factors $f_+^{D\pi(K)}(q^2)$. These include effective pole models, inspired by dispersion relations [11] or heavy-quark expansion arguments [12], the z-expansion method [13], or relativistic quark model predictions [14].

In this thesis we present the first $N_f=2+1+1$ LQCD calculation of the vector and scalar form factors $f_+^{D\pi(K)}(q^2)$ and $f_0^{D\pi(K)}(q^2)$ governing the semileptonic $D\to\pi(K)\ell\nu$ decays, using the gauge configurations generated by the European Twisted Mass Collaboration (ETMC) with $N_f=2+1+1$ dynamical quarks, which include in the sea, besides two light mass-degenerate quarks, also the strange and the charm quarks with masses close to their physical values [16, 17]. At variance with most of the existing LQCD calculations (see, e.g., Ref. [5]), which provide only the value of the vector form factor at zero 4-momentum transfer, we have evaluated both the vector and scalar form factors in the whole experimentally accessible range in q^2, i.e. from $q^2=0$ up to $q^2_{\rm max}=(M_D-M_{\pi(K)})^2$. An overall agreement with the momentum dependence of the experimental data from BELLE [6], BABAR [7, 8], CLEO [9] and BESIII [10] has been found, although some deviations have been observed at high values of q^2. The knowledge of the form factors in the full kinematical range allowed us to perform the first determination of the CKM matrix elements $|V_{cd}|$ and $|V_{cs}|$ in a truly consistent way within the SM, employing directly Eq. (2) without making use of any other assumption. We show that a more precise and consistent determination of $|V_{cd}|$ and $|V_{cs}|$, compared to those based only on the vector form factor at $q^2=0$, can be obtained. The determination of the vector and scalar form factors and the extraction of $|V_{cd}|$ and $|V_{cs}|$ have been presented in Refs. [18, 19] (see also Refs. [20, 21] for preliminary results).

In our calculations quark momenta are injected on the lattice using non-periodic boundary conditions [22, 23] and the matrix elements of both vector and scalar currents are determined for a plenty of kinematical configurations, in which parent and child mesons are either moving or at rest. Data coming from different kinematical conditions exhibit a remarkable breaking of the Lorentz symmetry due to hypercubic effects for both the $D\to\pi$ and the $D\to K$ semileptonic form factors. We show also that hypercubic artifacts may be largely affected by the difference between the parent and the child meson masses, which may represent an important warning in the case of the determination of the form factors governing semileptonic B-meson decays. We present the subtraction of such hypercubic effects and the determination of the Lorentz-invariant semileptonic vector and scalar form factors after the combined extrapolations to the physical pion mass and to the continuum limit. At zero 4-momentum transfer the results of our study are:

$$f_+^{D\to\pi}(0)=0.612\ (35) \qquad , \qquad f_+^{D\to K}(0)=0.765\ (31)\ , \tag{3}$$

which are consistent within the errors with the FLAG [5] averages $f_+^{D\to\pi}(0)=0.666\ (29)$, based on the result of Ref. [24], and $f_+^{D\to K}(0)=0.747\ (19)$ from Ref. [25], both obtained

at $N_f = 2 + 1$. Using Eq. (2) to combine the momentum dependence of the semileptonic vector form factors $f_+^{D\to\pi}(q^2)$ and $f_+^{D\to K}(q^2)$ with the differential rates measured for the semileptonic $D \to \pi\ell\nu$ and $D \to K\ell\nu$ decays by BELLE [6], BABAR [7, 8], CLEO [9] and BESIII [10], we get our determination of the CKM matrix elements $|V_{cd}|$ and $|V_{cs}|$:

$$|V_{cd}| = 0.2345\ (83) \qquad , \qquad |V_{cs}| = 0.978\ (35)\,, \tag{4}$$

where the errors take into account both lattice calculation and experimental uncertainties. Including the determination of $|V_{cb}|$ from B-meson decays [26], the unitarity test of the second-row of the CKM matrix yields

$$|V_{cd}|^2 + |V_{cs}|^2 + |V_{cb}|^2 = 1.013\ (68)\ , \tag{5}$$

which confirms unitarity at the percent level of precision.

The thesis is organized as follows. In Chap. 1 we introduce the main features of Flavor Physics in the SM, together with an introduction on semileptonic decays of pseudoscalar into pseudoscalar mesons. Chap. 2 is dedicated on Quantum Chromodynamics (QCD): after a brief description of the theory in the continuum and infinite volum limit, the framework of LQCD is described. A special focus is dedicated to the Wilson Twisted Mass (Wtm) action, which is the one employed in our simulations. In Chap. 3 we present the determination of the vector and scalar form factors $f_+^{D\pi(K)}(q^2)$ and $f_0^{D\pi(K)}(q^2)$. Evidences of Lorentz symmetry breaking lattice artifacts in the momentum dependence of these quantities are shown together with the strategy adopted in order to extract the physical, Lorentz invariant, form factors. In this Chapter we present also the extraction of the CKM matrix elements $|V_{cd}|$ and $|V_{cs}|$, obtained for the first time by combining the momentum dependence of the vector form factors $f_+^{D\to\pi(K)}(q^2)$ with the experimental determinations of the decay rates for the $D \to \pi(K)\ell\nu$ processes. A summary of the present work, together with the main achievements, are then reported in the conclusions. Finally, at the end of the thesis, an appendix shows our parametrization of the vector and scalar form factors $f_+^{D\to\pi(K)}(q^2)$ and $f_0^{D\to\pi(K)}(q^2)$ extrapolated to the physical pion point and to the continuum and infinite volume limits.

Chapter 1

Flavor Physics in the Standard Model

The Standard Model of Particle Physics is a quantum field theory based on the gauge group

$$SU(3)_C \otimes SU(2)_L \otimes U(1)_Y \,. \tag{1.1}$$

$SU(3)_C$ is the *color* symmetry of QCD, the theory which describes strong interactions, while $SU(2)_L \otimes U(1)_Y$ is the symmetry of electroweak interactions, spontaneously broken by the Higgs potential in $U(1)_{e.m.}$.

In the SM the fundamental fermionic constitutents of matter are quarks and the leptons, each of them characterized by a different type, referred to as *flavor*, so that the physics that describes transitions between these particles is named *Flavor Physics*. The SM Lagrangian $\mathcal{L}_{SM}$ can be decomposed in different sectors, which differ in both the content of fields and the symmetry properties:

$$\mathcal{L}_{SM} = \mathcal{L}_{Gauge} + \mathcal{L}_{Fermions} + \mathcal{L}_{Higgs} + \mathcal{L}_{Yukawa}. \tag{1.2}$$

The sectors $\mathcal{L}_{Gauge}$, $\mathcal{L}_{Fermions}$ and $\mathcal{L}_{Higgs}$ are invariant not only under the gauge group (1.1), but also under the global symmetry of *flavor*

$$U(3)^5 = U(3)_{Q_L} \otimes U(3)_{u_R} \otimes U(3)_{d_R} \otimes U(3)_{L_L} \otimes U(3)_{\ell_R} \,, \tag{1.3}$$

whose breaking is produced by the Yukawa sector, which is also responsible for the origin of fermion masses. However $U(3)^5$ is not completely broken by $\mathcal{L}_{Yukawa}$, so various interesting accidental symmetries survive. These are:

- Barion number B conservation,
- Lepton number L conservation,
- Lepton Flavor conservation,
- absence of FCNCs at tree level.

Accidental symmetries provide strong constraints on the possible structure of NP lagrangians. Furthermore, being a consequence of the content of fields and of the request of renormalizability, they are generally violated by many extentions of the SM.

In this Chapter we briefly present the different contributions which compose Eq. (1.2), focusing on the aspects of flavor physics relevant for the present work. We firstly introduce the Glashow-Weinberg-Salam Theory, which describes the unification of the Electromagnetic and Weak interactions. Then we present the Yukawa sector and the origin of fermion masses. A specific Section is dedicated to the CKM matrix, being the determination of its elements $|V_{cd}|$ and $|V_{cs}|$ the main goal of this work. We conclude the Chapter showing the general features of semileptonic decays between pseudoscalar mesons and their expression in terms of hadronic form factors.

1.1 Glashow-Weinberg-Salam Theory

The Glashow-Weinberg-Salam theory describes the unification of Electromagnetic and Weak interactions, whose nature is characterized by the gauge symmetry $SU(2)_L \otimes U(1)_Y$. The fermionic content of the theory is made up of five fields of spin 1/2, each of them appearing in three distinct families of flavor. We have:

$$\begin{gathered} Q_L^i = \begin{pmatrix} u^i \\ d^i \end{pmatrix}_L \to (3,2)_{+1/3} \quad L_L^i = \begin{pmatrix} \nu^i \\ \ell^i \end{pmatrix}_L \to (1,2)_{-1} \\ u_R^i \to (3,1)_{+4/3} \qquad d_R^i \to (3,1)_{-2/3} \qquad \ell_R^i \to (1,1)_{-2} \end{gathered} \tag{1.4}$$

where $i = (1,2,3)$ is the flavor index. The notation $C \to (A,B)_Y$ indicates that the field C belongs to the rappresentation A of $SU(3)_C$, B of $SU(2)_L$ and has weak hypercharge Y. For each field, the electric charge Q, the third component of the weak isospin T^3 and the weak hypercharge Y are reported in Tab. 1.1. These quantities are related by the Gell-Mann-Nishijima formula:

$$Q = T^3 + \frac{Y}{2}\,. \tag{1.5}$$

The fields Q_L^i, u_R^i and d_R^i represent quarks, while L_L^i and ℓ_R^i correspond to the leptons.

	ν_L^ℓ	ℓ_L^-	ℓ_R^-	u_L	d_L	u_R	d_R	ϕ^+	ϕ^0
Q	0	-1	-1	$2/3$	$-1/3$	$2/3$	$-1/3$	1	0
T^3	$1/2$	$-1/2$	0	$1/2$	$-1/2$	0	0	$1/2$	$-1/2$
Y	-1	-1	-2	$1/3$	$1/3$	$4/3$	$-2/3$	1	1

Table 1.1: Values of Q, T^3 and Y of the SM's particles.

Expanding in the flavor index we have:

$$\begin{cases} u^i_{\substack{L\\R}} = \; u_{\substack{L\\R}},\; c_{\substack{L\\R}},\; t_{\substack{L\\R}} \;, \\ d^i_{\substack{L\\R}} = \; d_{\substack{L\\R}},\; s_{\substack{L\\R}},\; b_{\substack{L\\R}} \;, \\ \ell^i_{\substack{L\\R}} = \; e_{\substack{L\\R}},\; \mu_{\substack{L\\R}},\; \tau_{\substack{L\\R}} \;, \\ \nu^i_L = \; \nu_{e_L},\; \nu_{\mu_L},\; \nu_{\tau_L} \;, \end{cases} \tag{1.6}$$

where labels L (left) and R (right) indicate the chirality of the different fields.

The spontaneous breaking of the gauge group $SU(2)_L \otimes U(1)_Y$ is given by the Higgs field, which is a scalar doublet belonging to the fundamental representation of $SU(2)_L$:

$$\phi = \begin{pmatrix} \phi^+ \\ \phi^0 \end{pmatrix} \rightarrow (1,2)_{+1} \;. \tag{1.7}$$

The above relation implies that a generic gauge transformation acting on the Higgs field is of the form

$$\phi \rightarrow e^{i\alpha^a \tau^a} e^{i\beta/2} \phi \;, \tag{1.8}$$

where $\tau^a = \sigma^a/2$ $(a = 1, 2, 3)$, being σ^a the Pauli matrices.

1.1.1 Gauge bosons

The lagrangian of the Glashow-Weinberg-Salam theory consists of the first three terms of Eq. (1.2), which are given by the following expressions:

$$\mathcal{L}_{Gauge} = -\frac{1}{4} \sum_{a=1}^{3} (W^a)^{\mu\nu} (W^a)_{\mu\nu} - \frac{1}{4} B^{\mu\nu} B_{\mu\nu} \;, \tag{1.9}$$

$$\mathcal{L}_{Fermionic} = \sum_{fermions} i \bar{\psi}_f \not{D} \psi_f \;, \tag{1.10}$$

$$\mathcal{L}_{Higgs} = (D^\mu \phi)^* (D_\mu \phi) - V(\phi) = (D^\mu \phi)^* (D_\mu \phi) + \mu^2 \phi^* \phi - \lambda (\phi^* \phi)^2 \;, \tag{1.11}$$

where D_μ is the *covariant derivative*. For a $SU(2)_L$ doublet ψ_L and a $SU(2)_L$ singlet ψ_R it is defined as:[1]

$$D_\mu \psi_L = \left[\partial_\mu - i g \, T^a W^a_\mu \; - i g' \frac{Y}{2} B_\mu \right] \psi_L \,, \tag{1.12}$$

$$D_\mu \psi_R = \left[\partial_\mu - i g' \frac{Y}{2} B_\mu \right] \psi_R \,, \tag{1.13}$$

being $T^a = \tau^a$ and Y the generators of the gauge groups $SU(2)_L$ and $U(1)_Y$, while W^a_μ and B_μ are the corresponding gauge bosons. Since T^a $(a = 1, 2, 3)$ and Y commute between

[1] We neglect the contributions of strong interactions, which are described in the next Chapter.

them, the two gauge groups are characterized by two distint coupling constants g and g'. Furthermore, as regards $\mathcal{L}_{Fermions}$, no quark and lepton masses appear in (1.10): these parameters enter in the SM through the Yukawa sector.

The potential $V(\phi)$ in (1.11) gives rise to the vacuum expectation value (vev) of the Higgs field

$$\langle\phi\rangle = \frac{1}{\sqrt{2}}\begin{pmatrix}0\\ v\end{pmatrix} , \tag{1.14}$$

which is invariant under transformations of the form (1.8) where the parameters satisfy the following relations:

$$\alpha^1 = \alpha^2 = 0 , \qquad \alpha^3 = \beta . \tag{1.15}$$

This property ensures the theory to have a massless gauge boson, corresponding to the combination (1.15), while the three remaining gauge bosons acquire a mass through the Higgs mechanism [27, 28]. These masses arise from evaluating the kinetic term of $\mathcal{L}_{Higgs}$ at the value v of the ϕ's vev:

$$\begin{aligned}(D^\mu\phi)^*(D_\mu\phi) \to \frac{1}{2}\begin{pmatrix}0 & v\end{pmatrix}\left(gW^a_\mu\tau^a + g'\frac{Y}{2}B_\mu\right)\left(gW^{b\mu}\tau^b + g'\frac{Y}{2}B^\mu\right)\begin{pmatrix}0\\ v\end{pmatrix} = \\ = \frac{1}{2}\frac{v^2}{4}\left[g^2(W^1_\mu)^2 + g^2(W^2_\mu)^2 + (-gW^3_\mu + g'B_\mu)^2\right] ,\end{aligned} \tag{1.16}$$

whence, by a redefinition of the fields, we obtain

$$W^\pm_\mu = \frac{1}{\sqrt{2}}(W^1_\mu \mp iW^2_\mu) \qquad \text{with mass} \quad M_W = g\,\frac{v}{2} , \tag{1.17}$$

$$Z^0_\mu = \frac{1}{\sqrt{g^2+g'^2}}(gW^3_\mu - g'B_\mu) \quad \text{with mass} \quad M_Z = \frac{v}{2}\sqrt{g^2+g'^2} , \tag{1.18}$$

and the massless gauge boson

$$A_\mu = \frac{1}{\sqrt{g^2+g'^2}}(g'W^3_\mu + gB_\mu) , \tag{1.19}$$

which is, as we expected, nothing but the photon. In terms of $W^\pm_\mu$, Z^0_μ and A_μ, the covariant derivative (1.12) assume the form:[2]

$$\begin{aligned}D_\mu\psi_L = \Bigg[\partial_\mu - i\frac{g}{\sqrt{2}}(W^+_\mu T^+ + W^-_\mu T^-) - i\frac{1}{\sqrt{g^2+g'^2}}Z^0_\mu\left(g^2T^3 - g'^2\frac{Y}{2}\right) + \\ - i\frac{gg'}{\sqrt{g^2+g'^2}}A_\mu\left(T^3 + \frac{Y}{2}\right)\Bigg]\psi_L ,\end{aligned}$$

where $T^\pm = T^1 \pm iT^2$ and from which it is straightforward to identify the electric charge e and the corresponding operator Q as:

$$e = \frac{gg'}{\sqrt{g^2+g'^2}} , \tag{1.20}$$

$$Q = T^3 + \frac{Y}{2} , \tag{1.21}$$

[2]The analogous equation for $SU(2)_L$ singlet can be obtained by setting $T^\pm = T^3 = 0$.

which explain the origin of the Gell-Mann-Nishijima formula presented above.

The transformation matrix which connects the basis (W^3, B) with the fields (Z^0, A) can be expressed in terms of the *weak mixing angle* θ_w:

$$\begin{pmatrix} Z^0 \\ A \end{pmatrix} = \begin{pmatrix} \cos\theta_w & -\sin\theta_w \\ \sin\theta_w & \cos\theta_w \end{pmatrix} \begin{pmatrix} W^3 \\ B \end{pmatrix} \ . \tag{1.22}$$

This parametrization together with Eqs. (1.18,1.19) implies

$$\cos\theta_w = \frac{g}{\sqrt{g^2 + g'^2}} \, , \tag{1.23}$$

$$\sin\theta_w = \frac{g'}{\sqrt{g^2 + g'^2}} \, , \tag{1.24}$$

so that we find the following relations for the coupling constants g and g':

$$e = g\sin\theta_w = g'\cos\theta_w \quad \Longrightarrow \quad g = \frac{e}{\sin\theta_w} \, . \tag{1.25}$$

Eq. (1.25) shows that all the couplings of the W and Z bosons depend only on the parameters e and θ_w. Furthermore, their masses are not independent of each other: using Eq. (1.23) with the expression of M_W in (1.17) we obtain

$$M_W = M_Z \cos\theta_w \ . \tag{1.26}$$

Finally we can rewrite the covariant derivative (1.20) in terms of the electric charge, the operator Q and the weak mixing angle, obtaining:

$$D_\mu = \partial_\mu - \frac{ig}{\sqrt{2}}(W^+_\mu T^+ + W^-_\mu T^-) - \frac{ig}{\cos\theta_w} Z^0_\mu (T^3 - \sin^2\theta_w Q) - ieA_\mu Q \, . \tag{1.27}$$

1.1.2 Couplings to fermions

Considering the fermionic lagrangian $\mathcal{L}_{Fermions}$ and using Eq. (1.27) in order to make explicit the presence of the gauge bosons in $\not{D}$, we have:

$$\begin{aligned} \mathcal{L}_{Fermionic} = \ & i\,\bar{Q}^i_L \not{\partial} Q^i_L + \mathrm{i}\,\bar{L}^i_L \not{\partial} L^i_L + \mathrm{i}\,\bar{u}^i_R \not{\partial} u^i_R + \mathrm{i}\,\bar{d}^i_R \not{\partial} d^i_R + \mathrm{i}\,\bar{e}^i_R \not{\partial} e^i_R + \\ & + g\left[W^+_\mu J^{+\mu}_W + W^-_\mu J^{-\mu}_W + Z^0_\mu J^\mu_Z \right] + eA_\mu J^\mu_{e.m.} \ , \end{aligned} \tag{1.28}$$

where the currents $J_W^{+\mu}$, $J_W^{-\mu}$, J_Z^μ and $J_{e.m.}^\mu$ are given by the following relations:

$$J_W^{+\mu} = \frac{1}{\sqrt{2}}\left[\bar{u}_L^i \gamma^\mu d_L^i + \bar{\nu}_L^i \gamma^\mu \ell_L^i\right] , \tag{1.29}$$

$$J_W^{-\mu} = \left(J_W^{+\mu}\right)^\dagger = \frac{1}{\sqrt{2}}\left[\bar{d}_L^i \gamma^\mu u_L^i + \bar{\ell}_L^i \gamma^\mu \nu_L^i\right] , \tag{1.30}$$

$$\begin{aligned} J_Z^\mu = \frac{1}{\cos\theta_w}\Bigg[&\frac{1}{2}\bar{\nu}_L^i \gamma^\mu \nu_L^i + \left(\sin^2\theta_w - \frac{1}{2}\right)\bar{\ell}_L^i \gamma^\mu \ell_L^i + \sin^2\theta_w \bar{\ell}_R^i \gamma^\mu \ell_R^i + \\ &+\left(\frac{1}{2} - \frac{2}{3}\sin^2\theta_w\right)\bar{u}_L^i \gamma^\mu u_L^i + \left(\frac{1}{3}\sin^2\theta_w - \frac{1}{2}\right)\bar{d}_L^i \gamma^\mu d_L^i + \\ &-\frac{2}{3}\sin^2\theta_w\, \bar{u}_R^i \gamma^\mu u_R^i + \frac{1}{3}\sin^2\theta_w\, \bar{d}_R^i \gamma^\mu d_R^i\Bigg] , \end{aligned} \tag{1.31}$$

$$J_{e.m.}^\mu = \frac{2}{3}\bar{u}^i \gamma^\mu u^i - \frac{1}{3}\bar{d}^i \gamma^\mu d^i - \bar{\ell}^i \gamma^\mu \ell^i \ . \tag{1.32}$$

Let's observe that while neutral currents involve both left-handed and right-handed particles, the charged ones involve only left-handed particles. Furthermore $J_{e.m.}^\mu$ has couplings that do not depend on the chirality: it is indeed the usual electromagnetic vector current.

From Eqs. (1.29-1.31) we can derive the behavior of weak interactions at low energies, namely when $E \ll M_W, M_Z$. The following relation (in the Feynman gauge)

$$\langle W_\mu^+(p) W_\nu^-(p)\rangle = \frac{-ig^{\mu\nu}}{p^2 - M_W^2} \underset{M_W^2 \gg p^2}{\approx} \frac{ig^{\mu\nu}}{M_W^2} , \tag{1.33}$$

shows how the high value of the W mass causes the contraction of the propagator, making the transition pointlike. So for example, the tree-level process $e^- u \to \nu_e d$ can be described by the lagrangian

$$\mathcal{L} = \frac{g^2}{2M_W^2}\left[\bar{u}_L \gamma^\mu d_L + \bar{\nu}_{eL} \gamma^\mu e_L\right]\left[\bar{d}_L \gamma^\mu u_L + \bar{e}_L \gamma^\mu \nu_{eL}\right] , \tag{1.34}$$

that is a *current-current* interaction, characterized by the Fermi costant through the relation

$$\frac{G_F}{\sqrt{2}} = \frac{g^2}{8M_W^2} \ . \tag{1.35}$$

A similar argument could be used for neutral current transitions which involve the Z boson. Low energy theories like (1.34) are called *Effective Theories*: among them, the Fermi Theory is the simplest example.

1.2 The Yukawa Sector

In the Glashow-Weinberg-Salam theory fermions are massless. In order to solve this problem it is necessary to extend the lagrangian (1.9-1.11) introducing new couplings, which compose the Yukawa Sector:

$$\mathcal{L}_{Yukawa} = -(Y_d)_{ij} \bar{Q}_L^i \phi\ d_R^j - (Y_u)_{ij} \bar{Q}_L^i \tilde{\phi}\ u_R^j - (Y_l)_{ij} \bar{L}_L^i \phi\ \ell_R^j + h.c. \ , \tag{1.36}$$

where $\tilde{\phi} = i\tau_2\phi^\dagger$. This sector is crucial in the SM description: its structure allows us not only to introduce fermion masses, but also characterizes the properties of quark mixing and CP violation, being particularly sensitive to the presence of NP.

Expanding Eq. (1.36) around the Higgs vev we have:

$$\mathcal{L}_{Yukawa} = -\frac{v\,(Y_d)_{ij}}{\sqrt{2}}\,\bar{d}_L^i d_R^j - \frac{v\,(Y_u)_{ij}}{\sqrt{2}}\,\bar{u}_L^i u_R^j - \frac{v\,(Y_\ell)_{ij}}{\sqrt{2}}\,\bar{\ell}_L^i \ell_R^j + \dots\,,^{3} \tag{1.37}$$

where we identify $m_i \equiv \frac{v}{\sqrt{2}} Y_i$ – with $i = u, d, \ell$ – as the mass matrices of quarks and leptons, whose diagonalization allows us to get the basis of mass eigenstates. Since m_i $(i = u, d, \ell)$ are generic 3×3 complex valued matrices, their diagonalization require the use of bi-unitary transformations:

$$\begin{cases} U_{uL}^\dagger\, m_u\, U_{uR} \equiv m_u^D = \mathrm{diag}(m_u, m_c, m_t)\ , \\ U_{dL}^\dagger\, m_d\, U_{dR} \equiv m_d^D = \mathrm{diag}(m_d, m_s, m_b)\ , \\ U_{\ell L}^\dagger\, m_\ell\, U_{\ell R} \equiv m_\ell^D = \mathrm{diag}(m_e, m_\mu, m_\tau)\ , \end{cases} \tag{1.38}$$

where U_{iL} and U_{iR} are unitary matrices. Eq. (1.38) suggests that the basis of mass eigenstates can be obtained by performing an independent rotation of the left- and right-handed components of the up and down quarks and leptons. More precisely, applying the following transformation

$$\begin{cases} u_{R/L} \to U_{uR/L}\, u_{R/L}\,, \\ d_{R/L} \to U_{dR/L}\, d_{R/L}\,, \\ \ell_{R/L} \to U_{\ell R/L}\, \ell_{R/L}\,, \end{cases} \tag{1.39}$$

we have

$$\begin{cases} \bar{u}_L^{\,i}(m_u)_{ij} u_R^j \ \to\ \bar{u}_L^{\,i}\, U_{uL}^\dagger (m_u)_{ij} U_{uR}\, u_R^j = (m_u^D)_{ij}\, \bar{u}_L^{\,i} u_R^j\,, \\ \bar{d}_L^{\,i}(m_d)_{ij} d_R^j \ \to\ \bar{d}_L^{\,i}\, U_{dL}^\dagger (m_d)_{ij} U_{dR}\, d_R^j = (m_d^D)_{ij}\, \bar{d}_L^{\,i} d_R^j\,, \\ \bar{\ell}_L^{\,i}(m_\ell)_{ij} \ell_R^j \ \to\ \bar{\ell}_L^{\,i}\, U_{\ell L}^\dagger (m_\ell)_{ij} U_{\ell R}\, \ell_R^j = (m_\ell^D)_{ij}\, \bar{\ell}_L^{\,i} \ell_R^j\,, \end{cases} \tag{1.40}$$

so that the rotated fields (1.39) correspond to the basis of mass eigenstates.

1.3 Charged and Neutral currents

Applying rotation (1.39) to the fermionic fields, the weak charged currents (1.29,1.30) are modified by the presence of the Cabibbo-Kobayashi-Maskawa matrix V_{CKM} [3, 4]. In the new basis, $J_W^{+\mu}$ takes the form:[4]

$$J_W^{+\mu} \approx \left[\bar{u}_L^{\,i}\gamma^\mu d_L^{\,i} + \bar{\nu}_L^{\,i}\gamma^\mu \ell_L^{\,i} + h.c.\right] \ \to\ \left[(V_{\mathrm{CKM}})_{ij}\, \bar{u}_L^{\,i}\gamma^\mu d_L^{\,j} + \bar{\nu}_L^{\,i}\gamma^\mu \ell_L^{\,i} + h.c.\right], \tag{1.41}$$

[3] The dots indicate interactions with the Higgs boson and the Goldstone bosons.

[4] $J_W^{-\mu}$ can be obtained considering the relation $J_W^{-\mu} = (J_W^{+\mu})^\dagger$.

where the CKM matrix, which is given by

$$V_{\rm CKM} = U_{u_L}^{\dagger} U_{dL} \,, \tag{1.42}$$

describes the mixing between the mass eigenstates (d, s, b) and the interaction eigenstates (d', s', b'):

$$\begin{pmatrix} d' \\ s' \\ b' \end{pmatrix} = \begin{pmatrix} V_{ud} & V_{us} & V_{ub} \\ V_{cd} & V_{cs} & V_{cb} \\ V_{td} & V_{ts} & V_{tb} \end{pmatrix} \begin{pmatrix} d \\ s \\ b \end{pmatrix} \,. \tag{1.43}$$

Eq. (1.41) shows how $V_{\rm CKM}$ modifies the weak charged currents only in the quark sector, leaving unchanged the leptonic one. This is due to the approximation $m_\nu = 0$, which allows us to extend the rotation $U_{\ell L}$ of Eq. (1.39) also to neutrinos:

$$\nu_L \;\to\; U_{\ell L}\, \nu_L \,. \tag{1.44}$$

Such a rotation reabsorbs the effect of the transformation on ℓ_L, so that, in moving from the basis of interaction eigenstates to that of mass eigenstates, the leptonic charged currents remain unchanged.

On the other hand J_Z^μ and $J_{e.m.}^\mu$ are invariant under transformations (1.39), so these currents are said to be diagonal in flavor. This property can be easily pointed out rewriting Eqs. (1.31,1.32) in the following compact way:

$$J_{e.m.}^\mu = \sum_f Q_f\, \bar{\psi}_f \gamma^\mu \psi_f \;, \tag{1.45}$$

$$J_Z^\mu \;= \sum_f \bar{\psi}_f \gamma^\mu (v_f - a_f \gamma^5) \psi_f \;, \tag{1.46}$$

where $v_f = T_f^3 - 2Q_f \sin^2\theta_W$ and $a_f = T_f^3$. It is straightforward to understand how every unitary matrix applied on a field ψ is cancelled by the hermitian conjugate related to the transformation of the field $\bar{\psi}$. In other words we have that neutral currents do not show any mixing in the different flavors, and this translates into one of the fundamental properties of the SM: the absence of FCNCs at tree-level.

1.4 The Cabibbo Kobayashi Maskawa matrix

Let's now discuss more deeply the properties of the mixing matrix $V_{\rm CKM}$ introduced in the last Section. First of all we highlight the number of indipendent parameters that characterize its structure and how such parameters are related to CP violation. The CKM matrix is a 3×3 complex matrix, so it is given by 18 real parameters: 9 angles and 9 phases. On the other hand $V_{\rm CKM}$ is unitary, thus we can use 9 unitarity constraint relations in order to reduce its free parameters. Furthermore, exploiting the quark fields phase redefinition freedom ($6 - 1 = 5$ arbitrary phases) one concludes that $V_{\rm CKM}$ depends only on 4 real parameters, three angles and one phase, which, together with fermion masses, constitute the free parameters of the flavor quark sector of the Standard Model.

1.4.1 CP violation

The phase of the CKM matrix determines the presence of CP violation in weak interactions. In fact CP symmetry acts on $\mathcal{L}_{Yukawa}$ turning its operators into the hermitian conjugates, leaving unchanged their coefficients, which are given by the couplings Y_d and Y_u. As an example, for the coupling to down type quarks we have:

$$(Y_d)_{ij}\,\bar{Q}_L^i\,\phi\,d_R^j + (Y_d^*)_{ij}\,\bar{d}_R^{\,i}\,\phi^\dagger Q_L^j \xrightarrow{CP} (Y_d)_{ij}\,\bar{d}_R^{\,i}\,\phi^\dagger Q_L^j + (Y_d^*)_{ij}\,\bar{Q}_L^i\,\phi\,d_R^j\ . \tag{1.47}$$

Now it's clear that if the couplings were real matrices the CP invariance would be a good symmetry of the theory. On the contrary the presence of a phase in $V_{\rm CKM}$, as it is shown in (1.47), makes it complex at least one of the two abovementioned couplings, determining the CP violation.

If we had only two generations of quarks, with the same argument developed so far, based now on a flavor symmetry of the type $U(2)_{Q_L}\otimes U(2)_{u_R}\otimes U(2)_{d_R}$, we would have only 5 free parameters, all reals (4 quark masses and the Cabibbo angle). This statement, together with the experimental observation of CP violation, induced M. Kobayashi and T. Maskawa [4] to postulate the existence of the third quark family.

Going back to Eq. (1.43) we remark that there are various parametrizations to express the form of the CKM matrix. Among them the *Standard* parametrization is given by:

$$V_{\rm CKM} = \begin{pmatrix} c_{12}c_{13} & s_{12}c_{13} & s_{13}e^{-i\delta} \\ -s_{12}c_{23} - c_{12}s_{23}s_{13}e^{i\delta} & c_{12}c_{23} - s_{12}s_{23}s_{13}e^{i\delta} & s_{23}c_{13} \\ s_{12}s_{23} - c_{12}c_{23}s_{13}e^{i\delta} & -s_{23}c_{12} - s_{12}c_{23}s_{13}e^{i\delta} & c_{23}c_{13} \end{pmatrix}, \tag{1.48}$$

where $c_{ij} = \cos\theta_{ij}$, $s_{ij} = \sin\theta_{ij}$ $(i,j = 1,2,3)$ and δ is the phase that causes the CP violation. From the experiments we have that $s_{13} \approx \mathcal{O}(10^{-3})$, $s_{23} \approx \mathcal{O}(10^{-2})$ and $c_{13} = c_{23} \approx 1$. As the four independent parameters we can consider:

$$s_{12} \approx |V_{us}|\,,\ s_{13} \approx |V_{ub}|\,,\ s_{23} \approx |V_{cb}|\,,\ \delta\ . \tag{1.49}$$

We remark that the phase $e^{i\delta}$ is always multiplied by the factors s_{12}, s_{13} and s_{23}, thus, for particular processes like the decays of K mesons, CP violation can be suppressed regardless of the value of δ.

Another important parametrization is the Wolfenstein Parametrization [29], that uses the hierarchical structure of the CKM matrix in order to expand each element in a power series of $\lambda = |V_{us}|$. It is expressed in such a way to respect the unitarity of the resulting matrix at the desired order of the expansion. At the order λ^4, we have:

$$V_{\rm CKM} = \begin{pmatrix} 1 - \frac{1}{2}\lambda^2 - \frac{1}{8}\lambda^4 & \lambda & A\lambda^3(\rho - i\eta) \\ -\lambda + \frac{1}{2}A^2\lambda^5[1 - 2(\rho + i\eta)] & 1 - \frac{1}{2}\lambda^2 - \frac{1}{8}\lambda^4(1 + 4A^2) & A\lambda^2 \\ A\lambda^3\left[1 - (\rho + i\eta)\left(1 - \frac{1}{2}\lambda^2\right)\right] & -A\lambda^2 + \frac{1}{2}A[1 - 2(\rho + i\eta)]\lambda^4 & 1 - \frac{1}{2}A^2\lambda^4 \end{pmatrix} \tag{1.50}$$

where the free parameters are λ, A, ρ and η, which are related to those of the Standard parametrization by the following equations:

$$\lambda = s_{12}\,,\quad A\lambda^2 = s_{23}\,,\quad A\lambda^3(\rho - i\eta) = s_{13}e^{-i\delta}\,. \tag{1.51}$$

This parametrization is the one that has the simplest structure but, being an approximate expression, it needs to be expanded in powers of λ to the order of the process we are intrested in.

Even if the CKM matrix is defined up to an arbitrary phase, all the physical observables must be independent from the convention used. In particular a measure of CP violation can be obtained computing the quantity

$$\mathrm{Im}[V_{ij}V_{kl}V_{il}^{*}V_{kj}^{*}] = J_{CP}\sum_{m,n}\varepsilon_{ikm}\varepsilon_{jln} \quad , \tag{1.52}$$

where J_{CP} is independent on the phase convention and is called the *Jarlskog invariant* [30]. It can be thought as a quantitative estimate of the size of CP violation in the SM.

1.4.2 Unitarity relations

The structure of the CKM matrix is also related to the *Unitarity Triangle* analysis. Unitarity of V_{CKM} implies the existence of nine conditions between its elements, which can be divided in two classes: three normalization relations and six orthogonality relations. These conditions are crucial in the SM description since their check is a powerful tool to derive bounds on the fundamental constants of the theory or to probe possible NP scenarios.

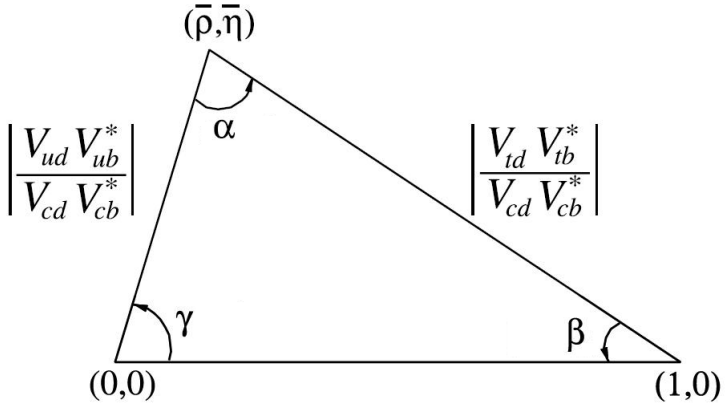

Figure 1.1: Unitarity Triangle in the complex plane $(\bar{\rho},\bar{\eta})$.

Normalization relations require that for each row (or column) the sum of the squared matrix elements must be equal to 1. One of the goal of this thesis is the determination of $|V_{cd}|$ and $|V_{cs}|$, so that we are able to test the unitarity constraint of the second-row of the CKM matrix (see Sections 3.5 and 3.6):

$$|V_{cd}|^2 + |V_{cs}|^2 + |V_{cb}|^2 = 1 \ . \tag{1.53}$$

On the other hand orthogonality relations can be represented as triangles in the plane $(\bar{\rho},\bar{\eta})$, where $\bar{\rho} = \rho(1-\frac{\lambda^2}{2})$ and $\bar{\eta} = \eta(1-\frac{\lambda^2}{2})$. It is convenient to consider unitarity conditions corresponding to triangles with sides that are of the same order of magnitude.

Using the Wolfenstein Parametrization it can be found that this is true for triangles coming from the orthogonality of the first and third rows or the first and third columns. Moreover these two triangles are equivalent at order $\mathcal{O}(\lambda^3)$, so that we can consider only the former, known as the *Unitary Triangle* (UT) of CKM matrix (see Fig. 1.1), which is given by the equation:

$$V_{ud}V_{ub}^* + V_{cd}V_{cb}^* + V_{td}V_{tb}^* = 0 \ . \tag{1.54}$$

Sides and angles of the UT depend on the absolute value of the $V_{\rm CKM}$ matrix elements, thus they are physical observables since they are independent of the phase convention. Furthermore all the triangles coming from orthogonality conditions have the same area:

$$A_\Delta = \frac{|J_{CP}|}{2} \ , \tag{1.55}$$

which shows the relation between unitarity triangles and the Jarlskog Invariant. Eq. (1.55) makes it clear how a measure of A_Δ corresponds to evaluate the size of CP violation.

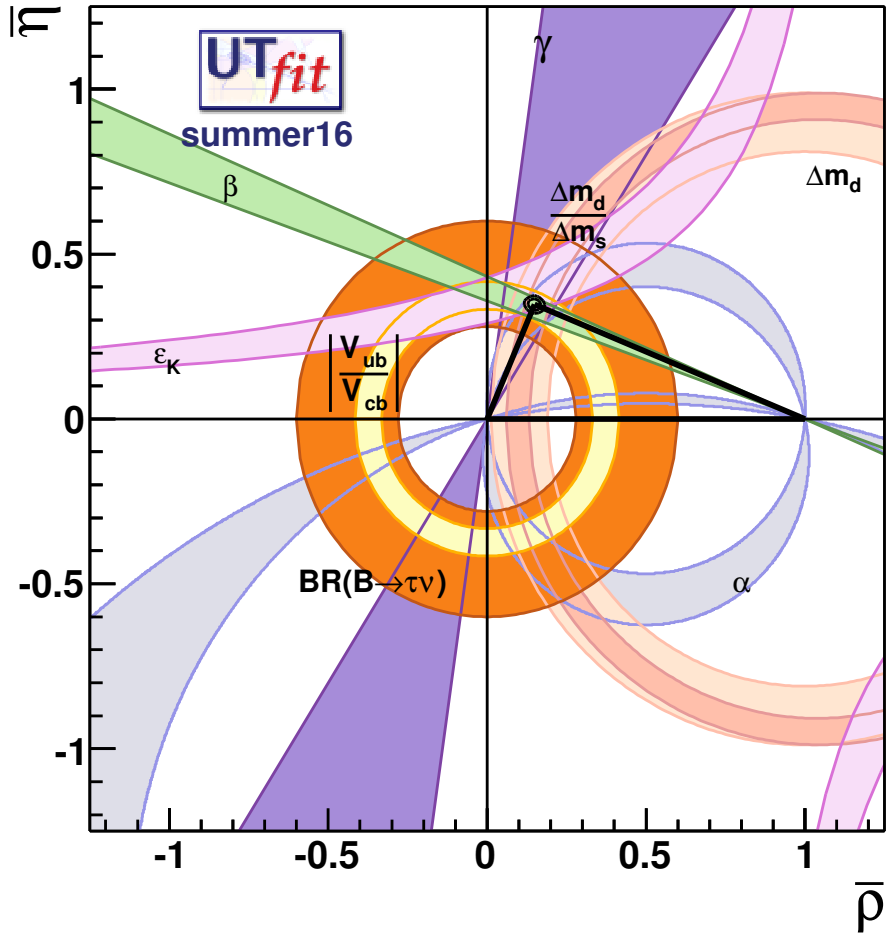

Figure 1.2: Bounds on the UT in the SM from the UTfit Collaboration [31].

Considering Eq. (1.54) and rescaling all by $V_{cb}^* V_{cd}$ we get

$$R_b = \left|\frac{V_{ud}V_{ub}^*}{V_{cd}V_{cb}^*}\right| = \left(1 - \frac{\lambda^2}{2}\right)\frac{1}{\lambda}\left|\frac{V_{ub}}{V_{cb}}\right| , \tag{1.56}$$

$$R_t = \left|\frac{V_{td}V_{tb}^*}{V_{cd}V_{cb}^*}\right| = \frac{1}{\lambda}\left|\frac{V_{td}}{V_{cb}}\right| , \tag{1.57}$$

which are two sides of the rescaled UT, the third one being equal 1 (see Fig. 1.1), while for the corners we find:

$$\alpha = \arg\left(-\frac{V_{td}V_{tb}^*}{V_{ud}V_{ub}^*}\right), \quad \beta = \arg\left(-\frac{V_{cd}V_{cb}^*}{V_{td}V_{tb}^*}\right), \quad \gamma = \arg\left(-\frac{V_{ud}V_{ub}^*}{V_{cd}V_{cb}^*}\right) . \tag{1.58}$$

Fig. (1.2) shows the bounds obtained by the UTfit Collaboration [31] using the more recent theoretical and experimental results, combining direct and indirect measurements. As can be seen, the intersection of the different bands forces the upper vertex of the triangle within a limited area, whose contours are related with the 68% and 95% of confidence level.

It is useful to emphasize that the CKM matrix elements, as well as the particle masses introduced in Sec. 1.2, are free parameters in the SM. This means that they are not fixed by the theory and cannot be measured directly by experiments. Therefore, a combination of experimental and theoretical inputs is required in order to determine them.

1.5 Semileptonic decays of pseudoscalar mesons

The golden modes for the extraction of the CKM matrix elements are represented by leptonic and semileptonic decays. Semileptonic decays are characterized by final states containing both hadrons and leptons. In what follows we will focus only on semileptonic decays

$$P \to P'\ell\nu_\ell , \tag{1.59}$$

where P and P' are both pseudoscalar mesons, ℓ is a charged lepton and ν_ℓ its corresponding neutrino. This case is more complicated with respect to the leptonic one because of the composition of the final state.

In the quark model pseudoscalar mesons are simply composed by a quark-antiquark pair so that, calling $P = Qq'$ and $P = qq'$, the process (1.59) can be described as $Q \to q\ell\nu_\ell$, with q' as a spectator. However all the hadrons, and mesons in particular, are more complex objects as they contain also *virtual* quark-antiquark pairs and gluons, which do not contribute to the quantum numbers of the entire particle. Furthermore at the energy scale characteristic of hadronic decays, strong interactions cannot be treated with perturbative methods because $\alpha_s \lesssim 1$. For this reason all the hadronic quantities involved in these kind of processes have to be evaluated using non-perturbative techniques. In this contest lattice QCD plays a primary role being a non perturbative approach based only on first principles. Fig. (1.3) shows a Feynman diagram for a process of the type (1.59), where the hadronic contributions of the see quark loops and gluon exchange are highlighted.

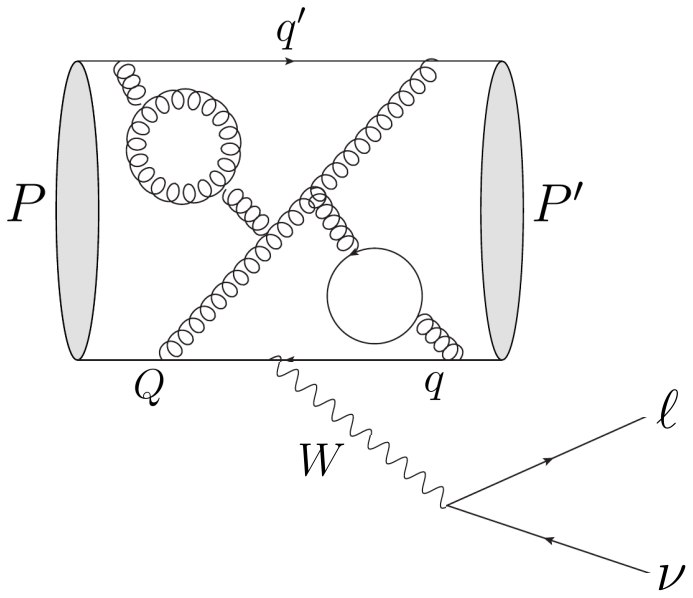

Figure 1.3: Example of the contribution of virtual quark-antiquark pairs and gluons in a semileptonic decay $P \to P'\ell\nu_\ell$.

The amplitude for the process at lowest order in weak interactions is:

$$\mathcal{M}(P \to P'\ell^-\bar{\nu}_\ell) = \frac{G_F}{\sqrt{2}} |V_{Qq}|\, H_\mu L^\mu \ , \tag{1.60}$$

where G_F is the Fermi constant, V_{Qq} is the CKM matrix element related to the quarks involved in the process, while H_μ and L^μ are the matrix elements of the hadronic and leptonic currents respectively:

$$L^\mu = \langle \ell^-\bar{\nu}_\ell | \bar{\ell}\gamma^\mu(1-\gamma^5)\nu_\ell|0\rangle \ , \tag{1.61}$$

$$H_\mu = \langle P'|\bar{q}\gamma^\mu(1-\gamma^5)Q|P\rangle \ . \tag{1.62}$$

In the case of pseudoscalar mesons both in the initial and final states, the contribution of the axial current to the hadronic matrix element vanishes, so that in Eq. (1.62) only the vector current survives:

$$H_\mu = \langle P'|\bar{q}\gamma^\mu(1-\gamma^5)Q|P\rangle = \langle P'|\bar{q}\gamma^\mu Q|P\rangle \equiv \langle V_\mu\rangle \ . \tag{1.63}$$

The vector matrix element $\langle V_\mu\rangle$, as required by the Lorentz symmetry, can be decomposed into two form factors $f_+(q^2)$ and $f_-(q^2)$:

$$\langle V_\mu\rangle = \langle P'(k)|V_\mu|P(p)\rangle = (p+k)_\mu\, f_+(q^2) + (p-k)_\mu\, f_-(q^2) \ , \tag{1.64}$$

where $f_+(q^2)$ is the vector form factor. It is also possible to define a scalar form factor

$$f_0(q^2) = f_+(q^2) + \frac{q^2}{M_D^2 - M_P^2}\, f_-(q^2) \ , \tag{1.65}$$

where $q_\mu = (p-k)_\mu$ is the momentum of the outgoing lepton pair and by construction we have the kinematic constraint $f_+(0) = f_0(0)$. In term of the scalar and vector form factors Eq. (1.64) takes the form:

$$\langle P'(k)|V_\mu|P(p)\rangle = \left(p + k - q\,\frac{m_P^2 - m_{P'}^2}{q^2}\right)_\mu f_+(q^2) + q_\mu\,\frac{m_P^2 - m_{P'}^2}{q^2}\,f_0(q^2)\ . \tag{1.66}$$

Using in the Feynman amplitude (1.60) the decomposition of Eq. (1.66) for the vector current and the expression (1.61) for the leptonic matrix element, we can get the SM prediction for the differential decay rate of a generic semileptonic transition between two pseudoscalar mesons:

$$\begin{aligned}\frac{d\Gamma(P\to P'\ell\nu)}{dq^2} = \frac{G_F^2|V_{Qq}|^2}{24\pi^3}\,\frac{(q^2-m_\ell^2)^2\sqrt{E_{P'}^2 - M_{P'}^2}}{q^4 M_P^2} \\ \cdot\left[\left(1+\frac{m_\ell^2}{2q^2}\right)M_P^2(E_{P'}^2 - M_{P'}^2)|f_+(q^2)|^2 + \frac{3m_\ell^2}{8q^2}(M_P^2 - M_{P'}^2)^2|f_0(q^2)|^2\right]\ .\end{aligned} \tag{1.67}$$

Finally since the contribution to the decay width due to the scalar form factor is proportional to m_ℓ, in the case of $\ell = e,\ \mu$ Eq. (1.67) can be simplified to

$$\frac{d\Gamma(P\to P'\ell\nu_\ell)}{dq^2} = \frac{G_F^2|V_{Qq}|^2}{24\pi^3}\ |\vec{p}_P|^3\ \left|f_+(q^2)\right|^2\ , \tag{1.68}$$

which is the equation we use in Sec. 3.6 in order to evaluate the CKM matrix elements $|V_{cd}|$ and $|V_{cs}|$.

Chapter 2

Lattice QCD

In this Chapter the main features of QCD regularized on a 4-dimensional lattice are presented. We start introducing the theory of strong interactions in the continuum, focusing on the content of fields - made up of quarks and gluons - and the symmetry properties under $SU(3)_C$. We then show how the formulation of QCD on the lattice provides both an infrared (IR) and an ultraviolet (UV) cutoff which regularize the theory. A brief presentation of the Wilson formulation of QCD on the lattice will be shown, and a special care will be devoted in the description of the Wilson Twisted mass action, which is the one used in our simulations, and the $\mathcal{O}(a)$ improvement it allows for. Last Sections are dedicated to the RI/MOM method, to an introduction on numerical simulations in LQCD, to the extrapolation of physical quantities from correlation functions, the twisted boundary conditions and the smearing techniques.

2.1 QCD in the continuum

Quantum Chromodynamics is the non abelian field theory that describes strong interactions. It is based on the symmetry group $SU(3)_C$ and its fundamental degrees of freedom are quarks and gluons.

Some features about quarks have been already presented in the previous Chapter. We remark here that they are spin-1/2 massive fermions which belong, as it is shown in Eq. (1.4), to the fundamental representation of $SU(3)_C$. They carry a color charge, that can be of three different types and that is the analogue for strong interactions of the electric charge of QED. In the following we will use for quarks the compact notation ψ^f_α, where f indicates the flavor label[1], while $\alpha = 1, 2, 3$ represents the color index.

Quarks interact with each other via gluons exchange, which are massless spin-1 bosons. In contrasts with QED, where photons are neutral particles, gluons can interact between them as they also carry color charges. They are the gauge bosons of QCD and are represented by real valued fields $A^a_\mu(x)$ $(a = 1, \dots 8)$, which are the color components of

[1]We remark the difference between this label and the flavor index i used in the previous Chapter. The former runs over all six quark's flavors ($f = u, d, s, c, b, t$), while the latter represents the families, so $i = 1, 2, 3$.

the gauge field $A_\mu(x)$:

$$A_\mu(x) \equiv A^a_\mu(x)\frac{\lambda^a}{2} \ , \tag{2.1}$$

where λ^a are the Gell-Mann matrices. $A_\mu(x)$ belongs to the adjoint representation of $SU(3)_C$, so it is hermitian and traceless.

2.1.1 The QCD lagrangian

The lagrangian of Quantum Chromodynamics is:[2]

$$\mathcal{L}_{QCD} = -\frac{1}{2}\mathrm{Tr}\left[F^{\mu\nu}(x)F_{\mu\nu}(x)\right] + \sum_f \bar{\psi}^f(x)\left(\mathrm{i}\not{D} - m^f\right)\psi^f(x) \ , \tag{2.2}$$

where the first contribution is given by the pure gluonic term, while the second one contains the couplings between fermions and gluons. This second term is characterized by the presence of the covariant derivative

$$D_\mu = \partial_\mu + \mathrm{i}gA_\mu(x) \ , \tag{2.3}$$

where g is the coupling constant of strong interactions.[3] Using this equation in (2.2) we find:

$$\sum_f \bar{\psi}^f(x)\left(\mathrm{i}\not{\partial} - m^f\right)\psi^f(x) - g\sum_f \bar{\psi}^f(x)\not{A}(x)\psi^f(x) \ , \tag{2.4}$$

where we recognize the kinetic term of quarks, with masses m^f depending on the specific flavor, and the interaction term between quarks and gluons. We remark that this interaction is the same for all flavors and it is similar to that between photons and charged particles in QED.

On the other hand the pure gluonic term is made up of the gauge field $A_\mu(x)$. It is characterized by the presence of the gauge strength tensor $F^{\mu\nu}(x)$, which is given by

$$F^{\mu\nu}(x) = \partial_\mu A_\nu(x) - \partial_\nu A_\mu(x) + \mathrm{i}\,g\left[A_\mu(x), A_\nu(x)\right] \ . \tag{2.5}$$

Using Eq. (2.1) it's possible to write also the stength tensor in color components:

$$F^{\mu\nu}(x) = F^a_{\mu\nu}(x)\frac{\lambda^a}{2} \ , \tag{2.6}$$

where we have

$$F^a_{\mu\nu}(x) = \partial_\mu A^a_\nu(x) - \partial_\nu A^a_\mu(x) - g\, f^{abc}\, A^b_\mu(x)\, A^c_\nu(x) \ , \tag{2.7}$$

and f^{abc} are the structure constants of $SU(3)$. Eq. (2.7) shows clearly the similarity between the strength tensor $F^{\mu\nu}$ with the corrisponding tensor of QED. In fact they

[2] Dirac and color indices are omitted.

[3] From now on we use g to indicate the coupling constant of $SU(3)_C$, and no longer that of $SU(2)_L$, as we did in the previous Chapter.

match up to the third term in (2.7), which is peculiar for non-abelian field theories and has deep physical consequences.

Using relation (2.6) we can get rid of the trace in (2.2) and we obtain

$$-\frac{1}{2}\mathrm{Tr}\left[F^{\mu\nu}F_{\mu\nu}\right] = -\frac{1}{2}F^{a\mu\nu}F^{b}_{\mu\nu}\underbrace{\mathrm{Tr}\left[\frac{\lambda^a}{2}\frac{\lambda^b}{2}\right]}_{\delta_{ab}/2} = -\frac{1}{4}F^{a\mu\nu}F^{a}_{\mu\nu}\ , \tag{2.8}$$

where the index a is summed over. Thus the gluonic part of $\mathcal{L}_{QCD}$ has the same structure of the pure gauge lagrangian of electromagnetism, but it is a generalization of it. The main difference with respect to QED arise from the last term in (2.7), i.e. from the gluonic self-interaction term. Expanding (2.6) and (2.7) in $\mathcal{L}_{QCD}$ we find that gluons engage with each other through a cubic and a quartic self-interaction. This is a remarkable hallmark of QCD as it gives rise to one of the most important feature of the theory: the confinement of color into hadrons. On the contrary let's notice that taking the limit $g \to 0$ in $\mathcal{L}_{QCD}$ all the interaction terms vanish and we get a free theory for quarks and gluons.

If we now rescale the gauge field $A_\mu(x)$ by the coupling constant:

$$A_\mu(x) \ \to \ \frac{1}{g}A_\mu(x)\ , \tag{2.9}$$

the physical content of the theory remains unchanged but now we can make explicit g in the lagrangian. We obtain:

$$\mathcal{L}_{QCD} = -\frac{1}{2g^2}\mathrm{Tr}\left[F^{\mu\nu}(x)F_{\mu\nu}(x)\right] + \sum_f \bar{\psi}^f(x)\left(\mathrm{i}\not{D} - m^f\right)\psi^f(x)\ , \tag{2.10}$$

where the coupling constant disappears from the covariant derivative and the strength tensor, that now become:

$$D_\mu = \partial_\mu + \mathrm{i}A_\mu(x)\ , \tag{2.11}$$

$$F^a_{\mu\nu}(x) = \partial_\mu A^a_\nu(x) - \partial_\nu A^a_\mu(x) - f^{abc}\,A^b_\mu(x)\,A^c_\nu(x)\ . \tag{2.12}$$

2.1.2 Gauge invariance of QCD

In the previous Section we wrote the QCD lagrangian without addressing the issue of the gauge invariance. Differently from the flavor symmetry, which is accidental in the limit of massless fermions, the color symmetry is required by the SM and it is exact. In order to have the invariance of QCD under $SU(3)_C$ we need to require that all the terms in the lagrangian (2.10) remain unchanged under group transformations.

Quark fields belong to the fundamental representation of $SU(3)_C$ so they transform, neglecting the flavor label, simply as

$$\begin{aligned}\psi_i(x) &\to \ \psi'_i(x) = \Omega(x)_{ij}\ \psi_j(x)\ ,\\ \bar{\psi}_i(x) &\to \ \bar{\psi}'_i(x) = \bar{\psi}_j(x)\ \Omega(x)^\dagger_{ji}\ ,\end{aligned} \tag{2.13}$$

where $\Omega(x) \in SU(3)_C$. This relations already guarantee the invariance of the fermionic mass term in (2.10):

$$\begin{aligned}\bar{\psi}'(x)\, m\, \psi(x)' \;&\to \bar{\psi}(x)\, \Omega(x)^\dagger\, m\, \Omega(x)\, \psi'(x) = \\ &= \bar{\psi}(x)\, \Omega(x)^\dagger\, \Omega(x)\, m\, \psi'(x) = \bar{\psi}(x)\, m\, \psi(x)\ ,\end{aligned} \tag{2.14}$$

having used the property $\Omega(x)^\dagger = \Omega(x)^{-1}$ of unitary matrices.

As for gluons, in order to understand how the gauge field $A_\mu(x)$ has to transform under $SU(3)_C$, let's go back and recall the fermionic term with the covariant derivative in $\mathcal{L}_{QCD}$. It has the same structure of the fermionic mass term but with m replaced by $\not{D}$. Therefore, since the Dirac matrices commute with every $\Omega(x) \in SU(3)_C$, in order to find the transformation rule for $A_\mu(x)$ we have to require that

$$D'_\mu \psi'(x) = \Omega(x) D_\mu \psi(x)\ , \tag{2.15}$$

which makes automatically satisfied the condition

$$\bar{\psi}'(x) D'_\mu \psi'(x) = \bar{\psi}(x)\, \Omega(x)^\dagger \Omega(x)\, D_\mu \psi(x) = \bar{\psi}(x) D_\mu \psi(x)\ . \tag{2.16}$$

Expanding Eq. (2.15) we find

$$\begin{aligned}&(\partial_\mu + \mathrm{i} A'_\mu(x))\, \Omega(x)\, \psi(x) = \Omega(x)\, \partial_\mu \psi(x) + \mathrm{i}\, \Omega(x)\, A_\mu(x)\, \psi(x) \implies \\ \implies\ &\partial_\mu \Omega(x)\, \psi(x) + \mathrm{i} A'_\mu(x)\, \Omega(x)\, \psi(x) = \mathrm{i}\, \Omega(x)\, A_\mu(x) \psi(x)\ ,\end{aligned} \tag{2.17}$$

where the term with the derivative on the quark field has vanished, and being $\psi(x)$ an arbitrary field, we can drop it and simply consider the equation on the gauge field:

$$\partial_\mu \Omega(x) + \mathrm{i} A'_\mu(x)\, \Omega(x) = \mathrm{i}\, \Omega(x)\, A_\mu(x)\ . \tag{2.18}$$

Multiplying from the right side all the equation by $\Omega^\dagger(x)$ we obtain the trasformation rule for $A_\mu(x)$:

$$A'_\mu(x) = \Omega(x)\, A_\mu(x)\, \Omega(x)^\dagger + \mathrm{i} \partial_\mu \Omega(x)\, \Omega(x)^\dagger\ , \tag{2.19}$$

that, using the condition

$$\partial_\mu \Omega(x)\, \Omega(x)^\dagger + \Omega(x)\, \partial_\mu \Omega(x)^\dagger = \partial_\mu \left(\Omega(x) \Omega(x)^\dagger\right) = \partial_\mu(\mathbb{1}) = 0\ , \tag{2.20}$$

became

$$A'_\mu(x) = \Omega(x)\, A_\mu(x)\, \Omega(x)^\dagger - \mathrm{i}\, \Omega(x)\, \partial_\mu \Omega(x)^\dagger\ . \tag{2.21}$$

This equation represents the transformation rule of the gauge field $A_\mu(x)$ under $SU(3)_C$ which makes Eq. (2.15) satisfied.

Now that we have proved the invariance of the fermionic part of $\mathcal{L}_{QCD}$, what is left to do is to check that also the pure gluonic term is symmetric under $SU(3)_C$ transformations.

For this purpose we note that the strength tensor can be written in terms of covariant derivatives as

$$F_{\mu\nu}(x) = -\mathrm{i}\, [D_\mu(x), D_\nu(x)]\ , \tag{2.22}$$

so that its tranformation properties derive directly from those of $D_\mu(x)$. Looking at (2.15) it's straightforward to find that under gauge transformations the covariant derivative becomes

$$D_\mu(x) \;\rightarrow\; D'_\mu(x) = \Omega(x) D_\mu(x)\, \Omega(x)^\dagger \;. \tag{2.23}$$

Thus Eq. (2.22) implies the same transformation rules of $D_\mu(x)$ also for the strength tensor $F_{\mu\nu}(x)$:

$$F_{\mu\nu}(x) \;\rightarrow\; F'_{\mu\nu}(x) = \Omega(x) F_{\mu\nu}(x)\, \Omega(x)^\dagger \;. \tag{2.24}$$

Now it is easy to show the invariance of the pure gluonic term of $\mathcal{L}_{QCD}$. Using the property of the trace to be invariant under cyclic permutations in (2.10), we have

$$\begin{aligned} \mathrm{Tr}\left[F'^{\mu\nu}(x) F'_{\mu\nu}(x)\right] &= \mathrm{Tr}\left[\Omega(x)^\dagger\, F^{\mu\nu}\, \Omega(x)\, \Omega(x)^\dagger\, F_{\mu\nu}\, \Omega(x)\right] = \\ &= \mathrm{Tr}\left[\Omega(x)^\dagger\, F^{\mu\nu} F_{\mu\nu}\, \Omega(x)\right] = \mathrm{Tr}\left[\Omega(x)\, \Omega(x)^\dagger\, F^{\mu\nu} F_{\mu\nu}\right] = \\ &= \mathrm{Tr}\left[F^{\mu\nu}(x) F_{\mu\nu}(x)\right] \;. \end{aligned} \tag{2.25}$$

which proves, since the coupling constant g is not touched by gauge transformations, the symmetry of the pure gluonc term, and so of the entire $\mathcal{L}_{QCD}$, under $SU(3)_C$ transformations.

This complete our first look on QCD in the continuum space-time. The next step is to transpose the theory on the lattice. To conclude let's notice that although there is not a unique way to do this, all the features we have seen so far will be the main ingredients to approach the problem.

2.2 Regularization of QCD

In Quantum Field Theory (QFT) physical informations are contained in the Green functions, which are vacuum expectation values of the T-products of an arbitrary number of fields and can be obtained in the framework of path integrals. For instance, let us consider a theory with a scalar field ϕ and action $S[\phi]$, the *n-point* Green function is defined as

$$\langle 0|\, T\left\{\phi(x_1) \dots \phi(x_n)\right\}|0\rangle = \frac{\int \mathcal{D}[\phi]\, \phi(x_1) \dots \phi(x_n)\, \exp\left\{iS\left[\phi\right]\right\}}{Z} \;, \tag{2.26}$$

where $Z = \int \mathcal{D}[\phi]\, \exp\left\{iS\left[\phi\right]\right\}$ is the so-called *partition function*. Let's notice that although $\phi(x_1), \dots, \phi(x_n)$ appear in both sides of the equation, those on the l.h.s. are operators, and in fact they act on the vacuum state, while those on the r.h.s. are numerical quantities. The n-point Green function can be expressed in terms of the *generating functional*:

$$Z[J] = \int \mathcal{D}[\phi]\, \exp\left\{ iS\left[\phi\right] + i \int d^4x\, J(x)\, \phi(x) \right\} \;, \tag{2.27}$$

which reduces to the partition function (2.26) when we impose $J(x)$, called the *source* of the field $\phi(x)$, to be zero. By taking functional derivatives of $Z[J]$ we have that

$$\langle 0|\, T\left\{\phi(x_1) \dots \phi(x_n)\right\}|0\rangle = \frac{(-i)^n}{Z[J=0]} \frac{\delta^n Z[J]}{\delta J(x_1) \dots \delta J(x_1)}\bigg|_{J=0} \;. \tag{2.28}$$

However, Feynman integral (2.26) is not well defined as it is infinite dimensional. In fact the measure $\mathcal{D}[\phi]$ is a product of integration measures of the classical field variables at all points x of the space-time:

$$\mathcal{D}[\phi] = \prod_{x \in \mathbb{R}^4} d\phi(x) \ , \tag{2.29}$$

so it is given by an infinite number of terms. Furthermore in the expression of the Green functions we have the phase $e^{\,iS}$, which is an oscillating term. It is clear that in order to make sense to the path integral (2.26) we have to solve this two problems: we refer to this procedure as the *regularization* of the theory. The phase $e^{\,iS}$ can be transformed in a negative exponential by implementing the so-called *Wick rotation*. On the other hand the Feynman integral can be reduced to be finite-dimensional by discretizing the space-time on a 4-dimensional lattice. This procedure automatically gets rid of the divergencies which typically affect QFTs.

2.2.1 Wick rotation

In order to make the integral (2.26) convergent we have to perform the Wick rotation, that is a transformation from the Minkowskian space-time to the Euclidean one. In this way we obtain a theory that preserves the physical content of interest, although is not the real one. This rotation corresponds to the analytic prolongation of time in the complex field. To better undestand how this rotation works, let's start observing the simple case of a 2-point Green function with values of time x^0 and y^0 such that $x^0 > y^0$.[4] We have:

$$\begin{aligned} \langle 0|\, T\{\phi(x)\phi(y)\}\, |0\rangle \underset{x^0>y^0}{=} & \langle 0|\, \phi(x)\phi(y)|0\rangle = \\ & = \sum_n \langle 0|\, e^{iHx^0}\phi(0,\mathbf{x})\, e^{-iHx^0}\, |n\rangle\, \langle n|\, e^{iHy^0}\phi(0,\mathbf{y})e^{-iHy^0}|0\rangle = \\ & = \sum_n \langle 0|\phi(0,\mathbf{x})\, |n\rangle\, \langle n|\, \phi(0,\mathbf{y})|0\rangle\, e^{-iE_n(x^0-y^0)} \ , \end{aligned} \tag{2.30}$$

where we have used the completeness relation

$$\mathbb{1} = \sum_n |n\rangle\, \langle n| \ , \tag{2.31}$$

in which we consider an orthonormal basis for the Hilbert space, with energies ordered as $E_0 < E_1 < E_2 < \dots$. We can perform the analytic prolongation of time in the complex field by setting

$$x_0 \ \to \ x_0\, e^{i\alpha} \, , \quad y_0 \ \to \ y_0\, e^{i\alpha} \ , \tag{2.32}$$

so that the exponential in Eq. (2.30) becomes

$$e^{-iE_n(x^0-y^0)\, e^{i\alpha}} = e^{-iE_n(x^0-y^0)\, \cos\alpha}\ e^{E_n(x^0-y^0)\, \sin\alpha} \ . \tag{2.33}$$

[4] Although this is not the general case, it shows well the problem and can be easily generalized.

The first term on the r.h.s.is still oscillating, but the second one has a real-valued exponent, so it's no longer a complex phase.

Focusing on this second exponential, we have to be careful in choosing α: the energy E_n is positive and has no upper bound when increasing n, but also $(x_0 - y_0)$ is greater than zero by assumption[5], thus the choice of α is not completely arbitrary. If we take $\alpha > 0$ the exponent is positive, so the sum in (2.30) explodes to infinity, but if we set $\alpha < 0$ the exponential is negative, so this choice improves the convergence of the T-product (2.30). In this procedure we only have the constraint $\alpha < 0$, which allows us to set the particularly advantageous value $\alpha = -\pi/2$, in order to get

$$\langle 0|\, T\{\phi(x)\phi(y)\}\, |0\rangle = \sum_n \langle 0|\phi(0,\mathbf{x})\, |n\rangle\, \langle n|\, \phi(0,\mathbf{y})|0\rangle\, e^{-E_n(x^0-y^0)} \ , \tag{2.34}$$

where the oscillating term vanishes becouse $\cos\alpha = 0$. Transformation (2.32) with the condition $\alpha = -\pi/2$ is what is called Wick rotation.

Using labels M and E to indicate the Minkowskian and the Euclidean space-time variables, for a generic space-time point x this transformation is given by

$$\begin{aligned} x^0 = x^0_M \ &\rightarrow\ -\mathrm{i}\, x^0_E \equiv -\mathrm{i}\, x_4 \ , \\ x^i = x^i_M \ &\rightarrow\ \quad x^i_E \equiv x_i \ . \end{aligned} \tag{2.35}$$

Now it is straightforward to see that the relativistic distance becomes

$$x^2 = (x^0_E)(x_{0E}) + (x^i_E)(x_{iE}) = x_1^2 + x_2^2 + x_3^2 + x_4^2 \ , \tag{2.36}$$

that explain why this new space-time is called Euclidean. Since we have an Euclidean metric, we do not distinguish between covariant and contravariant indices, and we will conventionally use only contravariant ones.

Let's see how it works the analytic prolongation for the free scalar theory. In this case the 2-points Green function is given by the Feynman propagator:

$$\mathrm{i}\,\Delta_F(x-y) = \mathrm{i}\int \frac{d^4q}{(2\pi)^4} \frac{e^{\,i\,q^0(x_0-y_0)}\, e^{-i\,\mathbf{q}\,(\mathbf{x}-\mathbf{y})}}{q^2 - m^2} \ . \tag{2.37}$$

Looking at the temporal part of (2.37), when we use the analytic prolongation of time (2.32) we get

$$\int dq^0\, \frac{e^{\,i\,q^0(x_0-y_0)_E\, e^{i\alpha}}}{q^2 - m^2} \ , \tag{2.38}$$

and the above integral will be divergent for any choice of α because q^0 can be either positive or negative. This means that we cannot apply directly rotation (2.35) to the Feynman propagator. What we have to do is to perform the analytic prolongation in such a way that the exponent in (2.38) is purely imaginary. In order to do that we have to change the integration path while we rotate time, so that q^0 has a constant phase $e^{-i\alpha}$ that cancels the one of $(x_0 - y_0)$.

[5]Had we chosen $x_0 < y_0$, we would get $(y_0 - x_0)$ in (2.33), once again greater than zero. In fact this argument is indepent of the choice $x_0 > y_0$.

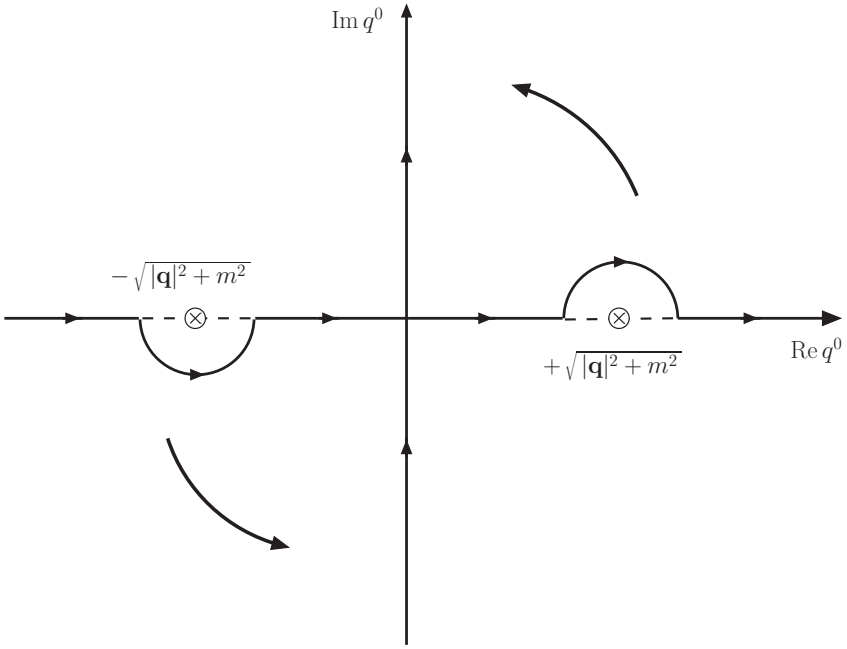

Figure 2.1: Wick rotation in the complex q^0 plane.

An integration path characterized by a constant phase is a straight line in the complex plane: we can only set $\alpha < 0$, otherwise we would move through the singularities $q^0 = \pm\sqrt{|\mathbf{q}|^2 + m^2}$. This is in agreement with the choice of setting $\alpha = -\pi/2$, which corresponds to rotate q^0 from the real to the imaginary axis. Thus when we perform the Wick rotation we have also to change the integration path in Eq. (2.37) and we obtain the Euclidean components of the four-momentum:

$$\begin{aligned} q^0_M &\rightarrow i q^0_E \equiv i q_4 \ , \\ q^i_M &\rightarrow q^i_E \ . \end{aligned} \tag{2.39}$$

Using (2.35) together with (2.39) the Feynman propagator becomes:

$$\begin{aligned} \mathrm{i}\,\Delta_F(x-y) \rightarrow \mathrm{i}\int \frac{(\mathrm{i}\,dq_4)\,d^3q}{(2\pi)^4}\frac{e^{i\,(i\,q_4)(-i)(x_4-y_4)}\,e^{-i\,\mathbf{q}\,(\mathbf{x}-\mathbf{y})}}{-q_4^2-|\mathbf{q}|^2-m^2} = \\ = \int \frac{d^4q}{(2\pi)^4}\frac{e^{i\,q_4(x_4-y_4)}\,e^{-i\,\mathbf{q}\,(\mathbf{x}-\mathbf{y})}}{q_4^2+|\mathbf{q}|^2+m^2} = \\ = \int \frac{d^4q}{(2\pi)^4}\frac{e^{i\,q_4(x_4-y_4)}\,e^{-i\,\mathbf{q}\,(\mathbf{x}-\mathbf{y})}}{q^2+m^2} \ , \end{aligned} \tag{2.40}$$

where now we indicate $q^2 = q_4^2 + |\mathbf{q}|^2$, exactly as in an euclidean space-time. We remark that the euclidean propagator (2.40) does not diverge anymore and it is free of singularites: the minus sign in the denominator has been replaced by the plus sign. All we showed here can be easily extended for a generic quantum field theory and keeps its validity for any n-points Green function.

2.2.2 Wick rotation of the QCD action

In order to complete the discussion about Wick rotation, what is left to do now is to see the implications of this transformation for the QCD action. First of all let's notice that when we perform the analytic prolongation of time in the complex field the gauge field components transform as

$$\begin{aligned} A_0^M(x) &\rightarrow \mathrm{i}\, A_4^E(x) \ , \\ A_i^M(x) &\rightarrow A_i^E(x) \ , \end{aligned} \tag{2.41}$$

while for the space-time derivatives we have

$$\begin{aligned} \partial_{0M} = \frac{\partial}{\partial x_M^0} &\rightarrow \frac{\partial}{-\mathrm{i}\,\partial x_E^0} = \mathrm{i}\,\partial_{0E} \ , \\ \partial_{iM} = \frac{\partial}{\partial x_M^i} &\rightarrow \frac{\partial}{\partial x_E^i} = \partial_{iE} \ . \end{aligned} \tag{2.42}$$

Taking the fermionic part of the QCD action and considering it for a single flavor, the action of the Wick rotation implies:

$$\begin{aligned} S_F^M[\psi,\bar\psi,A] = \int d^4x\ \bar\psi(x)\,(\mathrm{i}\gamma^\mu(\partial_\mu + \mathrm{i}\,A_\mu(x)) - m)\,\psi(x) \ \stackrel{\text{W. rot.}}{\longrightarrow} \\ \stackrel{\text{W. rot.}}{\longrightarrow} \int -\mathrm{i}\,d^4x^E\ \bar\psi(x)\left(\mathrm{i}\gamma^0(\mathrm{i}\,\partial_0^E + \mathrm{i}^2 A_4^E(x)) + \mathrm{i}\gamma^i(\partial_i^E + \mathrm{i}\,A_i^E(x)) - m\right)\psi(x) = \\ = \mathrm{i}\int d^4x^E\ \bar\psi(x)\left(\gamma_0(\partial_0^E + \mathrm{i}A_4^E(x)) + \mathrm{i}\gamma_i(\partial_i^E + \mathrm{i}\,A_i^E(x)) + m\right)\psi(x) = \\ = \mathrm{i}\int d^4x^E\ \bar\psi(x)\left(\gamma_\mu^E(\partial_\mu^E + \mathrm{i}A_\mu^E(x)) + m\right)\psi(x) \ , \end{aligned} \tag{2.43}$$

where we have introduced the Euclidean gamma matrices, which are related with the Minkowskian ones by the equations

$$\gamma_1^E = -\mathrm{i}\gamma_1^M, \ \ \gamma_2^E = -\mathrm{i}\gamma_2^M, \ \ \gamma_3^E = -\mathrm{i}\gamma_3^M, \ \ \gamma_4^E = \gamma_0^M \ , \tag{2.44}$$

and satisfy anti-commutation relations:

$$\{\gamma_\mu^E, \gamma_\nu^E\} = 2\,\delta_{\mu\nu}\,\mathbb{1} \ . \tag{2.45}$$

In addition to the matrices γ_μ^E ($\mu = 1,2,3,4$), we have also the Euclidean version of γ_5 as the product:

$$\gamma_5^E = \gamma_1^E\,\gamma_2^E\,\gamma_3^E\,\gamma_4^E \ . \tag{2.46}$$

From Eq. (2.43) we define the Euclidean fermionic action of QCD as

$$S_F^E[\psi,\bar\psi,A] = \int d^4x^E\ \bar\psi(x)\left(\gamma_\mu^E(\partial_\mu^E + \mathrm{i}A_\mu^E(x)) + m\right)\psi(x) \ . \tag{2.47}$$

Such a definition implies that the effect of the Wick rotation on the fermionic action can be summarized in the following compact way:

$$S_F^M[\psi,\bar\psi,A] \ \stackrel{\text{W. rot.}}{\longrightarrow} \ \mathrm{i}\,S_F^E[\psi,\bar\psi,A] \ . \tag{2.48}$$

For the case of the pure gluonic action we need to know the transformation properties of the strength tensor. Using Eqs. (2.41,2.42) in (2.5), we find:

$$\begin{aligned} F_{0i}^M(x) &\overset{\text{W. rot.}}{\longrightarrow} \mathrm{i}\, F_{0i}^E(x) \ , \\ F_{ij}^M(x) &\overset{\text{W. rot.}}{\longrightarrow} \mathrm{i}\, F_{ij}^E(x) \ , \end{aligned} \tag{2.49}$$

where $i, j = 1, 2, 3$. The above relations imply that the trace in (2.10) transforms as

$$\begin{aligned} \mathrm{Tr}\left[F^{\mu\nu}(x)F_{\mu\nu}(x)\right] &= \mathrm{Tr}\left[-2F_{0i}(x)F_{0i}(x) + F_{ij}(x)F_{ij}(x)\right] \overset{\text{W. rot.}}{\longrightarrow} \\ &\overset{\text{W. rot.}}{\longrightarrow} \mathrm{Tr}\left[\,2F_{0i}^E(x)F_{0i}^E(x) + F_{ij}^E(x)F_{ij}^E(x)\right] = \\ &= \mathrm{Tr}\left[F_{\mu\nu}^E(x)F_{\mu\nu}^E(x)\right] \ , \end{aligned} \tag{2.50}$$

and thus for the pure gluonic action we finally get:

$$\begin{aligned} S_G^M[A] = -\frac{1}{2\,g^2}\int d^4x\ \mathrm{Tr}\left[F^{\mu\nu}(x)F_{\mu\nu}(x)\right] \quad &\overset{\text{W. rot.}}{\longrightarrow} \\ \overset{\text{W. rot.}}{\longrightarrow} \mathrm{i}\,\frac{1}{2\,g^2}\int d^4x^E\ \mathrm{Tr}\left[F_{\mu\nu}^E(x)F_{\mu\nu}^E(x)\right] \ . \end{aligned} \tag{2.51}$$

If we now define the Euclidean pure gluonic action as

$$S_G^E[A] = \frac{1}{2\,g^2}\int d^4x^E\ \mathrm{Tr}\left[F_{\mu\nu}^E(x)F_{\mu\nu}^E(x)\right] \ , \tag{2.52}$$

we can extend relation (2.48) also to this case, and more generally to all the QCD action:

$$S_{QCD}^M[\psi, \bar{\psi}, A] \quad \overset{\text{W. rot.}}{\longrightarrow} \quad \mathrm{i}\, S_{QCD}^E[\psi, \bar{\psi}, A] \ . \tag{2.53}$$

This relation proves for QCD what we introduced for the general case at the beginning of this Section, i.e. that the phase $e^{\,iS}$ in the Green functions can be transformed by the Wick rotation in an negative exponential:

$$\exp\left(\mathrm{i}\, S_{QCD}^M\right) \quad \overset{\text{W. rot.}}{\longrightarrow} \quad \exp\left(-S_{QCD}^E\right) \ . \tag{2.54}$$

From here on we will only make use of the Euclidean formulation of the theory, so we'll neglect the label E but considering the Euclidean action of QCD.

2.2.3 Lattice regularization

Now that we have the Euclidean formulation of QCD we need to solve the problem of the infinite dimension of the Feynman integral (2.26), which actually is only a formal definition because of the infrared and ultraviolet divergences. In 1974 Kenneth Wilson proposed a formulation of QCD on a lattice that was the starting point for non perturbative numerical calculation in particle physics [32]. The idea is to discretize the space-time in a finite 4-dimensional lattice, so that the Feynman integral can be expressed in a well defined mathematical form.

The first step is to introduce a 4-dimensional lattice Λ:

$$\Lambda = \{\, n = (n_1, n_2, n_3, n_4) \,|\, n_1, n_2, n_3 = 0, 1, 2, ..., N-1;\; n_4 = 0, 1, 2, ..., N_T - 1\} \;, \quad (2.55)$$

where the vectors $n \in \Lambda$ indicate points of the space-time separated by the lattice spacing a:

$$x \longrightarrow an \qquad n \in \Lambda \,. \quad (2.56)$$

In each direction we consider N points, so the lattice Λ has a finite volume $V = L^3 \equiv (aN)^3$ and a finite extension in time $T = aN_T$, which means that we have to use a prescription in order to define the fields at the boundaries. As a starting point we choose periodic boundary conditions (BCs), i.e. we identify $n_\mu = N_{(T)}$ with $n_\mu = 0$ ($\mu = 1, 2, 3, 4$):

$$\Phi(n + aN_{(T)}\hat{\mu}) = \Phi(n) \,. \quad (2.57)$$

In the framework of LQCD the fields of the theory live only on the lattice sites, so we replace the space argument x by the label n:

$$\Phi(x) \longrightarrow \Phi(n) \quad n \in \Lambda \,. \quad (2.58)$$

In order to define a theory on the lattice we also need to discretize the derivatives. There's no single way to do it, but for small lattice constants a two solutions are given by the following replacements:

$$\partial_\mu \Phi(x) \longrightarrow \overrightarrow{\partial}_\mu \Phi(n) = \frac{\Phi(n + \hat{\mu}) - \Phi(n)}{a} \,, \quad (2.59)$$

$$\partial_\mu \Phi(x) \longrightarrow \overleftarrow{\partial}_\mu \Phi(n) = \frac{\Phi(n) - \Phi(n - \hat{\mu})}{a} \,, \quad (2.60)$$

where $\hat{\mu}$ denotes the unit vector in the μ-direction. Eqs. (2.59,2.60) are commonly called the *foreward* and *backward* derivatives. Using the Taylor expansion it is straightforward to see that these two quantities are equal to the usual derivative up to terms of order $\mathcal{O}(a)$. However, if we combine forward and backward derivatives as

$$\frac{1}{2}\left(\overrightarrow{\partial}_\mu + \overleftarrow{\partial}_\mu\right)\Phi(n) = \frac{\Phi(n + \hat{\mu}) - \Phi(n - \hat{\mu})}{2a} \;, \quad (2.61)$$

we obtain an object which matches the field derivative up to order $\mathcal{O}(a^2)$.

When we consider a theory on a lattice Λ the functional integral (2.26) is finite-dimensional. In fact the integration measure (2.29) becomes:

$$\mathcal{D}[\Phi] = \prod_{x \in \mathbb{R}^4} d\Phi(x) \longrightarrow \prod_{n \in \Lambda} d\Phi(n) \;, \quad (2.62)$$

which is the product of a finite number of terms, and so it represents the measure of a well defined multidimensional integral. The lattice provides also both an infrared and an ultraviolet cutoff, where the former is due to the fact that the lattice has a finite volume V, while the latter is a consequence of the discretization. Considering the expression of

the field Φ in the momentum space, which is given by the Fourier transform of $\Phi(n)$, we have

$$\Phi(\vec{p},t) = \sum_{\vec{n}} \Phi(n)\, \exp\{-ia\vec{p}\cdot\vec{n}\}\ , \tag{2.63}$$

which means that each component p_i $(i = 1,2,3)$ of the momentum is cutoff at the first Brioullin zone:

$$\Phi\big(\vec{p} + (2\pi/a)\,\hat{i}, t\big) = \Phi(\vec{p},t) \implies |p_i| \leq \frac{\pi}{a}\,. \tag{2.64}$$

Eq. (2.64) shows how the lattice spacing a, and more precisely its inverse a^{-1}, constitutes an ultraviolet cutoff for a theory on the lattice. On the other hand we can consider $\Phi(n)$, expressed in the space-time, as the Fourier transform of $\Phi(\vec{p},t)$. We have:

$$\Phi(n) = \frac{1}{V}\sum_{\vec{p}} \Phi(\vec{p},t)\exp\{ia\vec{p}\cdot\vec{n}\}\ , \tag{2.65}$$

through which, using Eq. (2.57), we find

$$\begin{aligned} &\frac{1}{L}\sum_{p_i}\psi(\vec{p},t)\exp\{iap_in_i\}\exp\{iap_iN\} = \frac{1}{L}\sum_{p_i}\psi(\vec{p},t)\exp\{iap_in_i\} \implies \\ \implies\ &\exp\{ip_iL\} = 1 \implies p_i = \frac{2\pi k_i}{aN}\ \text{ with }\ k_i = 0,1,2,\ldots,N-1\,, \end{aligned} \tag{2.66}$$

which shows how the lattice provides also an infrared cutoff for our theory.

2.3 Partition function of QCD

To write the generating functional in QCD we have to introduce three sources, one for each field in the action. In the Euclidean space-time we have:

$$\begin{aligned} Z[\boldsymbol{\eta},\bar{\boldsymbol{\eta}},J] = &\int \mathcal{D}[A]\left(\prod_f \mathcal{D}[\psi^f]\,\mathcal{D}[\bar{\psi}^f]\right)\times \\ \times\exp&\left\{-S_{QCD}[\boldsymbol{\psi},\bar{\boldsymbol{\psi}},A] + \int d^4x\left[\sum_f\Big(\bar{\eta}^{\,f}(x)\psi_f(x) + \bar{\psi}^f(x)\eta_f(x)\Big) + J(x)A(x)\right]\right\}\ , \end{aligned} \tag{2.67}$$

where we use symbols in bold to represent the dependence of fields on different flavors. Quark fields and their corresponding sources are anti-commuting complex variables (*Grassmann variables*) which satisfy the following commutation relations:

$$\big\{\overline{\xi},\overline{\xi}\big\} = \{\xi,\xi\} = \big\{\overline{\xi},\xi\big\} = 0\ . \tag{2.68}$$

This means that $\bar{\xi}^{\,2} = \xi^2 = 0$, so any generic function $f(\xi,\bar{\xi})$ can be expanded as a Taylor series in the simple form:

$$f(\xi,\bar{\xi}) = c_0 + c_1\,\xi + c_2\,\overline{\xi} + c_3\,\xi\overline{\xi}\ , \tag{2.69}$$

where all the higher other terms are zero, while the c_i $(i = 0, \ldots, 3)$ are just numerical coefficients. Furthermore, also derivation and intragration rules are different for Grassman variables with respect usual commuting ones. In particulare we have:

$$\frac{\partial}{\partial\xi}\frac{\partial}{\partial\overline{\xi}} = -\frac{\partial}{\partial\overline{\xi}}\frac{\partial}{\partial\xi} \ , \qquad \frac{\partial}{\partial\xi}\,\overline{\xi} = -\overline{\xi}\frac{\partial}{\partial\xi} \ , \tag{2.70}$$

$$\int d\overline{\xi}d\xi = \int d\overline{\xi}d\xi\,\overline{\xi} = \int d\overline{\xi}d\xi\,\xi = 0 \ , \tag{2.71}$$

$$\int d\xi\,\xi = \int d\overline{\xi}\,\overline{\xi} = \int d\overline{\xi}d\xi\,\xi\,\overline{\xi} = 1 \ . \tag{2.72}$$

Eqs. (2.71,2.72) can be used to find the expression of gaussian integrals of Grassman variables, which reduce to the simple form:

$$\int \left(\prod_{i=1}^{N} d\overline{\xi}_i d\xi_i\right) \exp\left\{-\sum_{i,j=1}^{N} \overline{\xi}_i M_{ij} \xi_j\right\} = \det[M]. \tag{2.73}$$

If we now consider the fermionic part of the generating functional (2.67) and define $M_f[A] \equiv \left(\gamma_\mu(\partial_\mu + iA_\mu(x)) + m^f\right)$ in the fermion action (2.47), we can write:

$$\begin{aligned} Z_F[\boldsymbol{\eta}, \bar{\boldsymbol{\eta}}, A] = \int \left(\prod_f \mathcal{D}[\psi^f]\,\mathcal{D}[\bar{\psi}^f]\right) \times \\ \times \exp\left\{-\int d^4x \sum_f \left(\bar{\psi}^f(x) M_f[A] \psi^f(x) - \bar{\eta}^{\,f}(x)\psi_f(x) - \bar{\psi}^f(x)\eta_f(x)\right)\right\} \ . \end{aligned} \tag{2.74}$$

To solve this integral it is convenient to perform the following transformation:

$$\begin{aligned} \psi^f(x) &\to \xi^f(x) + M_f^{-1}\,\eta^f \equiv \xi^f(x) + \widetilde{\psi}^f(x) \ , \\ \overline{\psi}^f(x) &\to \overline{\xi}^f(x) + \bar{\eta}^f M_f^{-1} \equiv \overline{\xi}^f(x) + \widetilde{\overline{\psi}}^f(x) \ , \end{aligned} \tag{2.75}$$

where ξ^f and $\overline{\xi}^f$ are new integration variables, while $\widetilde{\psi}^f$ and $\widetilde{\overline{\psi}}^f$ are constant fields. The change of variables (2.75) leaves invariant the integration measure and allow us to write the fermionic generating functional in the form:

$$\begin{aligned} Z_F[\boldsymbol{\eta}, \bar{\boldsymbol{\eta}}, A] = \exp\left\{\int d^4x \sum_f \bar{\eta}^f M_f^{-1} \eta^f\right\} \int \left(\prod_f \mathcal{D}[\xi^f]\,\mathcal{D}[\bar{\xi}^f]\right) \times \\ \times \exp\left\{-\int d^4x \sum_f \bar{\xi}^f M_f\,\xi^f\right\} = \exp\left\{\int d^4x \sum_f \bar{\eta}^f M_f^{-1} \eta^f\right\} \prod_f \det[M_f], \end{aligned} \tag{2.76}$$

where, for a given flavor, the quantity $\det[M_f]$ is called *fermionic determinant*. Differentiating this result with respect to η and $\bar{\eta}$ we find an expression for the fermionic

expectation value of Grassman variables that comes under the name of *Wick's theorem*. The simplest case is given by the 2-point function:

$$\langle \psi^f(y)\bar{\psi}^f(x)\rangle_F = \frac{1}{Z_F[\boldsymbol{\eta}=0,\bar{\boldsymbol{\eta}}=0,A]}\frac{\delta^2 Z_F}{\delta\bar{\eta}^f(y)\delta\eta^f(x)}\bigg|_{\eta^f,\bar{\eta}^f=0} = M_f[A]^{-1}\ , \tag{2.77}$$

where $\langle\ldots\rangle$ represents the analytic continuation of the T-product in the Euclidean space-time, while the label F indicates that the expectation value is calculated using the fermionic action S_F. Eq. (2.76) can be used to rewrite the QCD partition function (2.67) in terms of an effective action depending on gluon fields only. Setting to zero all sources in Z_F and and using the matrix property $\det[M] = \exp\{\,\mathrm{Tr}[\log(M)]\}$ we find

$$\begin{aligned} Z_{QCD} &= \int \mathcal{D}[A]\exp\left\{-S^{\mathrm{eff}}_{QCD}[A]\right\} = \\ &= \int \mathcal{D}[A]\exp\left\{+\,\mathrm{Tr}\left[\log\left(\sum_f M_f[A]\right)\right] - \frac{1}{2g^2}\int d^4x\,\mathrm{Tr}\left[F_{\mu\nu}(x)F_{\mu\nu}(x)\right]\right\}\ . \end{aligned} \tag{2.78}$$

The fermion determinant produces the sea quarks corrections, which are given by the exponential of fermionic loops with an arbitrary number of insertions of gauge fields. It describes the fermionic vacuum where virtual pairs of quarks and antiquarks are created and annihilated. Its numerical evaluation is time-consuming and computationally expensive and for this reason, up to the late nineties, lattice calculations were performed neglecting the fermion determinant in numerical simulations. This corresponds to perform the limit $m_q \to \infty$, in which the sea quarks decouple from the theory, and is known as the *quenched approximation*. Nowadays, most of the lattice calculations are *unquenched*, i.e. are performed considering the contribution of dynamical sea quarks. The present work, is developed using the gauge configurations produced by the ETM Collaboration includes the effects of four flavors of dynamical quarks (up, down, strange and charm).

2.4 Fermionic action

We start the analysis of the QCD formulation on the lattice from the fermionic action. In particular let us consider the free term of Eq. (2.47), which is:

$$S_F^0\left[\psi,\bar{\psi}\,\right] = \int d^4x\ \bar{\psi}(x)\left(\gamma_\mu\partial_\mu + m_0\right)\psi(x)\ , \tag{2.79}$$

where we use the symbol m_0 to indicate the *bare* quark mass. Using substitutions (2.58,2.61) it is straightforward to write the lattice version of S_F^0. We get:

$$S_F^0\left[\psi,\bar{\psi}\,\right] = a^4\sum_{n\in\Lambda}\ \bar{\psi}(n)\bigg[\sum_{\mu=1}^{4}\gamma_\mu\frac{\psi(n+\hat{\mu})-\psi(n-\hat{\mu})}{2a} + m_0\,\psi(n)\bigg], \tag{2.80}$$

where we have also transformed the space-time integral in a sum over the lattice sites:

$$\int d^4x\ \longrightarrow\ a^4\sum_{n\in\Lambda}\ . \tag{2.81}$$

Eq. (2.80) can also be written in the compact form:

$$S_F^0\left[\psi,\bar{\psi}\,\right] = a^4 \sum_{n,m\in\Lambda} \bar{\psi}(n)\, D(n,m)\, \psi(m)\ , \tag{2.82}$$

where the Dirac operator $D(n,m)$ is defined as:

$$D(n,m) = \sum_{\mu=1}^{4} \frac{1}{2a}\gamma_\mu \left[\delta_{m,n+\hat{\mu}} + \delta_{m,n-\hat{\mu}}\right] + m_0\, \delta_{mn}\ . \tag{2.83}$$

2.4.1 Gauge invariance of the fermionic action

In Eq. (2.80) we have introduced the lattice formulation for free fermions. In order to regularize the fermionic action, however, we have to consider also the interaction between quarks and gluons. We thus need to see how the property of gauge invariance of QCD under $SU(3)_C$ transformations traslates on the lattice.

Let us define $\Omega(n)$ as the lattice $SU(3)_C$ gauge transformation, being n a generic lattice site. Fermionic fields transform according to the fundamental representation of $SU(3)$:

$$\begin{aligned} \psi_i(n) &\to\ \ \psi_i'(n) = \Omega(n)_{ij}\ \psi_j(n)\ , \\ \bar{\psi}_i(n) &\to\ \ \bar{\psi}_i'(n) = \bar{\psi}_j(n)\ \Omega(n)^\dagger_{ji}\ , \end{aligned} \tag{2.84}$$

so the mass lagrangian term is automatically invariant as in the continuum case (2.14). For the discretized derivative terms in (2.80) this is not the case, so we have to define a lattice version of the covariant derivative.

This can be done introducing the field $U_\mu(n)$, which is an element of the gauge group $SU(3)$, related to the gauge field $A_\mu(n)$ through the expression:

$$U_\mu(n) = \exp\left(\mathrm{i}aA_\mu(n)\right)\ . \tag{2.85}$$

Eq. (2.85) implies for $U_\mu(n)$ the following transformation relation:

$$U_\mu(n) \to U_\mu'(n) = \Omega(n)\, U_\mu(n)\, \Omega(n+\hat{\mu})^\dagger\ , \tag{2.86}$$

which shows that $U_\mu(n)$ is an oriented field (along the $\hat{\mu}$ direction), attached to the link connecting the lattice sites n and $n+\hat{\mu}$. For this reason $U_\mu(n)$ is called *link variable*. We can also define the link variable that points in negative μ direction:

$$U_{-\mu}(n) \equiv U_\mu(n-\hat{\mu})^\dagger\ , \tag{2.87}$$

which has gauge transformation properties:

$$U_{-\mu}(n) \to U_{-\mu}'(n) = \Omega(n)\, U_{-\mu}(n)\, \Omega(n-\hat{\mu})^\dagger, \tag{2.88}$$

and so it connects the lattice site n with $n-\hat{\mu}$. With the introduction of the link variables we can generalize the free fermionic action (2.80) to the so-called *naive fermion action*:

$$S_F[\psi,\bar{\psi},U\,] = a^4 \sum_{n\in\Lambda}\ \bar{\psi}(n)\left[\sum_{\mu=1}^{4}\gamma_\mu \frac{1}{2}\left(\nabla_\mu + \nabla_\mu^*\right) + m_0\right]\psi(n)\ , \tag{2.89}$$

where we have defined ∇_μ and ∇^*_μ such that

$$\nabla_\mu \psi(n) \equiv \frac{U_\mu(n)\,\psi(n+\hat{\mu}) - \psi(n)}{a} = \frac{U_\mu(n)\,\delta_{n+\hat{\mu},m} - \delta_{n,m}}{a}\,\psi(m)\ , \tag{2.90}$$

$$\nabla^*_\mu \psi(n) \equiv \frac{\psi(n) - U_{-\mu}(n)\psi(n-\hat{\mu})}{a} = \frac{\delta_{n,m} - U_{-\mu}(n)\,\delta_{n-\hat{\mu},m}}{a}\,\psi(m)\ . \tag{2.91}$$

From Eq. (2.89) we can read the Dirac operator for the naive fermion action, which takes the form:

$$D(n,m) = \sum_{\mu=1}^{4} \gamma_\mu \frac{U_\mu(n)\,\delta_{n+\hat{\mu},m} - U_{-\mu}(n)\,\delta_{n-\hat{\mu},m}}{2a} + m_0\,\delta_{n,m}\ . \tag{2.92}$$

2.4.2 The doubling problem

Naive regularization is the minimal approach to translate the continuum action on the lattice. However it introduces in the theory new and unwanted degrees of freedom. This can be shown explicitly by computing the *quark propagator*:

$$S(n,m) = \langle \psi_\alpha(n) \bar{\psi}_\beta(m) \rangle = D^{-1}_{\alpha\beta}(n,m)\ . \tag{2.93}$$

Let us consider for simplicity the case of free fermions, which corresponds to take $U_\mu(n) \equiv \mathbb{1}$. Imposing periodic BCs on the lattice, $D(n,m)$ can be obtained in the momentum-space using the Fourier transform (FT):

$$\begin{aligned} \widetilde{D}\,(p,q) &= \frac{1}{VT} \sum_{n,m\in\Lambda} e^{-ip\cdot na}\ D(n,m)\ e^{iq\cdot ma} = \\ &= \frac{1}{VT} \sum_{n\in\Lambda} e^{-i(p-q)\cdot na}\ \left(\sum_{\mu=1}^{4} \gamma_\mu \frac{e^{+iq_\mu a} - e^{-iq_\mu a}}{2a} + m_0 \mathbb{1} \right) = \\ &= \delta(p-q) S^{-1}(p)\ , \end{aligned} \tag{2.94}$$

where $S^{-1}(p)$ is given by:

$$S^{-1}(p) = \frac{\mathrm{i}}{a} \sum_{\mu=1}^{4} \gamma_\mu \sin\left(p_\mu a\right) + m_0 \mathbb{1}\ . \tag{2.95}$$

In order to calculate $S(n,m)$ we simply need to compute the inverse of Eq. (2.95) and then invert the FT. We obtain:

$$S(n,m) = \frac{1}{VT} \sum_{p\in\widetilde{\Lambda}} \frac{-\mathrm{i} \sum_{\mu=1}^{4} \gamma_\mu \frac{\sin(p_\mu a)}{a} + m_0\,\mathbb{1}}{\sum_{\mu=1}^{4} \frac{\sin(p_\mu a)^2}{a^2} + m_0^2}\ e^{ip\cdot(n-m)a}\ . \tag{2.96}$$

The quark propagator (2.96) keeps in the continuum limit the physical pole at $p^2 = m_0^2$, which is associated with the particle mass. However on the lattice the situation is more complicated and the propagator for free fermions has additional poles. In order to

understand this problem let's consider the case of massless fermions. When p_μ is either 0 or π/a the function $\sin(p_\mu a)$ is equal 0, so if all the four-momentum components take one of these two values we find a pole. Our lattice Dirac operator has therefore 16 poles, one of which being

$$p = (0, 0, 0, 0) \ , \tag{2.97}$$

corresponding to $m_0^2 = 0$, while the remaining fifteen, the so-called *doublers*, are pure lattice artifacts.

2.4.3 Wilson fermions

In order to solve the doubling problem, Wilson proposed [32] to add to the Dirac propagator of the naive fermion action a new term, the so-called *Wilson term*, proportional to the lattice spacing a, so that it vanishes when we perform the continuum limit. In this way the action reads:

$$S_F^W[\psi, \bar{\psi}, U\,] = a^4 \sum_{n\in\Lambda} \bar{\psi}(n) \left[\sum_{\mu=1}^{4} \gamma_\mu \frac{1}{2} \left(\nabla_\mu + \nabla_\mu^* \right) - a\, \frac{r}{2} \sum_{\mu=1}^{4} \nabla_\mu \nabla_\mu^* + m_0 \right] \psi(n) \ , \tag{2.98}$$

where r is called the *Wilson parameter*. The new term modifies the Dirac operator (2.92), which becomes the *Wilson-Dirac operator*:

$$D_W(n, m) = \left(m_0 + \frac{4\, r}{a} \right) \delta_{n,m} - \frac{1}{2a} \sum_{\mu=\pm1}^{\pm4} \left(r\, \mathbb{1} - \gamma_\mu \right) U_\mu(n)\, \delta_{n+\hat{\mu},m} \ , \tag{2.99}$$

where we have defined $\gamma_{-\mu} \equiv -\gamma_\mu$.

If we return to the quark propagator (2.93), we find that it has been modified in the following way

$$S(n, m) = \frac{1}{VT} \sum_{p\,\in\tilde{\Lambda}} \frac{-\mathrm{i} \sum_{\mu=1}^{4} \gamma_\mu \frac{\sin(p_\mu a)}{a} + m(p_\mu)\, \mathbb{1}}{\sum_{\mu=1}^{4} \frac{\sin(p_\mu a)^2}{a^2} + m(p_\mu)^2}\ e^{ip\cdot(n-m)a} \ , \tag{2.100}$$

where the mass term is

$$m(p_\mu) = m + \frac{2\, r}{a} \sin\left(\frac{p_\mu\, a}{2} \right) \ . \tag{2.101}$$

Eq. (2.101) manifests the solution of the doubling problem. In fact on one hand the extra term in $m(p)$ vanishes when we consider $p = (0, 0, 0, 0)$, so the physical pole is not modified by the Wilson term. On the other hand when we consider the doublers, we have that each component $p_\mu = \pi/a$ provides an extra contribution $2r/a$ to the unphysical degrees of freedom. This means that for any finite value of r, the doublers become very heavy in the limit $a \to 0$, so that they decouple from the theory. In particular setting $r = 1$ and considering a typical lattice simulation where the inverse of the lattice spacing is around 2 GeV, the 15 doublers have a mass of at least 4 GeV, so their presence can be safely ignored in the computations.

Even if the Wilson term solves the doubling problem, it has however a bad side effect. In particular it explicitly breaks chiral simmetry, which is recovered in the massless limit only. This problem is not specific of the *Wilson action* (2.98), but comes from a general property of QCD expressed by the Nielsen-Ninomiya No-Go theorem [33], which states that it is impossible to discretize QCD in a way that is simultaneously free of the doubling problem and which reproduces the correct chiral limit. The breaking of the chiral symmetry on the lattice has important consequences. In fact although the naive fermion action is affected by $O(a^2)$ discretization errors, it introduces in the theory also errors at the order $O(a)$. Another important effect (see Sec. 2.8.2) is that the quark mass term is no longer safe against additive renormalization contributions which do not depend on the bare quark mass. It is therefore convenient to introduce a so-called *critical mass*, which can be subtracted to the bare quark mass

$$m_q = m_0 - m_{cr} \ , \tag{2.102}$$

such that the chiral point is well defined. This can be done, in the case of two degenerate quark flavors, setting m_{cr} in order to have a vanishing mass for the lightest pseudoscalar meson.

2.5 Pure gauge action

In the last Section we have studied the discretization of the fermionic part of the QCD lagrangian on the lattice and we have introduced the link fields $U_\mu(n)$ in order to preserve the gauge symmetry $SU(3)_C$. Now we want to repeat the analogous procedure for the pure gauge action (2.52).

In order to achieve this result we have to introduce a new object called *Plaquette*, which is a product of four link variables defined as

$$\begin{aligned} U_{\mu\nu}(n) &= U_\mu(n) U_\nu(n+\hat{\mu}) U_{-\mu}(n+\hat{\mu}+\hat{\nu}) U_{-\nu}(n+\hat{\nu}) = \\ &= U_\mu(n) U_\nu(n+\hat{\mu}) U_\mu(n+\hat{\nu})^\dagger U_\nu(n)^\dagger \ . \end{aligned} \tag{2.103}$$

The plaquette is the minimal non-trivial loop on the lattice and corresponds to the square defined by the points x and $x+\hat{\mu}+\hat{\nu}$. It is important because we can build an object which is gauge invariant just taking its trace. In fact under $SU(3)_C$ transformation we have:

$$\mathrm{Tr}\left[U_{\mu\nu}(n)\right] \longrightarrow \mathrm{Tr}\left[\Omega(n) U_{\mu\nu}(n) \Omega(n)^\dagger\right] = \mathrm{Tr}\left[\Omega(n)^\dagger \Omega(n) U_{\mu\nu}(n)\right] = \mathrm{Tr}\left[U_{\mu\nu}(n)\right] \ . \tag{2.104}$$

Wilson found for the gauge action the following expression:

$$S_G[U] = \frac{\beta}{3} \sum_{n\in\Lambda} \sum_{\mu<\nu} \mathrm{Re}\left\{ \mathrm{Tr}[\mathbb{1} - U_{\mu\nu}(n)] \right\}, \tag{2.105}$$

which is the combination of a sum over all plaquettes, with each plaquette counted with only one orientation, together with a sum over Lorentz indices. The factor β is the *inverse coupling* and is given by

$$\beta = \frac{6}{g^2} \ , \tag{2.106}$$

so that in the continuum limit $S_G[U]$ correctly reduces to (2.52).

To see that the *Wilson gauge action* (2.105) has the correct behavior in the limit $a \to 0$ let us consider the Baker-Campbell-Hausdorff formula:

$$\exp(A)\exp(B) = \exp\left(A + B + \frac{1}{2}[A,B] + \dots\right) , \tag{2.107}$$

through which we can express the plaquette in powers of the lattice spacing as:

$$\begin{aligned} U_{\mu\nu}(n) = \exp\Big[&+ \mathrm{i}aA_\mu(n) + \mathrm{i}aA_\nu(n+\hat{\mu}) - \frac{a^2}{2}[A_\mu(n), A_\nu(n+\hat{\mu})] + \\ &- \mathrm{i}aA_\mu(n+\hat{\nu}) - \mathrm{i}aA_\nu(n) - \frac{a^2}{2}[A_\mu(n+\hat{\nu}), A_\nu(n)] + \\ &+ \frac{a^2}{2}[A_\nu(n+\hat{\mu}), A_\mu(n+\hat{\nu})] + \frac{a^2}{2}[A_\mu(n), A_\nu(n)] + \\ &+ \frac{a^2}{2}[A_\mu(n), A_\mu(n+\hat{\nu})] + \frac{a^2}{2}[A_\nu(n+\hat{\mu}), A_\nu(n)] + \mathcal{O}(a^3)\Big] . \end{aligned} \tag{2.108}$$

Now using in the last equation the Taylor expansion for the gauge field

$$A_\nu(n+\hat{\mu}) = A_\nu(n) + a\partial_\mu A_\nu(n) + \mathcal{O}(a^3) , \tag{2.109}$$

we have, up to $\mathcal{O}(a^3)$ terms:

$$U_{\mu\nu}(n) = \exp\Big[\mathrm{i}a^2\big(\partial_\mu A_\nu(n) - \partial_\nu A_\mu(n) + \mathrm{i}[A_\mu(n), A_\nu(n)]\big)\Big] = \exp\Big(\mathrm{i}a^2 F_{\mu\nu}(n)\Big) , \tag{2.110}$$

and so we finally find that:

$$S_G[U] = \frac{\beta}{3}\sum_{n\in\Lambda}\sum_{\mu<\nu}\mathrm{Re}\,\{\,\mathrm{Tr}[\mathbb{1} - U_{\mu\nu}(n)]\,\} = \frac{a^4}{2g^2}\sum_{n\in\Lambda}\sum_{\mu,\nu}\mathrm{Tr}[F_{\mu\nu}(n)^2] + \mathcal{O}(a^2). \tag{2.111}$$

which reduces to (2.52) if we perform the continuum limit.

In summary, the complete lattice QCD action can be written as:

$$S_{LQCD}[\psi, \bar{\psi}, U\,] = S_G[U\,] + \sum_f S_F^{W\,(f)}[\psi, \bar{\psi}, U\,] , \tag{2.112}$$

where $S_G[U\,]$ corresponds to Eq. (2.105), while for fermions we take the sum over all flavors of the Wilson fermion action (2.98).

2.6 Improvement

Wilson formulation of QCD on the lattice (2.112) is built in a way that it reduces to the continuum action in the Euclidean space-time. We have seen however that while $S_G[U\,]$ matches its continuum counterpart up to terms of order $\mathcal{O}(a^2)$, the fermionic action (2.98) is characterized by discretization effects at the order $\mathcal{O}(a)$.

This means that physical observables has a dependence on the lattice spacing a, such that the expectation value of a given operator O can be written as:

$$\langle O \rangle_{\rm Latt} = \langle O \rangle_{\rm Cont} + \mathcal{O}(a) + \mathcal{O}(a^2) + \dots \ , \tag{2.113}$$

where $\langle O \rangle_{\rm Latt}$ and $\langle O \rangle_{\rm Cont}$ represent the expectation values calculated respectively on the lattice and in the continuum. Depending on the operator we consider and the lattice QCD formulation we use, lattice artifacts can affect physical quantities up to 30%.

In order to decrease discretization effects it is possible to use a procedure, first proposed by Symanzik, known as *Symanzik improvement program* [34, 35]. It consists in adding both to the action and to operators a set of counterterms aimed to cancel discretization effects up to some power of the lattice spacing. These counterterms have to be operators with dimension greater than 4 and have to vanish in the continuum limit. Furthermore they must not to modify the symmetries of the regularized action. The coefficients of these counterterms are not known a priori, but have to be calculated either in perturbation theory or with some non-perturbative approach.

Another way to reduce discretization effects without the need of additional counterterms is to build the QCD action using specific assumptions which directly lead to an *automatic improvement*. This is the case of the Wilson Twisted Mass lattice QCD action [36, 37], which allows for an automatic $\mathcal{O}(a)$ improvement at *maximal twist* [38, 39], i.e. tuning m_0 to its critical value m_{cr}. The Wtm-LQCD at maximal twist has been used in this analysis for regularize fermions on the lattice. More details are given in Sec. 2.7.

2.6.1 Symanzik improvement

For small values of the lattice spacing a, the QCD action can be described in the continuum space-time as a local effective theory given by

$$S_{\rm eff} = S_0 + a\, S_1 + a^2\, S_2 + \dots = \int d^4x \left\{ \mathcal{L}_0(x) + a\, \mathcal{L}_1(x) + a^2\, \mathcal{L}_2(x) + \dots \right\} \ , \tag{2.114}$$

where $\mathcal{L}_0(x)$ represents the QCD lagrangian in the continuum, while the generic $\mathcal{L}_k(x)$ is a linear combination of local operators of dimension $4+k$. As we anticipated above these operators must have the symmetries of the regularized theory.

Cutoff effects manifest themselves not only in the action as in Eq. (2.114), but they enter also local operators which compose the correlation functions. Let us consider a gauge invariant operator $\phi(x)$ made up of quaks and gluons. Assuming this field is not mixed with other operators by renormalization, we expect the renormalized n-point Green function

$$G(x_1, x_2, \dots, x_n) = (\mathcal{Z}_\phi)^n \, \langle \phi(x_1)\phi(x_2) \dots \phi(x_n) \rangle \ , \tag{2.115}$$

to have a well defined continuum limit if we take $x_1 \neq x_2 \neq \dots \neq x_n$. The factor $\mathcal{Z}_\phi$ in Eq. (2.115) is the renormalization constant (RC) for the field ϕ. The renormalized field $\Phi(x) \equiv \mathcal{Z}_\phi \phi(x)$ can be represented in the local effective theory as the effective operator

$$\Phi_{\rm eff}(x) = \Phi_0 + a\, \Phi_1 + a^2\, \Phi_2 + \dots \ , \tag{2.116}$$

where, as well as for Eq. (2.114), Φ_0 is the renormalized field in the continuum limit, while Φ_k stands for a combination of local operators with appropriate dimensions and symmetry properties.

Combining together Eqs. (2.114) and (2.116) for the action and fields, we can then expand the n-point Green function (2.115) in powers of the lattice spacing. In particular at the order $\mathcal{O}(a)$ we find:

$$\begin{aligned} G(x_1,\ldots,x_n) = &\langle \Phi_0(x_1)\ldots\Phi_0(x_n)\rangle_{\text{Cont}} + \\ &- a\int d^4y\,\langle \Phi_0(x_1)\ldots\Phi_0(x_n)\mathcal{L}_1(y)\rangle_{\text{Cont}} + \\ &+ a\sum_k \langle \Phi_0(x_1)\ldots\Phi_1(x_k)\ldots\Phi_0(x_n)\rangle_{\text{Cont}} + \mathcal{O}(a^2)\ , \end{aligned} \tag{2.117}$$

where $\langle\ldots\rangle_{\text{Cont}}$ indicates that the expectation values on the r.h.s. must be computed using the action S_0. In Eq. (2.117) the dependence on the lattice spacing is not only given by the explicit factors a. Cutoff effects originate also from Φ_1 and $\mathcal{L}_1$, which are, as we know, linear combinations of local operators. In particular although such local operators does not depend on a, a residual dependence on the lattice spacing lies in the coefficients of the linear combinations. Such coefficients can be calculated in perturbation theory as polynomial functions of $\ln a$ and am_0.

The prescription proposed by Symanzik is to add to the action and operators a set of counterterms needed to cancel discretization effects at a given order, which is tipically $\mathcal{O}(a^2)$ for the pure gauge action and $\mathcal{O}(a)$ for the fermionic one. In this way we can get rid of the extra terms in Eq. (2.117) and reduce contaminations of lattice artifacts to the physical quantities.

For the Wilson action (2.98) we have that, requiring the symmetries of $S_F^W[\psi,\bar\psi,U\,]$, the leading correction term $\mathcal{L}_1(x)$ can be written as the linear combination

$$\mathcal{L}_1(x) = c_1\mathcal{O}_1(x) + c_3\mathcal{O}_3(x) + c_5\mathcal{O}_5(x)\ , \tag{2.118}$$

where $\mathcal{O}_1$, $\mathcal{O}_3$ and $\mathcal{O}_5$ are the dimension-5 operators

$$\mathcal{O}_1(x) = \bar\psi(x)\sigma_{\mu\nu}F_{\mu\nu}(x)\psi(x)\ , \tag{2.119}$$

$$\mathcal{O}_3(x) = m_0\,\text{Tr}\,[F_{\mu\nu}(x)F_{\mu\nu}(x)] \tag{2.120}$$

$$\mathcal{O}_5(x) = m_0^2\,\bar\psi(x)\psi(x)\ , \tag{2.121}$$

and $\sigma_{\mu\nu} \equiv [\gamma_\mu,\gamma_\nu]/2\text{i}$. The two terms $\mathcal{O}_3(x)$ and $\mathcal{O}_5(x)$ up to some factor are already present in the original action, so they can be accounted for simply by a redefinition of the bare parameters m_0 and β. This means that the $\mathcal{O}(a)$ improvement can be obtained by adding to the Wilson action only the contribution of $\mathcal{O}_1$, which is called the *clover term*. We find:

$$S_F^{\text{Imp}}[\psi,\bar\psi,U\,] = S_F^W[\psi,\bar\psi,U\,] + c_{\text{sw}}\,a^5\sum_{n\in\Lambda}\sum_{\mu<\nu}\bar\psi(n)\frac{1}{2}\sigma_{\mu\nu}F_{\mu\nu}(n)\psi(n)\ , \tag{2.122}$$

where the constant c_{sw} is the *Sheikholeslami-Wohlert coefficient* [40], which depends on the coupling constant g and guarantees the subtraction of the $\mathcal{O}(a)$ effects from the action.

The use of $S_F^{\rm Imp}[\psi,\bar\psi,U\,]$, instead of the Wilson action (2.98), is already sufficient for the improvement of on-shell quantities such as hadron masses. However for a full $\mathcal{O}(a)$ improvement of the Green functions, and so to improve the determinations of the hadronic matrix elements, also operators O need to be improved. In this case, since currents with arbitrary quantum numbers may be constructed, there is not a general method to obtain the $O(a)$ improvement.

The Symanzik program has been extended also to the gauge sector [41, 42, 43]. At first order it requires to add to the gauge action (2.105) all possible closed paths made up of 6 links, which means to consider rectangle and chair-shaped paths besides simple plaquettes. The simplest case is the *tree-level* Symanzik improved action in which only rectangle contributions are taken into account and the gauge action reads:

$$S_G[U] = \frac{\beta}{3}\sum_{n\in\Lambda}\left\{ b_0 \sum_{\mu<\nu} \mathrm{Re}\left\{\,\mathrm{Tr}[\mathbb{1}-U_{\mu\nu}(n)]\,\right\} + b_1 \sum_{\mu,\,\nu} \mathrm{Re}\left\{\,\mathrm{Tr}[\mathbb{1}-U^{1\times 2}_{\mu\nu}(n)]\,\right\}\right\}, \quad (2.123)$$

where $U_{\mu\nu}(n)$ are the usual plaquettes, while $U^{1\times 2}_{\mu\nu}(n)$ are 1×2 loops corresponding to:

$$U^{1\times 2}_{\mu\nu}(n) = U_\mu(n)U_\mu(n+\hat\mu)U_\nu(n+2\hat\mu)U_{-\mu}(n+2\hat\mu+\hat\nu)U_{-\mu}(n+\hat\mu+\hat\nu)U_{-\nu}(n+\hat\nu)\ . \quad (2.124)$$

The coefficients b_0 and b_1 can be computed perturbatively and are fixed to the values $b_1=-1/12$ and $b_0=1-8b_1$. In our analysis we consider the *Iwasaki gluon action* [44], which corresponds to the improved gauge action (2.123) where also the chair-shaped paths are included.

2.7 Twisted Mass Action

The basic formulation of the twisted mass action describes QCD with two mass-degenerate flavors of Wilson fermions. As we anticipated in Sec. 2.6 this lattice action has been used in our simulations to regularize fermions, mainly because it has the great advantage of automatically provide the $\mathcal{O}(a)$ improvement of correlation functions.

Let us consider a field χ that in addition to Dirac and color indices carry also a flavor index with $N_f=2$ values. It represents a degenerate quark doublet that we can write as:

$$\chi = \begin{pmatrix}\chi_u\\ \chi_d\end{pmatrix}\ . \quad (2.125)$$

The twisted mass QCD action for the flavor doublet χ reads:

$$S_F^{tm}[\chi,\bar\chi,U\,] = a^4\sum_{n\in\Lambda}\ \bar\chi(n)\left[\sum_{\mu=1}^{4}\gamma_\mu\frac{1}{2}\left(\nabla_\mu+\nabla^*_\mu\right) - a\,\frac{r}{2}\sum_{\mu=1}^{4}\nabla_\mu\nabla^*_\mu + m_0 + \mathrm{i}\mu_q\gamma_5\tau^3\right]\chi(n)\ , \quad (2.126)$$

which is given by adding to the Wilson action (2.98) the mass term $\mathrm{i}\mu_q\gamma_5\tau^3$. The real parameter μ_q is the so-called *twisted mass*, while τ^3 represents the third Pauli matrix of the flavor group $SU(2)_f$.

The twisted mass term was originally introduced as it provides an useful infrared regularization [45]. In particular the Wilson-Dirac operator (2.99) is not protected against zero modes even at finite values of the quark mass. This means that, because of the dependence of D_W on the gauge field U, when we perform numerical simulations the Wilson-Dirac operator fluctuates as the the gauge field changes. Thus the occurrence of *exceptional configurations* may lead to large fluctuations in observable quantities, which correspond to unusually small eigenvalues of the Wilson-Dirac operator. On the contrary with the addition of the twisted mass term, Dirac operator becomes

$$D_{\text{twist}}(n,m) = D_W(n,m) + \mathrm{i}\mu_q\gamma_5\tau^3\,\delta_{n,m}\ , \tag{2.127}$$

and satisfy the condition

$$\det\left[D_{\text{twist}}\right] = \det\left[D_W^\dagger D_W + \mu_q^2\right] > 0\ , \tag{2.128}$$

so it is protected against zero modes for any finite value of μ_q.

Let us now consider the continumm limit of the twisted mass action (2.126):

$$S_F^{tm}[\chi,\bar\chi,U\,] \longrightarrow \int d^4x\,\bar\chi(x)\left[\gamma_\mu D_\mu + m_q + \mathrm{i}\mu_q\gamma_5\tau^3\right]\chi(x)\ , \tag{2.129}$$

where $m_q = m_0 - m_{cr}$. We can perform on the fields χ and $\bar\chi$, which are referred to as the *twisted basis*, the axial transformations:

$$\psi = e^{\,\mathrm{i}\alpha\gamma_5\tau^3/2}\,\chi\ , \tag{2.130}$$

$$\bar\psi = \bar\chi\, e^{\,\mathrm{i}\alpha\gamma_5\tau^3/2}\ , \tag{2.131}$$

which leaves invariant the form of Eq. (2.126) and produces just a mere transformation of the mass parameters m_q and μ_q:

$$\begin{aligned} M &= m_q\cos(\alpha) + \mu_q\sin(\alpha)\ ,\\ \mu_q' &= -m_q\sin(\alpha) + \mu_q\cos(\alpha)\ . \end{aligned} \tag{2.132}$$

In particular if we consider the following value for the rotation angle

$$\alpha \equiv \arctan\left(\frac{\mu_q}{m_q}\right)\ , \tag{2.133}$$

we have that $\mu_q' = 0$ and the action (2.129) reduces to the standard QCD with mass parameter M:

$$S_F^{tm}[\psi,\bar\psi,U\,] \longrightarrow \int d^4x\,\bar\psi(x)\left[\gamma_\mu D_\mu + M\right]\psi(x)\ . \tag{2.134}$$

The value (2.133) for α is called the *twist angle* and the corresponding mass M is named *polar mass*. In terms of these two parameters the mass term in Eq. (2.129) can be written as

$$m_q + \mathrm{i}\mu_q\gamma_5\tau^3 = M e^{\,\mathrm{i}\alpha\gamma_5\tau^3}\ , \tag{2.135}$$

which implies also the equations

$$\begin{cases} m_q = M\cos(\alpha) \\ \mu_q = M\sin(\alpha) \end{cases} \qquad \Longrightarrow \quad M = \sqrt{m_q^2 + \mu_q^2}\ . \tag{2.136}$$

Eq. (2.134) shows that in the continnum limit the twisted mass action is just a redefinition of the standard QCD formulation, which may be reached performing the axial rotations (2.130,2.131). For this reason the fields ψ and $\bar{\psi}$ are referred to as the *physical basis*.

However at finite lattice spacing the situation is different because the term D_W in the Wilson action breaks the chiral symmetry even if the mass parameter is set to zero. This means that the twisted mass term cannot be eliminated with a rotation of the fermionic fields and thus the Wilson action and the twisted mass action, which are equivalent when we take the continuum limit, are not equal for finite lattice spacings. In particular applying transformations (2.130,2.131) on the twisted mass action (2.126) we obtain its expression in the physical basis:

$$\begin{aligned} S_F^{tm}[\psi,\bar{\psi},U\,] = a^4 \sum_{n\in\Lambda}\ \bar{\psi}(n) \Bigg[\sum_{\mu=1}^{4} \gamma_\mu \frac{1}{2}\left(\nabla_\mu + \nabla_\mu^*\right) + \\ + \left(m_0 - a\,\frac{r}{2}\sum_{\mu=1}^{4}\nabla_\mu\nabla_\mu^* \right) e^{\,-\mathrm{i}\alpha\gamma_5\tau^3} + m_q \Bigg] \psi(n)\ , \end{aligned} \tag{2.137}$$

where in fact the Wilson term is not reabsorbed by the twist.

2.7.1 $\mathcal{O}(a)$ Improvement

In this Section we will present the fundamental property of the Wtm action of automatically provide the $\mathcal{O}(a)$ improvement of correlation functions of positive parity fields (renormalizable in a multiplicative way) when we work at maximal twist. The maximal twist corresponds to take in Eqs. (2.130,2.131) the rotation angle $\alpha = \pi/2$, which is equivalent to tune the bare quark mass m_0 to its critical value m_{cr}. Let us consider the Symanzik effective action (2.114) and the effective operator (2.116) at the first order in the lattice spacing:

$$S_{\text{eff}} = S_0 + a\,S_1 = \int d^4x\,\{\mathcal{L}_0(x) + a\,\mathcal{L}_1(x)\}\ , \tag{2.138}$$

$$\Phi_{\text{eff}}(x) = \Phi_0 + a\,\Phi_1\ . \tag{2.139}$$

In Eq. (2.139) the continuum action is given by

$$S_0 = \int d^4x\,\bar{\chi}(x)\left[\gamma_\mu D_\mu + \mathrm{i}\mu_q\gamma_5\tau^3\right]\chi(x)\ , \tag{2.140}$$

where the fact that $m_q = 0$ makes S_0 simmetric with respect to the chiral transformation

$$\mathcal{R}_5^{1,2} : \begin{cases} \chi(x) \longrightarrow \mathrm{i}\gamma_5\tau^{1,2}\,\chi(x) \\ \bar{\chi}(x) \longrightarrow \bar{\chi}(x)\,\mathrm{i}\gamma_5\tau^{1,2}\ . \end{cases} \tag{2.141}$$

As we know an operator O has a non-vanishing expectation value $\langle O \rangle_S$ only if it shares the same symmetries of the action S. In Sec. 2.6.1 we have seen that only the clover term $\mathcal{O}_1(x) = \bar{\chi}(x)\sigma_{\mu\nu}F_{\mu\nu}(x)\chi(x)$ contributes to the first order lagrangian $\mathcal{L}_1(x)$. However, this operator is odd with respect to the rotation (2.141), so if we consider $\Phi_0(x)$ to be invariant under the symmetries of the continuum action, we have

$$\langle \Phi_0(x_1) \dots \Phi_0(x_n)\mathcal{L}_1(y)\rangle_{\text{Cont}} = 0 \ , \tag{2.142}$$

and the second term in the r.h.s. of Eq. (2.117) vanishes.

In order to prove the automatic $\mathcal{O}(a)$ improvement of the twisted mass action we now have to show that also the last term in Eq. (2.117) is zero. We can use the property stating that if two operators have the same simmetries but differ by a unit in dimensionality they must have opposite chirality, which is the case of operators Φ_0 and Φ_1. Let us consider the transformation $\widetilde{\mathcal{D}} = \mathcal{D} \times [\mu_q \to -\mu_q]$, with

$$\mathcal{D} : \begin{cases} U_\mu(x) \longrightarrow U_\mu^\dagger(-x-\hat{\mu}) \\ \chi(x) \longrightarrow e^{3\mathrm{i}\pi/2}\,\chi(-x) \\ \bar{\chi}(x) \longrightarrow \bar{\chi}(-x)\,e^{3\mathrm{i}\pi/2} \end{cases} , \tag{2.143}$$

which *counts* the dimension of a given operator. The twisted mass action on the lattice is invariant under the composite symmetry $\mathcal{R}_5^{1,2} \times \widetilde{\mathcal{D}}$, and the same has to be true also for $\Phi_{\text{eff}}(x)$, otherwise we would have $\langle \Phi_{\text{eff}}(x)\rangle = 0$. In the continuum limit $\Phi_0(x)$ is equivalent to $\Phi_{\text{eff}}(x)$, so they must have the same symmetry properties: in particular being $\Phi_0(x)$ invariant under $\mathcal{R}_5^{1,2}$, it has to be invariant also with respect to $\widetilde{\mathcal{D}}$. On the other hand operator $\Phi_1(x)$ acquires a factor $e^{\mathrm{i}\pi} = -1$ when we perform the $\widetilde{\mathcal{D}}$ transformation, so it should be odd also with respect to $\mathcal{R}_5^{1,2}$ if we require for it to have a non-vanishing expectation value. In other words $\Phi_0(x)$ and $\Phi_1(x)$ have opposit chirality under $\mathcal{R}_5^{1,2}$ and so $\Phi_1(x)$ cannot enter the expansion (2.139). This means that also the last term in Eq. (2.117) is zero and thus it proofs that Wtm action, when is taken at the maximall twist, provide the automatic $\mathcal{O}(a)$ improvement of correlation functions.

The original demonstration of this property of the Wtm action has been carried out in Ref. [38]. In this work, the authors provide also a very useful method to extract energies and matrix elements which are automatically improved. They have shown that if quarks are arranged in SU(2) flavour doublets, $\mathcal{O}(a)$ discretization effects vanish in the average of correlators (see Sec. 2.10) computed with lattice actions having Wilson terms of opposite sign and a common value of the mass m_q. In this case, which is the one of the present work, automatically improved energies and matrix elements can be obtained simply by averaging the values of this quantities computed at opposites spatial momenta:

$$E_{\text{imp}}(\mathbf{k}) \equiv \frac{1}{2}\Big[E(\mathbf{k}) + E(-\mathbf{k})\Big] \ , \tag{2.144}$$

$$\langle O \rangle_{\text{imp}} \equiv \frac{1}{2}\Big[\,\langle A(E_A,\vec{p}_A)|O|B(E_B,\vec{p}_B)\rangle + P_O\,\langle A(E_A,-\vec{p}_A)|O|B(E_B,-\vec{p}_B)\rangle\,\Big] , \tag{2.145}$$

where A and B are two external states and P_O is the parity of the operator O.

2.7.2 Non-degenerate quarks

The twisted mass action (2.126), which describes QCD with two mass-degenerate flavors, can be reasonably considered to describe the u and d quarks, as their masses are very similar. When we consider the strange and charm quarks, however, the same formulation cannot be used. For this case, the twisted mass action can be extended to

$$S_F^{tm\,h}[\chi,\bar{\chi},U\,] = a^4 \sum_{n\in\Lambda}\ \bar{\chi}_h(n)\Bigg[\ \sum_{\mu=1}^{4}\gamma_\mu \frac{1}{2}\left(\nabla_\mu + \nabla_\mu^*\right) - a\,\frac{r}{2}\sum_{\mu=1}^{4}\nabla_\mu\nabla_\mu^* + \\ + m_0 + \mathrm{i}\mu_\sigma\gamma_5\tau^1 + \mathrm{i}\mu_\delta\tau^3\Bigg]\chi_h(n)\ , \tag{2.146}$$

which describes an $SU(2)$ pair of non-degenerate quarks:

$$\chi_h = \begin{pmatrix}\chi_s\\ \chi_c\end{pmatrix}\ . \tag{2.147}$$

In Eq. (2.146) h stands for *heavy*, m_0 and μ_σ are the untwisted and twisted bare masses, while μ_δ is the mass splitting along the τ^3 direction. In this case, the chiral rotation relating the heavy quark doublet in the twisted basis to the one in the physical basis is given by:

$$\psi_h = e^{\,\mathrm{i}\alpha_h\gamma_5\tau^1/2}\,\chi_h\ , \tag{2.148}$$

$$\bar{\psi}_h = \bar{\chi}_h\, e^{\,\mathrm{i}\alpha_h\gamma_5\tau^1/2}\ . \tag{2.149}$$

At maximal twist, which corresponds again to take $\alpha_h = \pi/2$, the physical renormalized strange and charm quark masses are related to the bare parameters μ_σ and μ_δ through the relations [39]:

$$m_s = \frac{1}{\mathcal{Z}_P}\left(\mu_\sigma - \frac{\mathcal{Z}_P}{\mathcal{Z}_S}\mu_\delta\right)\ , \tag{2.150}$$

$$m_c = \frac{1}{\mathcal{Z}_P}\left(\mu_\sigma + \frac{\mathcal{Z}_P}{\mathcal{Z}_S}\mu_\delta\right)\ . \tag{2.151}$$

This quantities can be obtained by tuning μ_σ and μ_δ such that the simulated K and D mensons have their physical masses. In Eqs. (2.150) and (2.151) $\mathcal{Z}_S$ and $\mathcal{Z}_P$ are the RCs of the scalar and pseudoscalar densities (see. Sec. 2.8.1).

Simulations used in this work are characterized by 4 dynamical quarks in the see: up and down quarks have been simulated as a degenerate doublet through the Wilson twisted mass action (2.126), while for the strange and charm quarks the non-degenerate case (2.146) has been considered. This setup is referred to as $N_f = 2+1+1$.

2.8 RI/MOM

In QFT divergent quantities like quark masses and coupling constants need to be renormalized in order to get finite determinations of physical observables. In Sec. 2.2.3 we

have shown how discretization of the space-time provides an UV cutoff for LQCD. This allows us to introduce renormalization constants (RCs) which reabsorb the divergences in the limit $a \to 0$. In this way we can relate determinations obtained on the lattice with renormalized quantities in the continuum limit.

The renormalization of a theory can be performed using either perturbative or non-perturbative approaches. Among the various perturbative methods the most popular is the modified Minimal Subtraction scheme ($\overline{\text{MS}}$), which is naturally defined within dimensional regularization at a given renormalization scale μ. $\overline{\text{MS}}$ can be implemented perturbatively on the lattice, although lattice perturbation theory is technically more difficult than in the continuum. For this reason non-perturbative renormalization schemes are often preferred to perturbative ones.

In this Section we present some details of the RI/MOM scheme (Regularization Independent at subtracted MOMentum) [46], which is a non-perturbative method where the renormalization conditions are imposed directly on Green functions in a fixed gauge and in the chiral limit. Renormalization conditions being imposed in the chiral limit imply RCs to be independent on fermion masses, so RI/MOM is defined a *mass-independent scheme*. The renormalization scale μ has to be chosen properly within a window

$$\Lambda_{QCD} \ll \mu \ll \frac{1}{a} \ , \tag{2.152}$$

where $\Lambda_{QCD} \ll \mu$ allows us to perform the matching between RI/MOM and other commonly adopted schemes such as the $\overline{\text{MS}}$, while the condition $\mu \ll \frac{1}{a}$ guarantees $\mathcal{O}(a)$ discretization effects to be small and under control.

2.8.1 Renormalization of bilinear operators

Let us consider a bare bilinear operator on the lattice:[6]

$$O_\Gamma(n) = \bar{\psi}^{(f)}(n)\Gamma\psi^{(f')}(n) \ , \tag{2.153}$$

and its expectation value $\langle p|O_\Gamma(n)|p\rangle$ between off-shell quark states $|p\rangle$, i.e. at zero momentum transfer. To fix the gauge, let us rotate the fields in the Landau gauge. Γ stands for a combination of gamma matrices which depends on the Lorentz structure of the field O_Γ: it can vary between different types which are summarized in Tab. 2.8.1.

The renormalized operator $\widehat{O}_\Gamma$ is built in such a way that it keeps finite even in the continuum limit $a \to 0$ and is related to the bare one through the equation:

$$\langle p|\widehat{O}_\Gamma|p\rangle\Big|_{p^2=\mu^2} = \mathcal{Z}_\Gamma(\mu)\,\langle p|O_\Gamma|p\rangle\Big|_{p^2=\mu^2} \ , \tag{2.154}$$

where $\mathcal{Z}_\Gamma$ is the RC of the field O_Γ and μ satisfies Eq. (2.152). In RI-MOM scheme renormalization conditions are applied on the amputated Green function in momentum space:

$$\Lambda_\Gamma(p) = S_f^{-1}(p)\,G_\Gamma(p)\,S_{f'}^{-1}(p) \ , \tag{2.155}$$

[6]Provided that $f \neq f'$, in the chiral limit the following discussion do not depend on the flavor of the quarks in the bilinear operator.

O_Γ Lorentz structure	Γ
Scalar (S)	$\mathbb{1}$
Pseudoscalar (P)	γ_5
Vector (V)	γ_μ
Axial (A)	$\gamma_5\gamma_\mu$
Tensor (T)	$\sigma_{\mu\nu}$

Table 2.1: Lorentz symmetry properties of the field O_Γ corresponding to different structures of the Γ matrix.

where $S_f(p)$ is the Landau gauge quark propagator

$$S_f(p) = \frac{1}{V}\sum_n e^{-iap\cdot n}\,\langle \psi^{(f)}(n)\bar{\psi}^{(f)}(0)\rangle \ , \tag{2.156}$$

while $G_\Gamma(p)$ is the non-amputated Green function in momentum space built from the operator $O_\Gamma(0)$ with the insertion of two external quark fields:

$$\begin{aligned} G_\Gamma(p) &= \frac{1}{V}\sum_{n,m} e^{-iap\cdot(n-m)}\,\langle \psi^{(f)}(n) O_\Gamma(0)\bar{\psi}^{(f')}(m)\rangle = \\ &= \frac{1}{V}\sum_{n,m} e^{-iap\cdot(n-m)}\,\langle \psi^{(f)}(n)\bar{\psi}^{(f)}(0)\,\Gamma\,\psi^{(f')}(0)\bar{\psi}^{(f')}(m)\rangle \ . \end{aligned} \tag{2.157}$$

In order to impose the renormalization conditions it is convenient to take the trace of the amputated Green function in Dirac and color indices, obtaining

$$\Omega_\Gamma(p) = \frac{1}{12}\,\mathrm{Tr}\left[P_\Gamma\,\Lambda_\Gamma(p)\right] \ , \tag{2.158}$$

where $1/12$ is the normalization factor of the trace (color$\times$spin $= 12$), while P_Γ is a projector chosen in such a way that $\Omega_\Gamma(p) = 1$ at tree-level: corresponding to $\Gamma = \{\mathbb{1}, \gamma_5, \gamma_\mu, \gamma_\mu\gamma_5\}$ we have $P_\Gamma = \left\{\mathbb{1}, \gamma_5, \frac{1}{4}\gamma_\mu, -\frac{1}{4}\gamma_\mu\gamma_5\right\}$.

The RI-MOM scheme consists in imposing the renormalization condition on the projected amputated Green function in momentum space:

$$\widehat{\Omega}_\Gamma(p)\big|_{p^2=\mu^2} = \frac{\mathcal{Z}_\Gamma(\mu)}{\mathcal{Z}_\psi(\mu)}\,\Omega_\Gamma(p)\bigg|_{p^2=\mu^2} = 1 \ , \tag{2.159}$$

where $\sqrt{\mathcal{Z}_\psi}$ is the RC of the quark field, while the RI-MOM definition of $\mathcal{Z}_\psi$ is:

$$\mathcal{Z}_\psi(\mu) = -\frac{\mathrm{i}}{12}\,\mathrm{Tr}\left[\frac{\partial S_f^{-1}(p)}{\partial \not{p}}\right]\bigg|_{p^2=\mu^2} \ . \tag{2.160}$$

So the determination of RCs for quark bilinear operators requires the calculation of the quark propagator $S(p)$ and the amputated Green function $\Lambda_\Gamma(p)$. Moreover, being the RI/MOM a mass-independent scheme, dedicated lattice simulations with degenerate sea quarks $N_f = 4$ are required to perform the renormalization procedure. Progressively smaller dynamical quark mass values have to be used for a controlled extrapolation of massive RC to the chiral limit.

2.8.2 Renormalization of quark masses

The mass term in the RI/MOM scheme renormalizes just like bilinears. At maximal twist we have that the twisted mass μ_q gets only multiplicative renormalization contributions and the renormalized quark mass m_q is given by:

$$m_q = \mathcal{Z}_m \, \mu_q \ . \tag{2.161}$$

The Ward identity for the vector current implies that the product of the twisted mass μ_q and the pseudoscalar density P is renormalization group invariant. This means that we have an equality between the RC of the twisted mass and the inverse of the pseudoscalar density which reads:

$$\mathcal{Z}_m = \frac{1}{\mathcal{Z}_P} \ . \tag{2.162}$$

2.9 Numerical Simulations

In Sec. 2.2 we have seen how Green functions can be expressed as path integrals over classical fields. In a similar way, from Eq. (2.26) it follows that the expectation value of a physical observable $O\big(\psi, \bar{\psi}, A\big)$ in QCD can obtained as

$$\langle O \rangle = \frac{\int \mathcal{D}[\psi] \, \mathcal{D}[\bar{\psi}] \, \mathcal{D}[A] \, O\big(\psi, \bar{\psi}, A\big) \ e^{-S_{QCD}\left[\psi, \bar{\psi}, A\right]}}{Z_{QCD}} \ , \tag{2.163}$$

where the contribution of fermionic fields is solved exactly in terms of the fermion determinant, and the expectation value depends on gauge fields only. On the lattice, the path-integral (2.163) becomes finite dimensional and its expression is given by

$$\langle O \rangle = \frac{\int \mathcal{D}[U] \, O\big(\psi, \bar{\psi}, U\big) \ e^{-S_{\text{eff}}[U]}}{\int \mathcal{D}[U] e^{-S_{\text{eff}}[U]}} \ , \tag{2.164}$$

where

$$S_{\text{eff}}[U] = S_G[U] - \ \text{Tr} \left[\log \left(\sum_{f=1}^{N_f} M_f[U] \right) \right] \ . \tag{2.165}$$

The expectation value (2.164) involves a huge number of integrations even for small lattice grids, so it cannot be solved analytically except for very small lattices. The evaluation of physical quantities have to be performed numerically by the use of Monte Carlo techniques. The main idea is that the so-called *Boltzmann factor* $e^{-S_{\text{eff}}[U]}$ is very small for most of the gauge configurations U and only a small fraction of them, which minimize the action, give relevant contributions to the path-integral. Exploiting this property, LQCD gauge configurations are generated using the *importance sampling* procedure, i.e. according to a probability distribution given by the Boltzmann factor $P[U] = e^{-S_{\text{eff}}[U]}$ and using a Markov chain where each configuration U_i is obtained from the preceding one U_{i-1}.

Once a set of N_{cfg} configuration has been produced, the expectation value $\langle O \rangle$ can be approximated by the sample average

$$\langle O \rangle \simeq \widehat{O} = \frac{1}{N} \sum_{i=1}^{N} O(U_i) \ , \tag{2.166}$$

where $O(U_i)$ is an estimate of the observable O corresponding to configuration U_i and the deviation from the perfect equivalence is of the order $\mathcal{O}(1/\sqrt{N})$.

2.9.1 Statistical errors

The importance sampling procedure allows us to evaluate physical observables $\langle O \rangle$ through the sample average $\widehat{O}$. Now suppose we want not the average $\langle O \rangle$ itself, but some function of it, i.e. $f(\langle O \rangle)$. A good estimator for this quantity is given by $f(\widehat{O})$, which means that the equivalence $f(\langle O \rangle) = f(\widehat{O})$ holds for $N \to \infty$, being N the number of random configurations used to estimate $\langle O \rangle$. Clearly, besides the mean value, we want to provide also the uncertainty associated to $f(\langle O \rangle)$. The usual error propagation is often unreliable or impossible to determine. However, two methods useful to correctly evaluate statistical errors are the Jackknife and the Bootstrap [47], which have been used in this analysis and are described below.

Jackknife Method

Let us consider a sample of N_{cfg} uncorrelated gauge configurations. We can divide this set in $N_c = N_{cfg}/n_c$ *clusters*, each one being composed by n_c configurations. For each subset we can compute the sample average

$$\overline{O}_i = \frac{1}{n_c} \sum_{k=1}^{n_c} (O_k)_i \ , \qquad i = 1, 2, \ldots, N_c \ , \tag{2.167}$$

where $(O_k)_i$ corresponds to the k-th configuration of the i-th cluster. The N_c *jackknife averages* O_s^J are defined as

$$O_s^J = \frac{1}{N_c} \sum_{i=1, i \neq s}^{N_c - 1} \overline{O}_i \ , \tag{2.168}$$

where all the $\overline{O}_i$-values *except* $\overline{O}_s$ are considered in the average. For each O_s^J we can define the jackknife determination of the function $f(\langle O \rangle)$ as

$$f_s^J \equiv f(O_s^J) \ . \tag{2.169}$$

The *jackknife estimate* of $f(\langle O \rangle)$ is then given by

$$f(\langle O \rangle) \simeq \overline{f^J} = \frac{1}{N_c} \sum_{s=1}^{N_c} f_s^J \ , \tag{2.170}$$

whose statistical uncertainty can be proved to be

$$\sigma_J = \sqrt{N_c - 1}\ \sigma_{f^J}\ , \quad \text{where} \quad \sigma^2_{f^J} \equiv \overline{\left(f^J\right)^2} - \left(\overline{f^J}\right)^2 . \tag{2.171}$$

The factor $\sqrt{N_c - 1}$ takes into account the correlations between the different f^J_s. The presence of such correlations is clear because they have been extracted from the same set of configurations, excluding just one cluster at a time.

Bootstrap Method

The bootstrap method, like the jackknife, consists in a resampling of the N_{cfg} uncorrelated configurations. Let us consider two quantities $A(\langle O\rangle)$ and $B(\langle O\rangle)$ obtained from independent simulations. We want to combine them in order to find a new observable $C(\langle O\rangle)$ by a fitting procedure. We can build for A and B the jackknife averages A^J_s and B^J_s, with $s = 1, \dots N_c$, as in Eq. (2.168). These two sets of values are independent of each other because the determinations of $A(\langle O\rangle)$ and $B(\langle O\rangle)$ come from different simulations.

The bootstrap method consists of generating a random set of N_{boot} couples $\{A^J_s, B^J_{s'}\}$ and to perform a determination of $C(\langle O\rangle)$ corresponding to each of them. In this way we get N_{boot} values C^B_k, one for each couple of jackknife averages. The *bootstrap estimate* of $C(\langle O\rangle)$ is then given by

$$C(\langle O\rangle) \simeq \overline{C^B} = \frac{1}{N_{boot}} \sum_{k=1}^{N_{boot}} C^B_k\ , \tag{2.172}$$

where the uncertainty is

$$\sigma_B = \sqrt{(N_c - 1)\left|\overline{\left(C^B\right)^2} - \left(\overline{C^B}\right)^2\right|}\ . \tag{2.173}$$

In our analysis we picked $N_{boot} = 100$.

2.9.2 Systematic errors

Besides statistical uncertainties, LQCD results are characterized by systematic errors. Any quantity measured on the lattice depends on the lattice spacing a and the lattice size L, on quark masses, on the number of dynamical quark flavors N_f and on the method used to determine RCs. We list below the most significant systematic errors in current simulations. Details of this analysis are summarized in Tab. 3.1.

Input parameters: Any observable on the lattice depends on the value of free parameters - quark masses and lattice spacing - and on RCs. The determination of these quantities must be performed in order to extract physical results by further analysis. The way this determination is carried out, and the uncertainty on these parameters, induces a systematic error in the final results.

Discretization effects: Lattice determinations are characterized by discretization effects which depend on the lattice spacing a. This means that, in order to find physical quantities, we have to perform the continuum limit $a \to 0$. This is done by computing observables for different values of the lattice spacing, and then fitting them with a polynimial expression in a. Once the a dependence has been studied by the fitting procedure, the continuum limit is performed numerically by setting $a = 0$. Lattice spacings are typically chosen as small as possible in order to minimize the systematic effects of this procedure.

Lorentz symmetry breaking
A primary consequence of the discretization of the space-time is the breaking of the Lorentz symmetry. In fact the lattice is invariant only under discrete rotations by multiple of 90° in each direction of the Euclidean space-time. Therefore, LQCD observables may depend on hypercubic invariants. Although for most of hadronic quantities this effect is small and can be neglected, in this analysis we have observed and studied for the first time a sizable contribution of the Lorentz symmetry breaking due to lattice hypercubic effects in the behavior of the $D \to \pi(K)$ form factors. Details on the treatment and subtraction of such lattice artifacts are presented in Sec. 3.4.

Finite size effects (FSE): Besides discretization effects, also the use of finite lattice volumes generates artifacts which contaminate physical quantities. In many cases, as for observables computed in this analysis, FSE are exponentially suppressed by the quantity $M_\pi L$, where M_π is the pion-mass and L is the side of the simulated lattice. Clearly, values of $M_\pi L$ as big as possible ($M_\pi L \gg 1$) have to be required to reduce contributions due to the finite volume. We studied the amount of FSE by performing two simulations which share the same pion-mass and lattice spacing a, but corresponding to different volumes.

Chiral extrapolation: At the physical u- and d-quark masses the condition $M_\pi L \gg 1$ is computationally very expensive. For this reason, one usually generates observables for larger values of $m_{u/d}$ and then extrapolates to the physical point. For example, in a typical numerical simulation the value of the pion-mass ranges from 200 up to 500 MeV. Only recently lattice collaborations have reached the goal of simulating directly at the physical point.

Excited states: Hadronic quantities in LQCD are extracted from correlation functions, which are vacuum expectation values of the T-product of operators in Euclidean space-time. Such objects are characterized by a sum over al lot of states, each one suppressed by an exponential factor proportional to its energy. Physical quantities are then extracted by isolating the ground state, studying the large time distance behavior of correlators. However, a residual contamination of some excited states can induce a systematic error in the final result. More details are given in Sec. 2.10.

2.10 Correlation functions

Lattice QCD allows for a numerical calculation of euclidean correlation functions. The basic idea is to extract useful informations from the behavior of these correlators at large values of time. In this Section we introduce the standard procedure used for the calculation of meson masses, decay constants and matrix elements from 2- and 3- point correlators, which have been analyzed in this work in order to determine the form factors of the $D \to \pi(K)$ semileptonic decays.

2.10.1 Two-point correlators

The Euclidean two-point correlation function, for two generic operators O_1 and O_2, is given by

$$C_2(x) = \langle O_1(x) O_2^\dagger(0) \rangle \ , \tag{2.174}$$

where we recall that the symbol $\langle \ldots \rangle$, introduced in Eq. (2.77), represents the vacuum expectation value of the T-product in the Euclidean space-time. This quantity is the probability amplitude for the propagation of a state created by operator O_2, the *source*, in the space-time point $x = 0$ and annihilated by O_1, the *sink*, in the space-time point $x = (t, \vec{x})$. Choosing $t > 0$ and performing the Fourier transform with respect to spatial coordinates we obtain

$$C_2(\vec{p}, t) = \frac{1}{L^3} \sum_{\vec{x}} \langle 0 | \, O_1(\vec{x}, t) O_2^\dagger(0) \, | 0 \rangle \, e^{i\vec{p}\cdot\vec{x}} \ , \tag{2.175}$$

where we have a sum instead of an integral because of space-time discretization. If we insert between O_1 and O_2 the completeness relation

$$\mathbb{1} = \sum_n \frac{1}{2E_n} \, | E_n, \vec{p}_n \rangle \, \langle E_n, \vec{p}_n | \ , \tag{2.176}$$

where we consider covariantly normalized energy eigenstates with $E_0 < E_1 < E_2 < \ldots$, we find:

$$\begin{aligned} C_2(\vec{p}, t) &= \frac{1}{L^3} \sum_{\vec{x}} \sum_n \frac{1}{2E_n} \langle 0 | \, O_1(\vec{x}, t) \, | E_n, \vec{p}_n \rangle \, \langle E_n, \vec{p}_n | \, O_2^\dagger(0) \, | 0 \rangle \, e^{i\vec{p}\cdot\vec{m}a} \ = \\ &= \frac{1}{L^3} \sum_{\vec{x}} \sum_n \frac{1}{2E_n} \langle 0 | \, e^{Ht + i\vec{P}\cdot\vec{x}} O_1(0) e^{-Ht - i\vec{P}\cdot\vec{x}} \, | E_n, \vec{p}_n \rangle \, \langle E_n, \vec{p}_n | \, O_2^\dagger(0) \, | 0 \rangle \, e^{i\vec{p}\cdot\vec{x}} \ = \\ &= \frac{1}{L^3} \sum_{\vec{x}} \sum_n \frac{1}{2E_n} \langle 0 | \, O_1(0) \, | E_n, \vec{p}_n \rangle \, \langle E_n, \vec{p}_n | \, O_2^\dagger(0) \, | 0 \rangle \, e^{-E_n t - i(\vec{p_n} - \vec{p})\cdot\vec{x}} \ = \\ &= \sum_n \frac{1}{2E_n} \langle 0 | \, O_1(0) \, | E_n, \vec{p}_n \rangle \, \langle E_n, \vec{p}_n | \, O_2^\dagger(0) \, | 0 \rangle \, e^{-E_n t} \ , \end{aligned} \tag{2.177}$$

where we used the relation

$$O(x) = e^{Ht + i\vec{P}\cdot\vec{x}} O(0) e^{-Ht - i\vec{P}\cdot\vec{x}} \tag{2.178}$$

in order to translate operator O_1 from the space-time point x to the origin, and the lattice version of the 3-dimensional Dirac delta

$$\frac{1}{L^3}\sum_{\vec{x}} e^{-i(\vec{p}_n-\vec{p})\cdot\vec{x}} = \delta^3_{\vec{p}_n,\vec{p}}\,. \tag{2.179}$$

Eq. (2.177) shows that Euclidean 2-point correlation functions can be written as a sum over a lot intermediate states, each one weighted by the exponential factor $e^{-E_n t}$. For large values of time, this means that only the ground state contributes[7], so we obtain

$$C_2(\vec{p},t) \underset{t\gg a}{\longrightarrow} \frac{\langle 0|\, O_1(0)\,|E_0,\vec{p}_0\rangle\,\langle E_0,\vec{p}_0|\, O_2^\dagger(0)\,|0\rangle}{2E_0}\, e^{-E_0 t} \equiv \frac{Z_1 Z_2^\dagger}{2E_0}\, e^{-E_0 t}\ , \tag{2.180}$$

where we have defined

$$Z_i \equiv \langle 0|\, O_i(0)\,|E_0,\vec{p}_0\rangle\ . \tag{2.181}$$

On the lattice, Eq. (2.180) must be modified in order to include contributions from forward and backward propagation. Calling η the temporal parity of the 2-point correlator with respect to the transformation $t \to T-t$, we have

$$C_2(\vec{p},t) \underset{t\gg a}{\longrightarrow} \frac{Z_1 Z_2^\dagger}{2E_0}\left(e^{-E_0 t} + \eta\, e^{-E_0(T-t)}\right)\ , \tag{2.182}$$

which becomes:

$$C_2(\vec{p},t) \underset{t\gg a}{\longrightarrow} \frac{Z_O^2}{E_0}\cosh\left[\left(t-\frac{T}{2}\right)E_0\right]\ , \tag{2.183}$$

in the case $O_1 = O_2 \equiv O$ and $\eta = 1$.

Considering for O an interpolator of the form (2.153), with quantum numbers appropriate to create a meson from the vacuum, Eq. (2.183) can be used to determine the energy of the ground state and the decay constant, which is embedded in the matrix element Z_O, of the corresponding particle. As for E_0, a different determination can be performed using the so-called *effective mass*:

$$aM_{eff}(t) = \log\left[\frac{C_2(\vec{p},t)}{C_2(\vec{p},t+1)}\right]\ , \tag{2.184}$$

which reduces to the ground state energy (in lattice units) for large values of time:

$$aM_{eff}(t) \underset{t\gg a}{\longrightarrow} aE_0\,. \tag{2.185}$$

The name effective mass for M_{eff} is clearly related to the fact that for $\vec{p}=0$ the energy E_0 is nothing but the particle mass. An example of the dependence of the effective mass as a function of time is shown in Fig. (2.1) for the case of a light-light PS meson.

It is clear that the energy E_0 can determined through a constant fit of $M_{eff}(t)$ in the time region $[t_{min}, t_{max}]$ where data show the plateau. The condition $t \gg a$ in Eq. (2.184) means that t_{min} has to be chosen high enough for the contribution of excited state to be sufficiently suppressed. On the other hand, t_{max} is limited by the fact that the signals we want to isolate are exponentially suppressed by the factor $e^{E_0 t}$, which leads to noisy data for large values of time. Anyhow, the lattice time extension T constitutes an upper bound for t_{max}.

[7]States with energies $E_n > E_0$ are commonly called *excited states*.

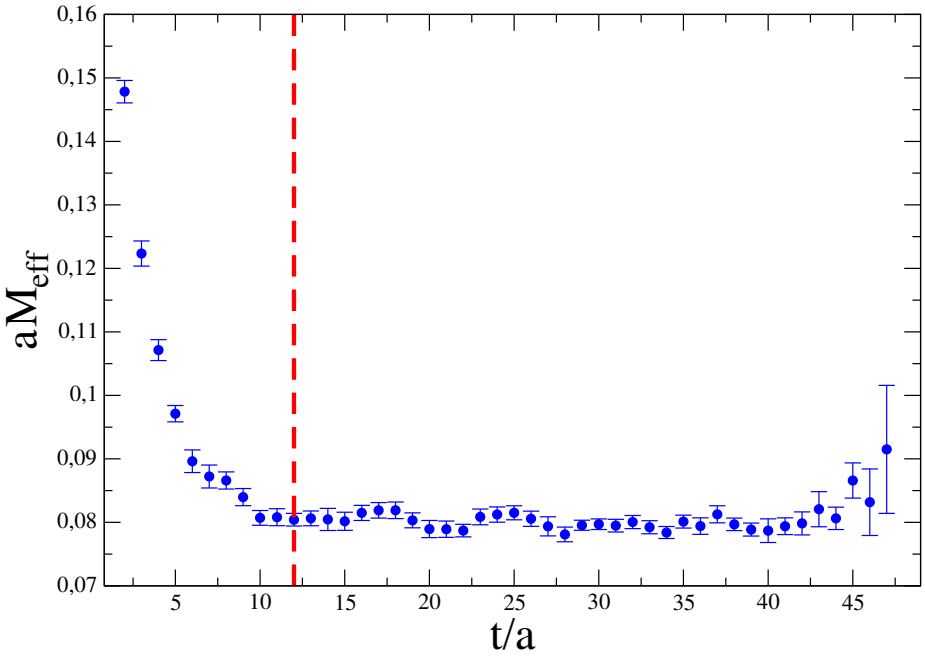

Figure 2.2: Example of a typical behavior of the effective mass (in lattice units) as a function of time. For high values of t/a a plateau, corresponding to the energy of the ground state, is clearly visible. The dashed red line indicates the point from which the contributions of excited states can be neglected.

2.10.2 Three-point correlators

Euclidean 3-point correlation functions can be used to extract matrix elements of currents connecting two external states. A 3-point correlator in the momentum space is given by

$$C_\Gamma^{AB}(t,t',\vec{p}_A,\vec{p}_B) = \frac{1}{L^3}\sum_{\vec{x},\vec{x}\,'} \langle 0|\, O_B(\vec{x}\,',t')\, O_\Gamma(\vec{x},t)\, O_A^\dagger(0)\,|0\rangle\, e^{i\vec{p}\cdot\vec{x}}\, e^{i\vec{p}\,'\cdot\vec{x}\,'}\,, \tag{2.186}$$

where O_A and O_B are interpolators which create the hadrons A and B from the vacuum, while O_Γ is an operator producing the transition between these two particles. As well as for the case of the 2-point correlator we can insert the completeness relation in Eq. (2.186). This time we have three operators, so the completeness relation can be used twice:

$$\begin{aligned} C_\Gamma^{AB}(t,t',\vec{p}_A,\vec{p}_B) =& \frac{1}{(L^3)^2}\sum_{\vec{x},\vec{x}\,'}\sum_{n,m}\frac{1}{(2E_n)(2E_m)}\,\langle 0|\, O_B(\vec{x}\,',t')\,|E_m,\vec{p}_m\rangle \times \\ & \times \langle E_m,\vec{p}_m|\, O_\Gamma(\vec{x},t)\,|E_n,\vec{p}_n\rangle\,\langle E_n,\vec{p}_n|\, O_A^\dagger(0)\,|0\rangle\, e^{i\vec{p}\cdot\vec{x}}\, e^{i\vec{p}\,'\cdot\vec{x}\,'}\,. \end{aligned} \tag{2.187}$$

The last expression can be further simplified through the same manipulations used for the 2-point function. Operators can be shifted to the origin according to Eq. (2.178), while the lattice version of the Dirac delta (2.179) can be used to eliminate the spatial volume

integration in $\vec{x}$ and $\vec{x}\,'$. We have

$$\begin{aligned} C_\Gamma^{AB}(t,t',\vec{p}_A,\vec{p}_B) = &\sum_{n,m} \frac{1}{4E_nE_m} \langle 0|\, O_B(0)\, |E_m,\vec{p}_m\rangle \times \\ &\times \langle E_m,\vec{p}_m|\, O_\Gamma(0)\, |E_n,\vec{p}_n\rangle \langle E_n,\vec{p}_n|\, O_A^\dagger(0)\, |0\rangle\, e^{-E_n t}\, e^{-E_m(t'-t)}\ , \end{aligned} \tag{2.188}$$

where we find again a sum over many intermediate states suppressed by negative exponential factors. In this case, in order to isolate the ground state we have to require not only $t \gg a$, but also the condition $t' - t \gg a$ to be fulfilled. For values of time satisfying this relations, the 3-point correlation function becomes

$$C_\Gamma^{AB}(t,t',\vec{p}_A,\vec{p}_B) \xrightarrow[t\gg a\ (t'-t)\gg a]{} \sum_{n,m} \frac{Z_A^\dagger Z_B}{4E_nE_m} \langle B(p_B)|\, O_\Gamma(0)\, |A(p_A)\rangle\, e^{-E_A t}\, e^{-E_B(t'-t)}\ , \tag{2.189}$$

which depends on the matrix element of the current $O_\Gamma(0)$. This quantity can be obtained in different ways. The simplest one is to compute the factors Z_A and Z_B from the 2-point functions and then extract $\langle B(p_B)|\, O_\Gamma(0)\, |A(p_A)\rangle$ through Eq. (2.189). A different method is to construct proper double ratios of 3-point correlators, which approach the wanted current matrix element for large values of time. This second method is the one used in this analysis. More details are shown in the next Chapter.

2.11 Twisted boundary conditions

In Sec. 2.2.3 we have seen how the finite volume of the lattice poses the problem of fixing some condition to treat the fields at the boundaries. In the spatial directions, labeled by $i = 1, 2, 3$, the tipical choice is given by periodic BCs, i.e. fermionic fields satisfies

$$\psi^f(n_i + N) = \psi^f(n_i)\,, \tag{2.190}$$

which is just a rewrite of Eq. (2.57), where $N = L/a$. Such conditions imply the following constraint on the lattice fields momenta:

$$p_\mu = \frac{2\pi k_\mu}{L} \ \text{ with } \ k_\mu = 0, 1, 2, \ldots, N-1\,, \tag{2.191}$$

which means that for tipical values of the lattice spacing $a^{-1} \approx 2\,\text{GeV}$ and a lattice size $L/a = 24$, the minumum achievable momentum is $\approx 0.5\,\text{GeV}$. This is very restrictive, expecially for physical observables that need to be studied as functions of p. In fact we are often interested in simulating particles with momenta much smaller than that and the possibility of arbitrary choice their values is very important.

The solution of this problem lies in the observation that there is no reason for having single valued fields. The only quantities that must be single valued are physical observables, and thus the action of our theory. This means that we can define a quark field $\widetilde{\psi}$ which satisfy spatial boundary conditions of the form

$$\widetilde{\psi}^f(n_i + N) = U_i^f \widetilde{\psi}^f(n_i)\,, \tag{2.192}$$

where U_i is a global simmetry of the action. The most generic U_i is the diagonal transformation in the flavor space

$$U_i^f = \exp\left\{2\pi i\theta_i^f\right\}\,, \tag{2.193}$$

which corresponds to the choice of the so-called *twisted boundary conditions*:

$$\widetilde{\psi}^f(n_i+N) = \exp\left\{2\pi i\theta_i^f\right\}\widetilde{\psi}^f(n_i)\,. \tag{2.194}$$

If we now consider Eq. (2.194) in the momentum space, by means of the Fourier transform of the fields, we find:

$$\begin{aligned}&\frac{1}{L}\sum_{p_i}\widetilde{\psi}^f(\vec{p},t)\exp\{iap_in_i\}\exp\{iap_iN\} = \frac{1}{L}\sum_{p_i}\widetilde{\psi}^f(\vec{p},t)\exp\{iap_in_i\}\exp\left\{2\pi i\theta_i^f\right\} \implies\\ &\implies \exp\left[i\left(p_i-\frac{2\pi\theta_i^f}{L}\right)L\right] = 1 \implies p_i = \frac{2\pi}{L}(k_i+\theta_i^f) \text{ with } k_i\in\mathbb{Z}\,,\end{aligned} \tag{2.195}$$

so that the spatial momenta are still quantized as for periodic boundary conditions, but now they are shifted by an arbitrary amount $2\pi\theta_i^f/L$. This continuous dependence on the parameter θ_i^f is very useful for phenomenological applications as it allows us to set the wanted values of the quark momenta.

Twisted BCs can be implemented on the lattice by defining a new quark field [22, 23]:

$$\psi_\theta^f(n) = \exp\left\{\frac{2\pi i\vec{\theta}^f\cdot\vec{x}}{L}\right\}\widetilde{\psi}^f(n)\,, \tag{2.196}$$

where $\widetilde{\psi}^f$ satisfies Eq. (2.194). The resulting field ψ_θ^f fulfills periodic BCs but obeys a modified Dirac equation given by

$$S_F\left[\psi,\bar{\psi}\,\right] = a^4\sum_f\sum_{n,m\in\Lambda}\bar{\psi}_\theta^f(n)\,D_\theta(n,m)\,\psi_\theta^f(m)\,, \tag{2.197}$$

where the new Dirac operator is related to the usual one by simply rephasing the gauge links by the four-vector $\theta^f = (\vec{\theta}^f, 0)$:

$$U_\mu(n)\to U_\mu^\theta(n) = \exp\left\{\frac{2\pi ia\theta_\mu}{L}\right\}U_\mu(n)\,. \tag{2.198}$$

We remark that the plaquette $P_{\mu\nu}(x)$ is left invariant by the rephasing of the gauge links.

2.12 Smeared interpolating fields

The 2- and 3- point correlation functions, as we have seen in Sec. 2.10, are given by a sum over many intermediate states $|E_n,\vec{p}_n\rangle$, each one suppressed by a factor e^{-E_nt}. We are interested in isolating only the ground-state contribution in order to extract physical quantities, and to do that we have to fit correlators at large values of time. When we

face with mesons containing heavy quarks we find that the time interval $[t_{min}, t_{max}]$, in which only the ground-state contributes, is shorter compared to that of light-light and light-strange mesons. This has a clear physical reason: on one hand the more the particles are heavy, the smaller the gap between the lowest energy state and the first excited state is; on the other hand if the energy of the ground-state is high, its contribution is strongly suppressed for values of time which are lower with respect to the case of light mesons. For these reasons, if the signal to noise ratio is too low or if there is too much excited states contamination, the evaluation of the ground state matrix element might be impossible.

In building the correlators, we consider interpolators $O_P^\dagger$ which create from the vacuum the particle P we are interested in, together with all excited states corresponding to the same quantum numbers:

$$O_P^\dagger |0\rangle = |P(\vec{p}_P)\rangle + |E_1, \vec{p}_1\rangle + |E_2, \vec{p}_2\rangle \dots \ . \tag{2.199}$$

Although any operator with the correct quantum numbers contributes to the physical state, some may be more suitable then others. The general idea is to consider *smeared* quark fields by constructing interpolators which couple better with the state $|P(\vec{p}_P)\rangle$ with respect to excited states. The overlap is represented by the matrix element of Eq. (2.181), so what is required is that

$$Z_P \gg Z_P^n \ , \quad \text{with} \quad Z_P^n = \langle 0| O_P(0) |E_n, \vec{p}_n\rangle \ \ (n = 1, 2, \dots) \ . \tag{2.200}$$

We know there are infinite operators useful for creating the particle we are interested in. Any average of these operators would be suitable for our purpose, thus the basic idea is to construct an advantageous average between the possible interpolating operators which has the best overlap with the state $|P(\vec{p}_P)\rangle$. In general we want to create our particle in a point of the continuum space-time but, once we carry this problem on the lattice there is no exact correspondence between a continuum point and a lattice point: the former will always lie in the interval between two consecutive lattice sites. However, the wave-function of a particle with mass M extends over a spatial region of dimension proportional to $1/M$. Thus by increasing the spatial extent of operators one can achieve a better overlap with the lower lying state and so obtain correlation functions with minor excited states contamination. This suggests the idea of constructing improved interpolating operators out of averages between the same operator calculated at different lattice points.

Since this work regards semileptonic decays between pseudoscalar mesons, we present the smearing procedure for the case of meson interpolators, which are tipically described by bilinear operators of the form (2.153). On the lattice, the overlap with the state of interest can be improved considerably by considering a more general meson operator, introduced by rewriting Eq.(2.153) as[8]

$$O_\Gamma^S(\vec{n}, t) = \sum_{\vec{n}_1, \vec{n}_2} \bar{\psi}(\vec{n}_1, t) S(\vec{n}, t; \vec{n}_1, \vec{n}_2) \psi(\vec{n}_2, t) \ , \tag{2.201}$$

where the distribution S combines fields at spatial lattice positions $\vec{n}_1$ and $\vec{n}_2$ in the vicinity of $\vec{n}$, and it is often chosen to be a factorizable function

$$S(\vec{n}, t; \vec{n}_1, \vec{n}_2) = S^i(\vec{n}, t; \vec{n}_1) \, \Gamma \, S^k(\vec{n}, t; \vec{n}_2) \, , \tag{2.202}$$

[8] We neglect the flavor index for notational convenience.

where the indices i and k indicate that the S-functions for ψ and $\bar{\psi}$ may differ. Eq. (2.202) allows us to write the generalized interpolator O^S_Γ in the form

$$O^S_\Gamma(n) = \bar{\psi}^{S^i}(n)\Gamma\psi^{S^k}(n) \,, \tag{2.203}$$

where we have introduced the so-called *smeared fermions*:

$$\bar{\psi}^{S^i}(\vec{n},t) = \sum_{\vec{n}_1} \bar{\psi}(\vec{n}_1,t)\, S^i(\vec{n},t;\vec{n}_1) \,, \tag{2.204}$$

$$\psi^{S^k}(\vec{n},t) = \sum_{\vec{n}_2} S^k(\vec{n},t;\vec{n}_2)\, \psi(\vec{n}_2,t) \,. \tag{2.205}$$

Various choices for the S-function shape can be used. The trivial case is given by

$$S^{i(j)}(\vec{n},t;\vec{n}_{1(2)}) \equiv L(\vec{n},t;\vec{n}_{1(2)}) = \delta_{\vec{n},\vec{n}_{1(2)}} \,, \tag{2.206}$$

which corresponds to a *local* interpolator O^L_Γ, situated on the single site $(\vec{n},t)$, so that the meson operator turns out to be the usual bilinear (2.153). A more useful possibility is to assume the shape of the wave function of meson states to be Gaussian-like, and build a creation operator with such form. This choice has been used to treat the simulated π-, K- and D-meson in the present work.

2.12.1 Gaussian smearing

The so-called *Gaussian smearing* [48], obtained using the *Jacobi method* [49], consist in choosing for the distribution function S the following form:

$$S(\vec{n},t;\vec{n}_1) = ML(\vec{n},t;\vec{n}_1) \,, \quad M = \sum_{m=0}^{N_G} k_G^m H^m_{\vec{n},\vec{n}_1}[U] \,, \tag{2.207}$$

where k_G represents the coupling with the nearest neighbors, N_G is the number of smearing steps and H connects different sites of the time slice (with t fixed to the time slice of the source) to the central site with gauge transporters:

$$H_{\vec{n},\vec{n}_1}[U] = \sum_{j=1}^{3} \left[U_\mu(\vec{n}+\hat{j},t)\, \delta_{\vec{n}+\hat{j},\vec{n}_1} + U_\mu(\vec{n}-\hat{j},t)\, \delta_{\vec{n}-\hat{j},\vec{n}_1} \right] . \tag{2.208}$$

Parameters N_G and k_G are free parameter, which have to be chosen in order to optimize the profile of the meson interpolator.

In building hadron correlators, smearing can be applied both to the source and the sink. We thus have four different 2-point correlation functions made out by all possible combinations of local and smeared operators:

$$C^{LL}_{ij}(x) = \langle O^L_i(x) O^L_j(0) \rangle \,, \tag{2.209}$$

$$C^{LS}_{ij}(x) = \langle O^L_i(x) O^S_j(0) \rangle \,, \tag{2.210}$$

$$C^{SL}_{ij}(x) = \langle O^S_i(x) O^L_j(0) \rangle \,, \tag{2.211}$$

$$C^{SS}_{ij}(x) = \langle O^S_i(x) O^S_j(0) \rangle \,. \tag{2.212}$$

In the same way we have four possible combinations for the 3-point correlators, which correspond to Eqs. (2.209-2.212) with the insertion of the current Γ between meson interpolators. The analysis of the vector and scalar form factors, which is presented in the next Chapter, has been performed by studying only 2- and 3-point correlation functions of the type SS, which allowed for a good suppression of excited states related to both the D and the $\pi(K)$ mesons. More details are given in Sec. 3.1.

Chapter 3

Vector and Scalar form factors

In this Chapter we present the determination of the vector and scalar form factors f_+ and f_0 of the $D \to \pi\ell\nu$ and $D \to K\ell\nu$ semileptonic decays. After a brief description in Sec. 3.1 of the setup used in our $N_f = 2+1+1$ simulations of QCD on the lattice, we show in Sec. 3.2 the analysis of 2- and 3- point correlators allowing for the extraction of the vector and scalar matrix elements $V_\mu = \bar{c}\gamma_\mu q$ and $S = \bar{c}q$, which are used to extrapolate the momentum dependence of $f_+^{D\to\pi(K)}$ and $f_0^{D\to\pi(K)}$. A Lorentz symmetry breaking due to hypercubic effects is clearly observed (Sec. 3.3) and included in the decomposition of the current matrix elements in terms of additional form factors. A global fit of all the data, performed by considering a simultaneous dependence on q^2, m_ℓ and a^2 of the vector and scalar form factors and a dependence on q^2 and m_ℓ for the hypercubic contributions, is described in Sec. 3.4. Results of $f_+^{D\to\pi(K)}(q^2)$ and $f_0^{D\to\pi(K)}(q^2)$ are shown in comparison with experimental determinations in Sec. 3.5. We conclude the Chapter (Sec. 3.6) with the extraction of the CKM matrix elements $|V_{cd}|$ and $|V_{cs}|$. This has been carried out by combining the momentum dependence of the vector form factors $f_+^{D\to\pi(K)}(q^2)$ with experimental values of the $D \to \pi(K)\ell\nu$ decay rates. We remark that such a method is fully consistent with the SM and does not need of any further assumption.

3.1 Simulation details

The gauge ensembles used in this work have been generated by the ETMC with $N_f = 2 + 1 + 1$ dynamical quarks, which include in the sea, besides two light mass-degenerate quarks, also the strange and the charm quarks [16, 17]. The ensembles are the same adopted in Ref. [50] to determine the up, down, strange and charm quark masses, using the experimental value of the pion decay constant f_π to set the lattice scale[1]. They have been used also to determine the leptonic decay constants f_K, $f_{D^{(*)}}$, $f_{D_s^{(*)}}$ and $f_{B^{(*)}}$ [51, 52], as well as the vector and scalar form factors of the semileptonic $K \to \pi\ell\nu$ decay [53].

The action used in the simulations is

$$S = S_G + S_F^{tm\,\ell} + S_F^{tm\,h}\,, \tag{3.1}$$

[1]With respect to Ref. [50] the number of independent gauge configurations adopted for the ensemble D15.48 has been increased to 90 to improve the statistics.

where S_G is the the Iwasaki gluon action [44], while $S_F^{tm\,\ell}$ and $S_F^{tm\,h}$ are the twisted mass quark actions at maximal twist and in the physical basis [36, 37, 38] for the light and heavy quarks respectively, whose expressions are given in Sec. 2.7. The action (3.1) is known to produce a mixing in the strange and charm sectors [37, 54]. In order to avoid it, for valence quarks we adopted the non-unitary setup described in Ref. [39], in which the valence strange and charm quarks are regularized as Osterwalder-Seiler (OS) fermions [55], while the valence up and down quarks have the same action of the sea. Thus, while we keep the light sector unitary, the action in the strange and charm sectors ($f = s,\, c$) reads

$$S_{OS}^f = a^4 \sum_{n\in\Lambda} \bar{\psi}^f(n) \Bigg[\sum_{\mu=1}^{4} \gamma_\mu \frac{1}{2} \left(\nabla_\mu + \nabla_\mu^*\right) - i\gamma_5 r_f \left(m_0 - \frac{a}{2} \sum_{\mu=1}^{4} \nabla_\mu \nabla_\mu^* \right) + \mu_f \Bigg] \psi^f(n) \;, \tag{3.2}$$

where $r_f = \pm 1$. The use of different lattice regularisations for the valence and sea heavy quarks avoids completely the effects of the strange and charm mixing without modifying the renormalization pattern of operators in massless schemes and produces only a modification of discretization effects. When constructing meson correlation functions the Wilson parameters of the two valence quarks have been always chosen to have opposite values, $r_c = r_s = r_d = -r_u$, so that the squared pseudoscalar (PS) meson mass differs from its continuum counterpart only by terms of $\mathcal{O}(a^2 m \Lambda_{QCD})$ [38]. Moreover, since we work at maximal twist, the automatic $\mathcal{O}(a)$-improvement described in Sec. 2.7.1 is guaranteed also for our non-unitary setup. The statistical accuracy of the correlators is significantly improved by using the all-to-all quark propagators evaluated with the so-called "one-end" stochastic method [56], which includes spatial stochastic sources at a single time slice chosen randomly (see Ref. [57], where the degenerate case of the electromagnetic pion form factor is discussed in details).

In the case of charm quarks it is a common procedure to adopt Gaussian-smeared interpolating fields [48] for both the source and the sink in order to suppress faster the contribution of the excited states, leading to an improved projection onto the ground state at relatively small time distances. For the values of the smearing parameters we set $k_G = 4$ and $N_G = 30$. In addition, we apply APE-smearing to the gauge links [58] in the interpolating fields with parameters $\alpha_{APE} = 0.5$ and $N_{APE} = 20$. The Gaussian smearing is applied as well also for the light and strange quarks. The values of M_π and M_K reported in Tab. 3.1 are consistent within the statistical errors with the corresponding ones listed in the Tab. 1 of Ref. [53], computed using local interpolating fields.

The QCD simulations have been carried out at three different values of the inverse bare lattice coupling β, to allow for a controlled extrapolation to the continuum limit, and at different lattice volumes. For each gauge ensemble we have used a number of gauge configurations corresponding to a separation of 20 trajectories to avoid autocorrelations. We have simulated quark masses in the range from $\simeq 3\, m_{ud}$ to $\simeq 12\, m_{ud}$ in the light sector, from $\simeq 0.7\, m_s$ to $\simeq 1.2\, m_s$ in the strange sector, and from $\simeq 0.7\, m_c$ to $\simeq 1.2\, m_c$ in the charm sector, where m_{ud}, m_s and m_c are the physical values of the average up/down, strange and charm quark masses respectively, as determined in Ref. [50]. The lattice spacings are found to be $a = \{0.0885\,(36), 0.0815\,(30), 0.0619\,(18)\}$ fm at $\beta = \{1.90, 1.95, 2.10\}$

respectively, the lattice volume goes from $\simeq 2$ to $\simeq 3$ fm and the pion masses, extrapolated to the continuum and infinite volume limits, range from $\simeq 210$ to $\simeq 450$ MeV (see Ref. [50] for further details).

ensemble	β	V/a^4	$a\mu_{sea} = a\mu_\ell$	$a\mu_s$	$a\mu_c$	M_π(MeV)	M_K(MeV)	M_D(MeV)	L(fm)	$M_\pi L$
A30.32	1.90	$32^3 \times 64$	0.0030	{0.0180,	{0.21256,	275	569	2015	2.84	3.96
A40.32			0.0040	0.0220,	0.25000,	315	578	2018		4.53
A50.32			0.0050	0.0260}	0.29404}	351	578	2018		5.04
A40.24		$24^3 \times 48$	0.0040			324	584	2024	2.13	3.49
A60.24			0.0060			386	599	2022		4.17
A80.24			0.0080			444	619	2037		4.79
A100.24			0.0100			495	639	2042		5.34
B25.32	1.95	$32^3 \times 64$	0.0025	{0.0155,	{0.18705,	258	545	1950	2.61	3.42
B35.32			0.0035	0.0190,	0.22000,	302	556	1944		3.99
B55.32			0.0055	0.0225}	0.25875}	375	578	1959		4.96
B75.32			0.0075			436	600	1965		5.77
B85.24		$24^3 \times 48$	0.0085			467	611	1974	1.96	4.63
D15.48	2.10	$48^3 \times 96$	0.0015	{0.0123,	{0.14454,	220	526	1928	2.97	3.31
D20.48			0.0020	0.0150,	0.17000,	254	533	1933		3.83
D30.48			0.0030	0.0177}	0.19995}	308	547	1939		4.65

Table 3.1: *Summary of the simulated sea and valence quark bare masses, of the π, K and D meson masses, of the lattice size L and of the product $M_\pi L$ for the various gauge ensembles used in this work. The values of M_K and M_D do not correspond to the simulated strange and charm bare quark masses shown in the 5^{th} and 6^{th} columns, but to the renormalized strange and charm masses interpolated at the physical values $m_s^{phys}(\overline{MS}, 2\text{ GeV}) = 99.6(4.3)\,\text{MeV}$ and $m_c^{phys}(\overline{MS}, 2\text{ GeV}) = 1.176(39)\,\text{GeV}$ determined in Ref. [50].*

Statistical errors on quantities directly extracted from the correlators have been evaluated through the jackknife procedure (using $N_c = 15$ clusters), while uncertainties on data obtained from independent ensembles of gauge configurations, like the errors of the fitting procedures, are evaluated using a bootstrap sampling (with $N_{boot} = 100$) as described in Sec. 2.9.1. In our study of the semileptonic $D \to \pi\ell\nu$ and $D \to K\ell\nu$ form factors we make use of the input parameters summarized in Tab. 3.2, obtained from the eight branches of the analysis carried out in Ref. [50]. The various branches have been calculated using different strategies, in order to take under control systematic errors, and differ by:

- The choice of the scaling variable used for the treatment of discretization effects and the extrapolation to the continuum limit. This quantity was taken to be either the Sommer parameter r_0/a [59] or the mass of a fictitious pseudoscalar (PS) meson made of two strange-like quarks $aM_{s's'}$;

- The chiral extrapolation, which was based either on Chiral Perturbation Theory

(ChPT) or on a polynomial expansion in the light quark mass (for the motivations see the discussion in Sec. 3.1 of Ref. [50]);

- The choice between two methods, denoted as M1 and M2 which differ by $\mathcal{O}(a^2)$ effects (see, e.g., Ref. [60]), used to determine non-perturbatively the values of the mass RC $\mathcal{Z}_m = 1/\mathcal{Z}_P$ [50].

	β	1^{st}	2^{nd}	3^{rd}	4^{th}
a^{-1}(GeV)	1.90	2.224(68)	2.192(75)	2.269(86)	2.209(84)
	1.95	2.416(63)	2.381(73)	2.464(85)	2.400(83)
	2.10	3.184(59)	3.137(64)	3.248(75)	3.163(75)
m_{ud}^{phys}(GeV)		0.00372(13)	0.00386(17)	0.00365(10)	0.00375(13)
m_{s}^{phys}(GeV)		0.1014(44)	0.1023(39)	0.0992(29)	0.1007(32)
m_{c}^{phys}(GeV)		1.183(34)	1.193(28)	1.177(25)	1.219(21)
$\mathcal{Z}_P$	1.90	0.5290(73)			
	1.95	0.5089(34)			
	2.10	0.5161(27)			

	β	5^{th}	6^{th}	7^{th}	8^{th}
a^{-1}(GeV)	1.90	2.222(67)	2.195(75)	2.279(89)	2.219(87)
	1.95	2.414(61)	2.384(73)	2.475(88)	2.411(86)
	2.10	3.181(57)	3.142(64)	3.262(79)	3.177(78)
m_{ud}^{phys}(GeV)		0.00362(12)	0.00377(16)	0.00354(9)	0.00363(12)
m_{s}^{phys}(GeV)		0.0989(45)	0.0995(39)	0.0962(27)	0.0975(30)
m_{c}^{phys}(GeV)		1.150(35)	1.158(27)	1.144(29)	1.182(19)
$\mathcal{Z}_P$	1.90	0.5730(42)			
	1.95	0.5440(17)			
	2.10	0.5420(10)			

Table 3.2: *The input parameters for the eight branches of the analysis of Ref. [50]. The renormalized quark masses and the RC Z_P are given in the $\overline{\rm MS}$ scheme at a renormalization scale of 2 GeV. With respect to Ref. [50] the table includes an update of the values of the lattice spacing and, consequently, of all the other quantities.*

Throughout this work the results corresponding to the various branches of the analysis are combined to form our averages and errors according to the following equations:

$$\overline{x} = \frac{1}{N}\sum_{i=1}^{N} x_i \,, \tag{3.3}$$

$$\sigma_x^2 = \frac{1}{N}\sum_{i=1}^{N} \sigma_i^2 + \frac{1}{N}\sum_{i=1}^{N} (\overline{x} - x_i)^2 \,, \tag{3.4}$$

where x_i and σ_i stand for the central value and the standard deviation corresponding to the i-th branche of our data samples respectively. In view of what explained above, $N = 8$ in this analysis. The basic simulation parameters and the masses of the π, K and D mesons corresponding to each ensemble used in this work are collected in Tab. 3.1.

3.2 Vector and Scalar matrix elements

The matrix element of the weak vector current $\widehat{V}_\mu$ between an initial D-meson state and a $\pi(K)$-meson final state decomposes, as shown in Eq. (1.64), into the two form factors $f_+(q^2)$ and $f_-(q^2)$:[2]

$$\langle \widehat{V}_\mu \rangle \equiv \langle P(p_P)|\widehat{V}_\mu|D(p_D)\rangle = (p_D + p_P)_\mu \, f_+(q^2) + (p_D - p_P)_\mu \, f_-(q^2) \ , \tag{3.5}$$

where $P = \pi(K)$ can be either the pion or the kaon and the 4-momentum transfer q is given by $q \equiv p_D - p_P$. In Sec. 1.5 we have also introduced the scalar form factor f_0, which is defined as

$$f_0(q^2) = f_+(q^2) + \frac{q^2}{M_D^2 - M_P^2} \ f_-(q^2) \ , \tag{3.6}$$

so that the kinematic identity $f_+(0) = f_0(0)$ is satisfied by definition. The scalar form factor is proportional to the 4-divergence of $\langle \widehat{V}_\mu \rangle$ so that, thanks to the Ward-Takahashi identity (WTI), f_0 can be determined from the matrix element of the scalar density $\widehat{S}$ between the D-meson and the $\pi(K)$-meson states:

$$\langle \widehat{S} \rangle \equiv \langle P(p_P)|\widehat{S}|D(p_D)\rangle = \frac{M_D^2 - M_P^2}{m_c - m_x} \ f_0(q^2) \ , \tag{3.7}$$

where $x = \ell(s)$. From Eqs. (3.5) and (3.7) it turns out that the determination of the scalar and vector form factors can be carried out by computing the matrix elements $\langle \widehat{V}_\mu \rangle$ and $\langle \widehat{S} \rangle$. These two quantities can be extracted from the large (Euclidean) time distance behavior of a convenient combination of 2- and 3-point correlation functions in LQCD.

As described in Eqs. (2.182) (with $\eta = 1$) and (2.189), at large time distances 2- and 3-point correlation functions behave as

$$C_2^{D(P)}\left(t', \vec{p}_{D(P)}\right) \quad \xrightarrow[t' \gg a]{} \quad \frac{|Z_{D(P)}|^2}{2E_{D(P)}} \left[e^{-E_{D(P)} t'} + e^{-E_{D(P)}(T - t')} \right] , \tag{3.8}$$

$$C_{\widehat{\Gamma}}^{DP}\left(t, t', \vec{p}_D, \vec{p}_P\right) \xrightarrow[t \gg a \, , \, (t'-t) \gg a]{} \frac{Z_P Z_D^*}{4 E_P E_D} \ \langle P(p_P)|\widehat{\Gamma}|D(p_D)\rangle \ e^{-E_D t} \, e^{-E_P (t'-t)} \ , \tag{3.9}$$

where Z_D and Z_P are the matrix elements $\langle 0| \, P_5^D(0) \, | \, D(\vec{p}_D)\rangle$ and $\langle 0| \, P_5^P(0) \, | \, P(\vec{p}_P)\rangle$, which depend on the meson momenta $\vec{p}_D$ and $\vec{p}_P$ because of the use of smeared interpolating fields, while E_D and E_P are the energies of the D and P mesons. These energies and matrix elements can be extracted directly by fitting the exponential behavior, given by the r.h.s of Eq. (3.8), of the corresponding 2-point correlation functions. The time intervals $[t_{\rm min}, \, t_{\rm max}]$

[2] As in Sec. 2.8.1 we use the hat symbol to indicate renormalized operators.

adopted for the fit (3.8) are listed in Tab. 3.3. We have checked that the extracted values of $E_{D(P)}$ are nicely reproduced (within the statistical errors) by the continuum-like dispersive relation $E^{\rm disp}_{D(P)} = \sqrt{M^2_{D(P)} + |\vec{p}_{D(P)}|^2}$, where $M_{D(P)}$ is the meson mass extracted from the 2-point correlator corresponding to the meson at rest. We decided to use for the analysis the energy values $E^{\rm disp}_{D(P)}$ instead of those directly extracted from the fit. As for the 3-point correlators (3.9) the usual choice of the time distance t' between the source and the sink is to maximize it, i.e. to put $t' = T/2$. Since we are using smeared interpolating fields, it is convenient to choose smaller values of t', which allow to decrease significantly the statistical noise satisfying at the same time the dominance of the ground-state signals. We have optimized the choice of the values of t' for the various lattice spacings and volumes, which can be read off in the last column of Tab. 3.3.

β	V/a^4	$[t_{\rm min},\, t_{\rm max}]_{(\ell\ell,\,\ell s)}/a$	$[t_{\rm min},\, t_{\rm max}]_{(\ell c)}/a$	t'/a
1.90	$32^3 \times 64$	[12, 31]	[8, 16]	18
	$24^3 \times 48$	[12, 23]	[8, 17]	18
1.95	$32^3 \times 64$	[13, 31]	[9, 18]	20
	$24^3 \times 48$	[13, 23]	[9, 18]	20
2.10	$48^3 \times 96$	[18, 40]	[12, 24]	26

Table 3.3: *Time intervals adopted for the extraction of the PS meson energies $E_{D(P)}$ and the matrix elements $Z_{D(P)}$ from the 2-point correlators in the light (ℓ), strange (s) and charm (c) sectors. The last column contains the values of the time distance t' between the source and the sink adopted for the 3-point correlators (3.9).*

In our lattice setup we employ maximally twisted fermions and therefore the vector and scalar currents, $\widehat{V}_\mu$ and $\widehat{S}$, renormalize multiplicatively [38]. Introducing the local bare currents $V_\mu = \bar{c}\gamma_\mu q$ and $S = \bar{c}q$, where $q = d(s)$, and keeping the same value for the Wilson parameters of the initial and final quarks, one has

$$\widehat{V}_\mu = \mathcal{Z}_V \cdot V_\mu = \mathcal{Z}_V\, \bar{c}\gamma_\mu q \ , \tag{3.10}$$

$$\widehat{S} = \mathcal{Z}_P \cdot S = \mathcal{Z}_P\, \bar{c}q \ , \tag{3.11}$$

where $\mathcal{Z}_V$ and $\mathcal{Z}_P$ are the renormalization constants (RCs) of the vector and pseudoscalar densities for standard Wilson fermions, respectively. As shown in Sec. (2.8.2) the twisted quark masses renormalize multiplicatively with a RC $\mathcal{Z}_m$ given by $\mathcal{Z}_m = 1/\mathcal{Z}_P$ [38], which means that the product $(m_c - m_q)\,\langle \widehat{S} \rangle$ is renormalization group invariant. Therefore, according to Eq. (3.7), the scalar form factor $f_0(q^2)$ is related to the (bare) matrix element $\langle S \rangle$ by

$$\langle S \rangle \equiv \langle P(p_P)|S|D(p_D)\rangle = \frac{M_D^2 - M_P^2}{\mu_c - \mu_q}\, f_0(q^2) \ , \tag{3.12}$$

where μ_q and μ_c are the bare light (strange) and charm quark masses, respectively.

As in the case of the semileptonic $K_{\ell 3}$ decay [53], the matrix elements $\langle S\rangle$ and $\langle \widehat{V}_\mu\rangle$ (see Eq. (3.5)) can be extracted from the time dependence of the ratios R_μ ($\mu = 0, 1, 2, 3$) and R_S of 2- and 3-point correlation functions, considering local bare currents V_μ and S, namely

$$R_\mu(t, \vec{p}_D, \vec{p}_P) \equiv 4\, p_{D\mu}\, p_{P\mu}\, \frac{C^{DP}_{V_\mu}(t, t', \vec{p}_D, \vec{p}_P)\, C^{PD}_{V_\mu}(t, t', \vec{p}_P, \vec{p}_D)}{C^{PP}_{V_\mu}(t, t', \vec{p}_P, \vec{p}_P)\, C^{DD}_{V_\mu}(t, t', \vec{p}_D, \vec{p}_D)}\ , \tag{3.13}$$

$$R_S(t, \vec{p}_D, \vec{p}_P) \equiv 4\, E_D\, E_P\, \frac{C^{DP}_{S}(t, t', \vec{p}_D, \vec{p}_P)\, C^{PD}_{S}(t, t', \vec{p}_P, \vec{p}_D)}{\widetilde{C}^{D}_2\,(t', \vec{p}_D)\ \widetilde{C}^{P}_2\,(t', \vec{p}_P)}\ , \tag{3.14}$$

where the correlation functions $\widetilde{C}_2^{D(P)}(t)$ are given by

$$\widetilde{C}_2^{D(P)}\left(t,\, \vec{p}_{D(P)}\right) \equiv \frac{1}{2}\left[C_2^{D(P)}\left(t,\, \vec{p}_{D(P)}\right) + \sqrt{C_2^{D(P)}\left(t,\, \vec{p}_{D(P)}\right)^2 - C_2^{D(P)}\left(\frac{T}{2},\, \vec{p}_{D(P)}\right)^2}\right]\ , \tag{3.15}$$

which at large time distances behave as

$$\widetilde{C}_2^{D(P)}\left(t,\, \vec{p}_{D(P)}\right) \xrightarrow[t\gg a]{} \frac{Z_{D(P)}}{2\, E_{D(P)}}\, e^{-E_{D(P)}t}\ , \tag{3.16}$$

i.e. without the backward signal. Note that the denominator of Eq. (3.13) is nothing but the numerator evaluated in the mass-degenerate limit for the valence quarks in the current. Such mass-degenerate quarks have the same lattice regularisation of the corresponding ones in the numerator, so that the RC $\mathcal{Z}_V$ is the same for the two terms in the ratio and therefore it cancels out.

At large time distances one has:

$$R_\mu(t, \vec{p}_D, \vec{p}_P) \xrightarrow[t\gg a\ (t'-t)\gg a]{} 4\, p_{D\mu}\, p_{P\mu}\, \frac{\langle P(p_P)|\widehat{V}_\mu|D(p_D)\rangle\, \langle D(p_D)|\widehat{V}_\mu|P(p_P)\rangle}{\langle P(p_P)|\widehat{V}_\mu|P(p_P)\rangle\, \langle D(p_D)|\widehat{V}_\mu|D(p_D)\rangle} = |\langle \widehat{V}_\mu\rangle|^2, \tag{3.17}$$

$$R_S(t, \vec{p}_D, \vec{p}_P) \xrightarrow[t\gg a\ (t'-t)\gg a]{} |\langle P(p_P)|S|D(p_D)\rangle|^2 = |\langle S\rangle|^2\ , \tag{3.18}$$

so that, up to lattice artefacts, the renormalized quantity $|\,\langle \widehat{V}_\mu\rangle\,|^2$ and the bare one $|\,\langle S\rangle\,|^2$ can be extracted directly from the plateau of R_μ and R_S, independently of the matrix elements Z_D and $Z_{\pi(K)}$ of the interpolating fields. In the r.h.s. of Eq. (3.17) we have used the fact that, due to the charge conservation, $\langle P(p_P)|\widehat{V}_\mu|P(p_P)\rangle = 2\, p_{P\mu}$ and $\langle D(p_D)|\widehat{V}_\mu|D(p_D)\rangle = 2\, p_{D\mu}$. Taking the square root of R_μ and R_S we can get the absolute value of the matrix elements $\langle \widehat{V}_\mu\rangle$ and $\langle S\rangle$, while their sign can be easily inferred from those of the correlators $C^{DP}_{V_\mu}(t, t', \vec{p}_D, \vec{p}_P)$ and $C^{DP}_{S}(t, t', \vec{p}_D, \vec{p}_P)$ in the relevant time regions. When a spatial component of the momentum of either the parent or the child meson is vanishing, the corresponding matrix element $\langle P(p_P)|V_i|P(p_P)\rangle$ (or $\langle D(p_D)|V_i|D(p_D)\rangle$) ($i = 1, 2, 3$) is also vanishing and the correlator $C^{PP}_{V_i}$ (or $C^{DD}_{V_i}$), cannot be used in the denominator of the r.h.s of Eq. (3.13). In these cases the quantity $2p_{Pi}\,/\langle P(p_P)|V_i|P(p_P)\rangle$

(or $2p_{Di}/\langle D(p_D)|V_i|D(p_D)\rangle$) is replaced by $2E_P/C_{V_0}^{PP}$ (or $2E_D/C_{V_0}^{DD}$). Moreover, if both the pion (kaon) and the D-meson are at rest, only two ratios, R_S and R_0, can be constructed, providing two independent determinations of the scalar form factor $f_0(q^2)$ at the kinematical end-point $q^2_{\rm max} = (M_D - M_P)^2$, which may differ by lattice artefacts.

In order to inject momenta on the lattice we use the same procedure adopted in Ref. [53] for the $K_{\ell 3}$ decays. In particular for the valence quark fields we impose twisted boundary conditions (BC's) [22, 23, 61] in the spatial directions and anti-periodic BC's in time. The sea dynamical quarks, on the contrary, have been simulated with periodic BC's in space and anti-periodic ones in time. The choice of using twisted BC's for the valence quark fields, as presented in Sec. (2.11), is crucial in order to remove the strong limitations to the accessible kinematical regions of momentum-dependent quantities like, e.g., form factors. Furthermore we remark that, as shown in Refs. [62, 63], for physical quantities which do not involve final state interactions (like, e.g., meson masses, decay constants and semileptonic form factors), the use of different BC's for valence and sea quarks produces only FSE which are exponentially small. The quark 3-momentum in our simulations is then given by

$$p = \frac{2\pi}{L}\left(\theta + n_x,\ \theta + n_y,\ \theta + n_z\right)\ , \tag{3.19}$$

where $n_{x,y,z}$ are integers and the θ values adopted for the different gauge ensembles, chosen to be democratically distributed along the three spatial directions, are collected in Tab. 3.4. In this way we obtain momenta with values ranging from $\approx 150\,\text{MeV}$ to $\approx 650\,\text{MeV}$ for all the various lattice spacings and volumes[3]. The 3-point correlation

β	V/a^4	θ
1.90	$32^3 \times 64$	$0.0,\ \pm 0.200,\ \pm 0.467,\ \pm 0.867$
	$24^3 \times 48$	$0.0,\ \pm 0.150,\ \pm 0.350,\ \pm 0.650$
1.95	$32^3 \times 64$	$0.0,\ \pm 0.183,\ \pm 0.427,\ \pm 0.794$
	$24^3 \times 48$	$0.0,\ \pm 0.138,\ \pm 0.321,\ \pm 0.596$
2.10	$48^3 \times 96$	$0.0,\ \pm 0.212,\ \pm 0.493,\ \pm 0.916$

Table 3.4: *Values of the parameter θ, appearing in Eq. (3.19), for the various ETMC gauge ensembles of Tab. 3.1.*

functions $C_{V_\mu}^{DP}(t, t', \vec{p}_D, \vec{p}_P)$ and $C_S^{DP}(t, t', \vec{p}_D, \vec{p}_P)$ have been simulated imposing periodic BC's to the spectator light quark and partially twisted BC's (3.19) to the initial c and final $u(s)$ quarks. With this choice the π, K and D meson (spatial) momenta are given by $\vec{p}_D = (2\pi/L)\,(\theta_D, \theta_D, \theta_D)$ and $\vec{p}_{\pi(K)} = (2\pi/L)\left(\theta_{\pi(K)}, \theta_{\pi(K)}, \theta_{\pi(K)}\right)$, where θ_D and $\theta_{\pi(K)}$ can assume for each gauge ensemble the values of the parameter θ given in Tab. 3.4.

[3]The correlators used in this work have been calculated within the PRACE project PRA067 *"First Lattice QCD study of B-physics with four flavors of dynamical quarks"*. The values of the quark momentum were not chosen having in mind the investigation of hypercubic effects in the semileptonic form factors. In particular the use of spatially symmetric values of the quark momentum (see Tab. 3.4) is not ideal for such a purpose.

As described in Sec. 2.7.1 the use of two kinematics with opposite spatial momenta of the initial and final mesons, given by opposite signs of the corresponding θ, allows for an $\mathcal{O}(a)$ improvement on the matrix elements $\langle \widehat{V}_\mu \rangle$ and $\langle S \rangle$ performing the following average:

$$\langle \widehat{V}_0 \rangle_{\rm imp} \equiv \frac{1}{2}\left[\langle P(E_P,\vec{p}_P)|\widehat{V}_0|D(E_D,\vec{p}_D)\rangle + \langle P(E_P,-\vec{p}_P)|\widehat{V}_0|D(E_D,-\vec{p}_D)\rangle \right] , \quad (3.20)$$

$$\langle \widehat{V}_i \rangle_{\rm imp} \equiv \frac{1}{2}\left[\langle P(E_P,\vec{p}_P)|\widehat{V}_i|D(E_D,\vec{p}_D)\rangle - \langle P(E_P,-\vec{p}_P)|\widehat{V}_i|D(E_D,-\vec{p}_D)\rangle \right] , \quad (3.21)$$

$$\langle S \rangle_{\rm imp} \equiv \frac{1}{2}\left[\langle P(E_P,\vec{p}_P)|S|D(E_D,\vec{p}_D)\rangle + \langle P(E_P,-\vec{p}_P)|S|D(E_D,-\vec{p}_D)\rangle \right] . \quad (3.22)$$

Furthermore since we are using democratically distributed momenta in the three spatial directions, the matrix elements of the spatial components of the vector current $\langle \widehat{V}_i \rangle_{\rm imp}$ are equal to each other. Therefore, in order to improve the statistics, we average them to get

$$\langle \widehat{V}_{\rm sp} \rangle_{\rm imp} \equiv \frac{1}{3}\left[\langle \widehat{V}_1 \rangle_{\rm imp} + \langle \widehat{V}_2 \rangle_{\rm imp} + \langle \widehat{V}_3 \rangle_{\rm imp} \right] . \quad (3.23)$$

The quality of the plateau for the matrix elements $\langle \widehat{V}_0 \rangle_{\rm imp}$, $\langle \widehat{V}_{\rm sp} \rangle_{\rm imp}$ and $\langle S \rangle_{\rm imp}$ is illustrated in Fig. 3.1 in the case of the $D \to \pi$ transition. The time intervals adopted for fitting Eqs. (3.17-3.18) are symmetric around $t'/2$ (see Tab. 3.3 for the values of t' for each specific gauge ensemble) and equal to $[t'/2-2,\ t'/2+2]$. These values are compatible with the dominance of the π, K and D mesons ground-state observed along the time intervals of Tab. 3.3 for the two-point correlation functions.

Thus, from the 2- and 3-point lattice correlators we are able to extract the three $\mathcal{O}(a)$-improved matrix elements $\langle \widehat{V}_0 \rangle_{\rm imp}$, $\langle \widehat{V}_{\rm sp} \rangle_{\rm imp}$ and $\langle S \rangle_{\rm imp}$. The standard procedure for determining the scalar and vector form factors $f_0(q^2)$ and $f_+(q^2)$ is to assume the following Lorentz-covariant decomposition

$$\langle P(p_P)|\widehat{V}_\mu|D(p_D)\rangle = P_\mu\ f_+(q^2) + q_\mu\ \frac{M_D^2 - M_P^2}{q^2}\left[f_0(q^2) - f_+(q^2) \right] + \mathcal{O}(a^2) , \quad (3.24)$$

$$\langle P(p_P)|S|D(p_D)\rangle = \frac{M_D^2 - M_P^2}{\mu_c - \mu_q} f_0(q^2) + \mathcal{O}(a^2) \quad (3.25)$$

with $P_\mu \equiv (p_D + p_P)_\mu$. Explicitly one has

$$\langle \widehat{V}_0 \rangle_{\rm imp} = (E_D + E_P) f_+(q^2) + (E_D - E_P)\frac{M_D^2 - M_P^2}{q^2}\left[f_0(q^2) - f_+(q^2) \right] + \mathcal{O}(a^2), \quad (3.26)$$

$$\langle \widehat{V}_{\rm sp} \rangle_{\rm imp} = \frac{2\pi}{L}\left\{ (\theta_D + \theta_P) f_+(q^2) + (\theta_D - \theta_P)\frac{M_D^2 - M_P^2}{q^2}\left[f_0(q^2) - f_+(q^2) \right] \right\} + \mathcal{O}(a^2) \quad (3.27)$$

$$\langle S \rangle_{\rm imp} = \frac{M_D^2 - M_P^2}{\mu_c - \mu_q} f_0(q^2) + \mathcal{O}(a^2) , \quad (3.28)$$

which represent a redundant mathematical system consisting of three equations depending on just two form factors. We then determine $f_0(q^2)$ and $f_+(q^2)$ by minimizing the χ^2-variable constructed using Eqs. (3.26-3.28). In the next Section we present and discuss the result of this determination in which, as anticipated, we found evidence for Lorentz symmetry breaking terms.

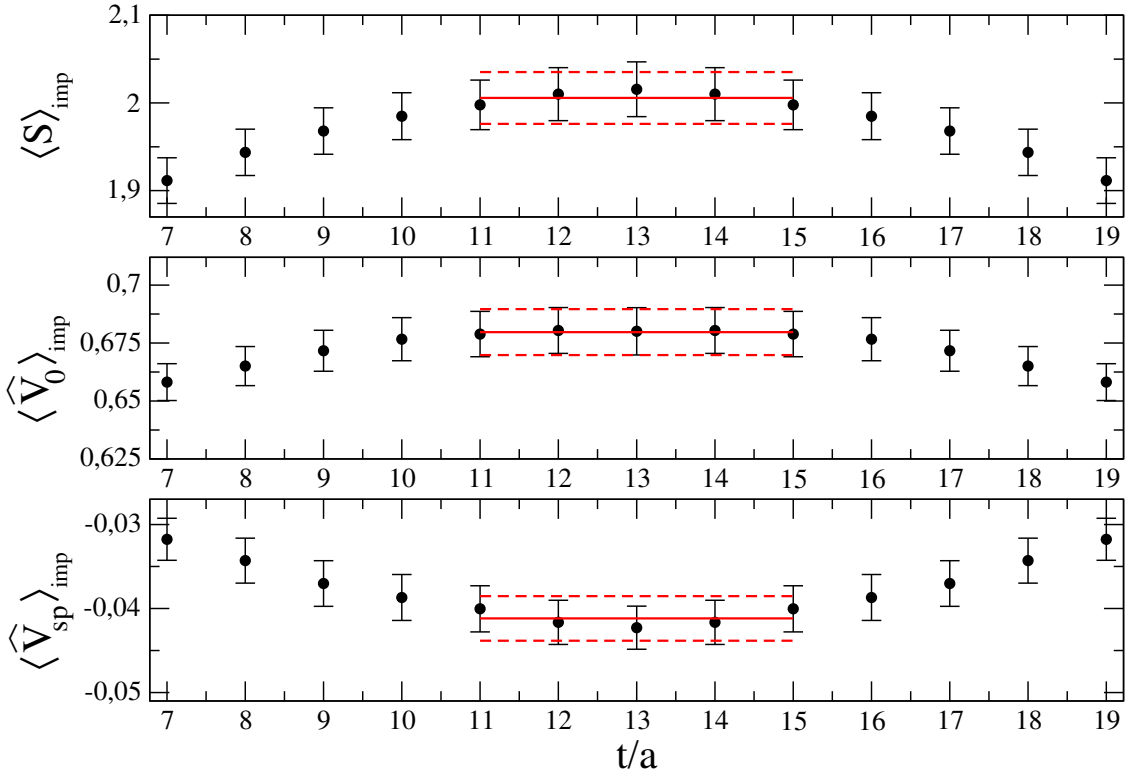

Figure 3.1: *Matrix elements* $\langle \widehat{V}_{\rm sp} \rangle_{\rm imp}$, $\langle \widehat{V}_0 \rangle_{\rm imp}$ *and* $\langle S \rangle_{\rm imp}$ *for the* $D \to \pi$ *case extracted from the ratios* R_μ *and* R_S *[see Eqs. (3.17) and (3.18)] for the ensemble D20.48 with* $\beta = 2.10$, $L/a = 48$, $a\mu_\ell = 0.0020$, $a\mu_c = 0.17$, $\vec{p}_D = -\vec{p}_\pi$ *and* $|\vec{p}_D| \simeq 150\,\text{MeV}$. *The meson masses are* $M_\pi \simeq 254\,\text{MeV}$ *and* $M_D \simeq 1933\,\text{MeV}$. *The horizontal red lines correspond to the plateau regions used to extract the matrix elements and to their central values and statistical errors.*

3.3 Form factors and hypercubic effects

After a small interpolation of our lattice data to the physical values of the strange and charm quark masses, $m_s^{phys}(2\,\text{GeV}) = 99.6\,(4.3)\,\text{MeV}$ and $m_c^{phys}(2\,\text{GeV}) = 1.176\,(3.9)\,\text{GeV}$ taken from Ref. [50], we determine the vector and scalar form factors $f_+^{D\pi(K)}$ and $f_0^{D\pi(K)}$ for each gauge ensemble and for each choice of the parent and child meson momenta. The momentum dependencies of the semileptonic form factors $f_+^{D\pi(K)}$ and $f_0^{D\pi(K)}$ are illustrated in the upper (lower) panels of Fig. 3.2, where different markers and colors correspond to different values of the child meson momentum for the ETMC ensemble A60.24, i.e. at fixed values of the parent and child meson masses as well as of the lattice spacing and volume. Therefore, if the Lorentz-covariant decomposition (3.24-3.25) were adequate to describe our data, the extracted form factors would depend only on the squared 4-momentum transfer q^2. This is not the case and an extra dependence on the value of the child meson momentum is clearly visible in Fig. 3.2 beyond the statistical uncertainties.

As is well known, the lattice breaks Lorentz symmetry and is invariant only under

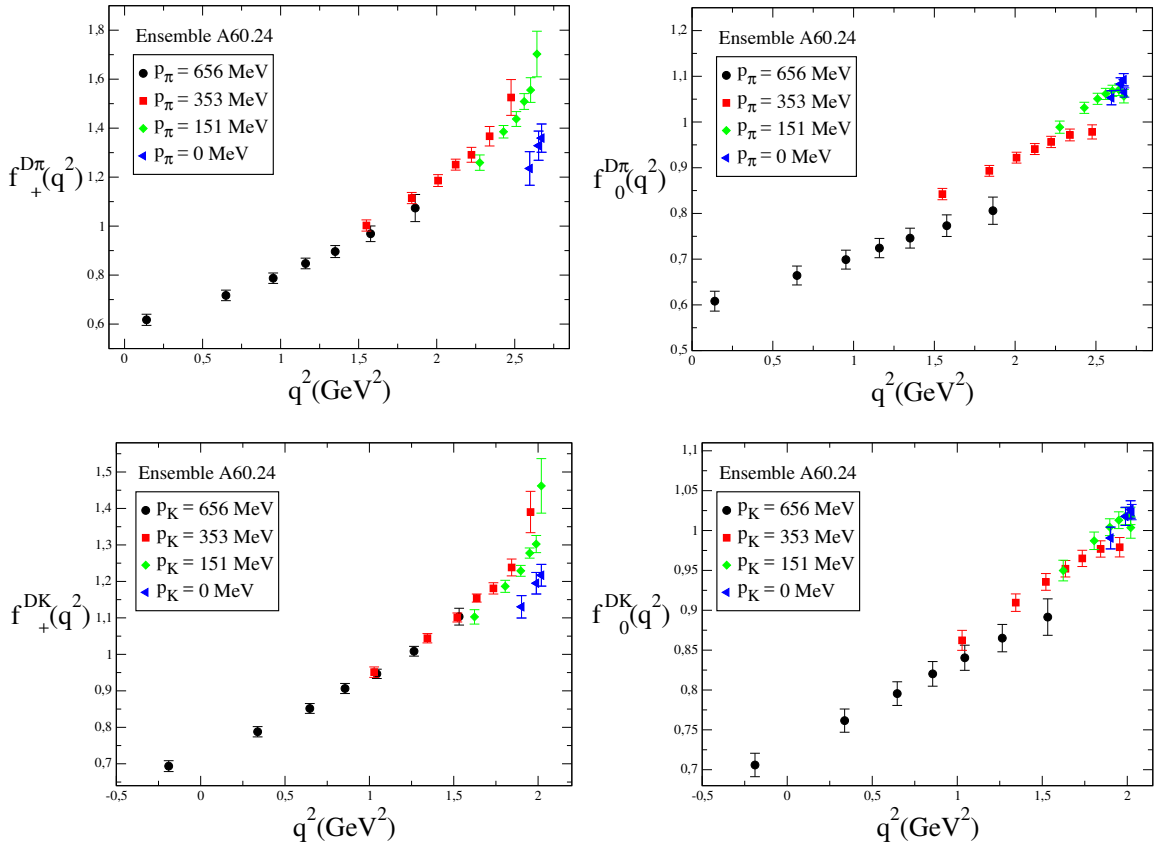

Figure 3.2: *Momentum dependence of the vector $f_+^{D\pi}$ (upper left panel), f_+^{DK} (lower left panel) and scalar $f_0^{D\pi}$ (upper right panel), f_0^{DK} (lower right panel) form factors in the case of the gauge ensemble A60.24 [50]. Different markers and colors distinguish different values of the child meson momentum. The simulated meson masses are $M_\pi \simeq 386$ MeV, $M_K \simeq 599$ MeV and $M_D \simeq 2022$ MeV, while the lattice spacing and spatial size are $a \simeq 0.0885$ fm and $L \simeq 2.13$ fm, respectively (see Tab. 3.1).*

discrete rotations by multiple of 90° in each direction of the Euclidean space-time. Therefore, the matrix elements (3.20-3.23), and consequently the form factors extracted from Eqs. (3.26-3.28), may depend also on hypercubic invariants[4]. Hypercubic effects are known to affect lattice calculations and they have been discussed for instance in Refs. [64, 65]. It is however the first time that these effects are observed in the D-meson semileptonic form factors. In Refs. [66] and [24, 25] $N_f = 2+1$ results for the $f_+^{D\pi(K)}$ form factor have been obtained by FNAL/MILC and HPQCD collaborations, respectively, using only a limited number of kinematic conditions, restricted in particular to the parent D-meson at rest. Also the ETMC reported $N_f = 2$ results for the D-meson semileptonic form factors in Ref. [67], but the kinematics were limited to the Breit-frame ($\vec{p}_D = -\vec{p}_P$). Recently in Ref. [68] both the $D \to \pi$ and $D \to K$ semileptonic transitions have been investigated

[4]Hypercubic symmetry is also broken on our lattices because of the different length of the temporal and spatial dimensions. This effect however is expected to be subdominant and will be neglected in what follows.

using $N_f = 2 + 1$ domain-wall fermions assuming the D-meson at rest, while in Ref. [69] the FNAL/MILC collaboration has addressed the determination of the semileptonic form factors, using $N_f = 2 + 1 + 1$ MILC ensembles with HISQ fermions and tuning properly the child meson momentum to reach directly $q^2 = 0$, but working only in the reference frame where the D-meson is at rest. We argue that all these choices may obscure the presence of hypercubic effects in the lattice data.

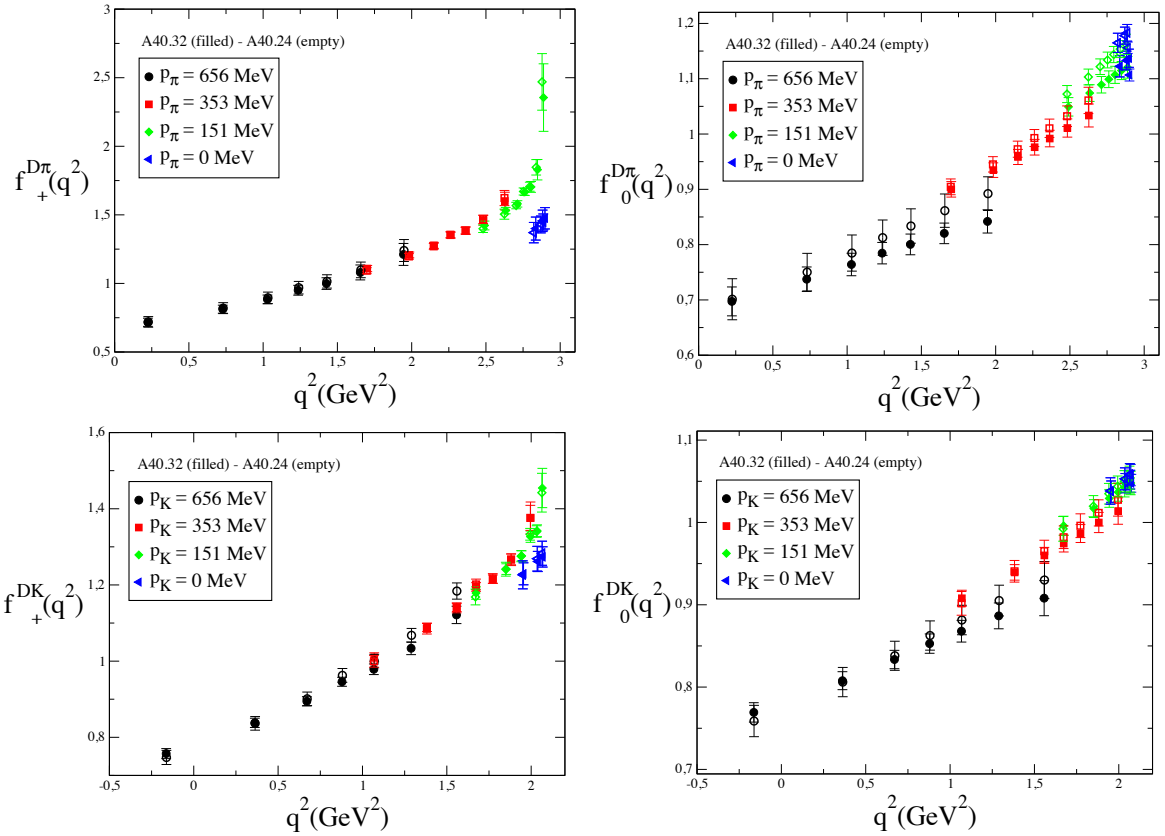

Figure 3.3: *Results for the vector (left panels) and scalar (right panels) form factors in the case of the $D \to \pi$ (upper panels) and $D \to K$ (lower panels) semileptonic decays versus q^2 for the gauge ensembles A40.24 and A40.32, which correspond to $a \simeq 0.0885$ fm, $M_\pi \simeq 320$ MeV, $M_K \simeq 580$ MeV, $M_D \simeq 2020$ MeV and two different lattice volumes $L/a = 24$ (empty markers) and $L/a = 32$ (filled markers), respectively. The different shape and color of the markers distinguish between different values of the child meson momentum.*

The behavior observed in Fig. 3.2 might be (at least partially) related to finite size effects (see, e.g., Ref. [70] for the case of $K_{\ell 3}$ decays). The possible impact of FSE has been investigated by comparing the results corresponding to the two gauge ensembles, A40.24 and A40.32, which share the same pion mass and lattice spacing, but have different lattice sizes, $L = 24a$ and $L = 32a$, respectively, as illustrated in Fig. 3.3. It can clearly be seen that for the $D \to \pi(K)$ semileptonic vector and scalar form factors FSE appear to be negligible within the current statistical uncertainties, except for the slope of the $D \to \pi$

scalar form factor (upper right panel in Fig. 3.3). Hypercubic effects for the two gauge ensembles A40.24 and A40.32 are found to be comparable and they do not appear to depend on the lattice size L. Thus, since in our setup all the current matrix elements are $\mathcal{O}(a)$-improved, the breaking of the Lorentz invariance is expected to be produced by $\mathcal{O}(a^2)$ hypercubic effects, whose subtraction will be discussed in the next Section in order to get the Lorentz-invariant semileptonic vector and scalar form factors.

Before closing the Section, it is worth noting that no evidence of hypercubic effects within the current statistical uncertainties was found in the case of the $K \to \pi\ell\nu$ semileptonic form factors analyzed in Ref. [53], where the same gauge configurations and the same parent and child momenta were adopted[5]. This suggests that the hypercubic artefacts may be governed by the difference between the parent and the child meson masses. Such an indication is confirmed by the results given in Fig. 3.4, where the transition between two charmed PS mesons with masses close to the D-meson one has been considered. The momentum dependencies of the corresponding form factors show no evidence of hypercubic effects within the statistical uncertainties. The dependence of hypercubic artefacts upon the mass difference between the parent and the child mesons is clearly a very important issue, which warrants further investigations. It may represent an important warning in the case of the determination of the form factors governing semileptonic B-meson decays into lighter mesons.

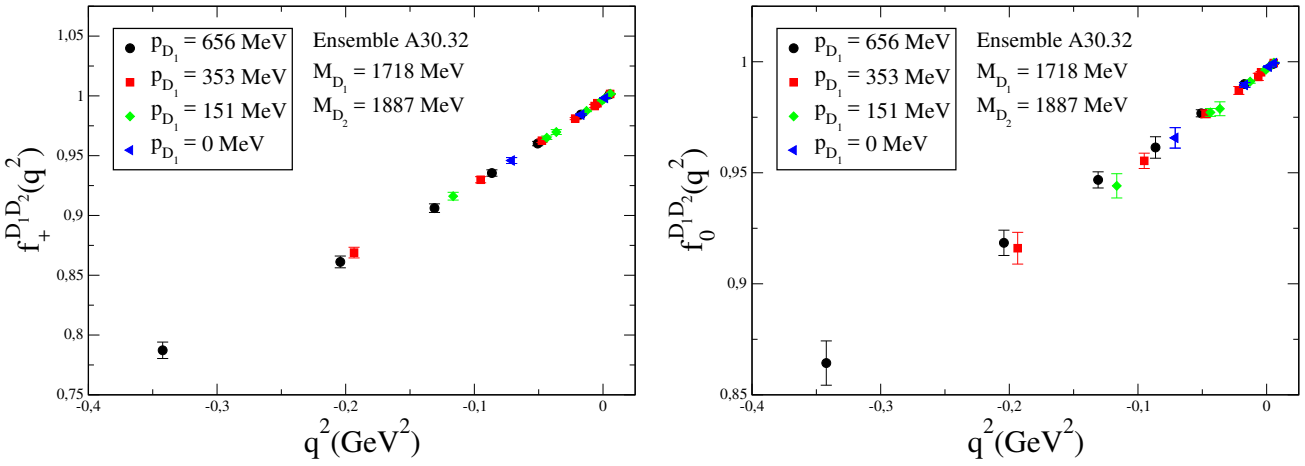

Figure 3.4: *Momentum dependence of the vector (left panel) and scalar (right panel) form factors regulating the semileptonic decay in which the parent and child mesons are two charmed PS mesons, D_1 and D_2, with masses close to the D-meson one. In this plot we have used the gauge ensemble A30.32, in which D_1 and D_2 have masses equal to* 1718 *MeV and* 1887 *MeV, respectively. Different markers and colors distinguish different values of the child meson momentum.*

[5]In Ref. [53] the vector and scalar form factors for the $K_{\ell 3}$ decays have been constructed using local interpolating fields for both the pion and the kaon. We have checked that no hypercubic effects are visible also in the case of smeared interpolating fields.

3.4 Subtraction of the hypercubic effects

As shown in the previous Section the form factors f_+ and f_0 for both the $D \to \pi$ and $D \to K$ decays exhibit a sizeable Lorentz-symmetry breaking due to hypercubic effects generated at finite lattice spacing. In order to find the mathematical expression of these lattice artefacts we have to remember that we are working in an Euclidean space-time, thus physical momenta enter observables directly simulated on the lattice through their Euclidean couterparts. This means that hypercubic effects in the vector and scalar form factors have to be investigated in terms of Euclidean momenta. As shown in Eq. (2.39) we have:[6]

$$q_\mu^E = (\vec{q},\ q_4) = (\vec{q},\ -iq_0)\ , \tag{3.29}$$

so that

$$\sum_\mu q_\mu^E q_\mu^E = -q^2\,. \tag{3.30}$$

Invariant quantities under hypercubic rotations can be constructed using q_μ^E and $P_\mu^E = (p_D + p_P)_\mu^E$ as:

$$q^{[n]}P^{[m]} \equiv \sum_\mu \left(q_\mu^E\right)^n \left(P_\mu^E\right)^m\ . \tag{3.31}$$

For $n+m=2$ we find three invariants, that respect also the Lorentz symmetry, i.e. q^2, $q\cdot P$ and P^2, which can be rewritten in terms of q^2 and the parent and child meson masses. For $n+m=4$ the hypercubic invariants are five:

$$q^{[4]},\quad q^{[3]}P^{[1]},\quad q^{[2]}P^{[2]},\quad q^{[1]}P^{[3]},\quad P^{[4]}\,, \tag{3.32}$$

where $q^{[4]}$ ($P^{[4]}$) stands for $q^{[4]}P^{[0]}$ ($q^{[0]}P^{[4]}$). In this Section we show that hypercubic lattice artifacts in the vector and scalar form factors can all be expressed at the order $\mathcal{O}(a^2)$ in terms of these quantities. The simplest way to do it is to study hypercubic effects not directly on f_+ and f_0, but on the vector and scalar currents, related to the form factors through Eq. (3.26-3.28).

3.4.1 Hypercubic effects in the vector current

As already shown in Fig. 3.2, the form factors $f_{+,0}$ calculated using Eqs. (3.26-3.28) do not depend on q^2 only. A possible way to describe the observed hypercubic effects is to address them directly on the vector and scalar matrix elements. We start by considering the following decomposition of the vector current:

$$\langle P(p_P)|\widehat{V}_\mu^E|D(p_D)\rangle = \langle\widehat{V}_\mu^E\rangle_{\rm Lor} + \langle\widehat{V}_\mu^E\rangle_{\rm hyp}\ , \tag{3.33}$$

in which $\langle\widehat{V}_\mu^E\rangle_{\rm Lor}$ is the Lorentz-covariant term

$$\langle\widehat{V}_\mu^E\rangle_{\rm Lor} = P_\mu^E\ f_+(q^2,a^2) + q_\mu^E\ \frac{M_D^2 - M_P^2}{q^2}\left[f_0(q^2,a^2) - f_+(q^2,a^2)\right]\ , \tag{3.34}$$

[6] We neglect the label M related to Minkowskian (physical) momenta.

while $\langle \widehat{V}_\mu^E \rangle_{\rm hyp}$ is given by

$$\langle \widehat{V}_\mu^E \rangle_{\rm hyp} = a^2 \left[\left(q_\mu^E\right)^3 \; H_1 + \left(q_\mu^E\right)^2 P_\mu^E \; H_2 + q_\mu^E \left(P_\mu^E\right)^2 \; H_3 + \left(P_\mu^E\right)^3 \; H_4 \right] , \tag{3.35}$$

where the quantities H_i ($i = 1, 2, 3, 4$) are additional hypercubic form factors. Note that in the Lorentz-covariant term (3.34) we have explicitly considered that the form factors $f_{+,0}$ can be affected by discretization errors of order $\mathcal{O}(a^2)$, which are unrelated to hypercubic effects and may depend on q^2 as well as on the parent and child meson masses. Eq. (3.35) is the most general structure, up to order $\mathcal{O}(a^2)$, that transforms properly under hypercubic rotations and is built with third powers of the components of the two momenta q_μ^E and P_μ^E. The Lorentz-invariance breaking effects are encoded in the four structures $\left(q_\mu^E\right)^3$, $\left(q_\mu^E\right)^2 P_\mu^E$, $q_\mu^E \left(P_\mu^E\right)^2$ and $\left(P_\mu^E\right)^3$ as well as in the hypercubic form factors H_i, for which we assume a dependence only on q^2 and the parent and child meson masses. Note that the decomposition (3.33-3.35) implies that the form factors $f_{+,0}$ calculated using Eqs. (3.26-3.28) do depend not only on q^2, but also on the five hypercubic invariants $q^{[4]}$, $q^{[3]}P^{[1]}$, $q^{[2]}P^{[2]}$, $q^{[1]}P^{[3]}$, $P^{[4]}$.

For the H_i form factors we adopt a simple polynomial form in terms of the z variable [71, 72]

$$H_i(z) = d_0^i + d_1^i z + d_2^i z^2 , \tag{3.36}$$

where z is defined as

$$z = \frac{\sqrt{t_+ - q^2} - \sqrt{t_+ - t_0}}{\sqrt{t_+ - q^2} + \sqrt{t_+ - t_0}} \tag{3.37}$$

with t_+ and t_0 given by

$$\begin{aligned} t_+ &= (M_D + M_P)^2 , \\ t_0 &= (M_D + M_P) \left(\sqrt{M_D} - \sqrt{M_P}\right)^2 . \end{aligned} \tag{3.38}$$

In Eq. (3.36) the coefficients $d_{0,1,2}^i$ are treated as free parameters.

3.4.2 Hypercubic effects in the scalar density

Let's now turn to the scalar density. As well as for the case of the vector current, we consider for the scalar matrix elements the following decomposition:

$$\langle P(p_P)|S|D(p_D)\rangle = \langle S \rangle_{\rm Lor} + \langle S \rangle_{\rm hyp} , \tag{3.39}$$

where $\langle S \rangle_{\rm Lor}$ is again the Lorentz-invariant term

$$\langle S \rangle_{\rm Lor} = \frac{M_D^2 - M_P^2}{\mu_c - \mu_q} f_0(q^2, a^2) , \tag{3.40}$$

while $\langle S \rangle_{\rm hyp}$ is given by

$$\langle S \rangle_{\rm hyp} = \frac{a^2}{\mu_c - \mu_q} \left[q^{[4]} \; \widetilde{H}_1 + q^{[3]}P^{[1]} \; \widetilde{H}_2 + q^{[2]}P^{[2]} \; \widetilde{H}_3 + q^{[1]}P^{[3]} \; \widetilde{H}_4 + P^{[4]} \widetilde{H}_5 \right] \tag{3.41}$$

with quantities $\widetilde{H}_i$ $(i = 1, 2, 3, 4, 5)$ representing additional hypercubic form factors.

The Ward-Takahashi Identity (WTI) relates the 4-divergence of the vector current to the scalar density. Let's introduce the WTI breaking term $\Delta^{\rm hyp}_{WTI}$ defined as

$$\begin{aligned} \Delta^{\rm hyp}_{WTI} &= (\mu_c - \mu_q)\,\langle P(p_P)|S|D(p_D)\rangle + q^E_\mu\,\langle P(p_P)|\widehat{V}^E_\mu|D(p_D)\rangle \\ &= (\mu_c - \mu_q)\,\langle S\rangle_{\rm hyp} + q^E_\mu\,\langle \widehat{V}^E_\mu\rangle_{\rm hyp} \end{aligned} \tag{3.42}$$

which implies

$$\begin{aligned} \Delta^{\rm hyp}_{WTI} &= a^2\Big[q^{[4]}\,(\widetilde{H}_1 + H_1) + q^{[3]}P^{[1]}\,(\widetilde{H}_2 + H_2) + q^{[2]}P^{[2]}\,(\widetilde{H}_3 + H_3) \\ &+ q^{[1]}P^{[3]}\,(\widetilde{H}_4 + H_4) + P^{[4]}\widetilde{H}_5\Big]\ . \end{aligned} \tag{3.43}$$

The quantity $\Delta^{\rm hyp}_{WTI}$ can be evaluated directly using the matrix elements $\langle\widehat{V}^E_\mu\rangle$ and $\langle S\rangle$. Its dependence on the parent child momenta is illustrated in Fig. 3.5 in the case of the gauge ensemble A30.32. It can be clearly seen that even if the WTI-violating term $\Delta^{\rm hyp}_{WTI}$

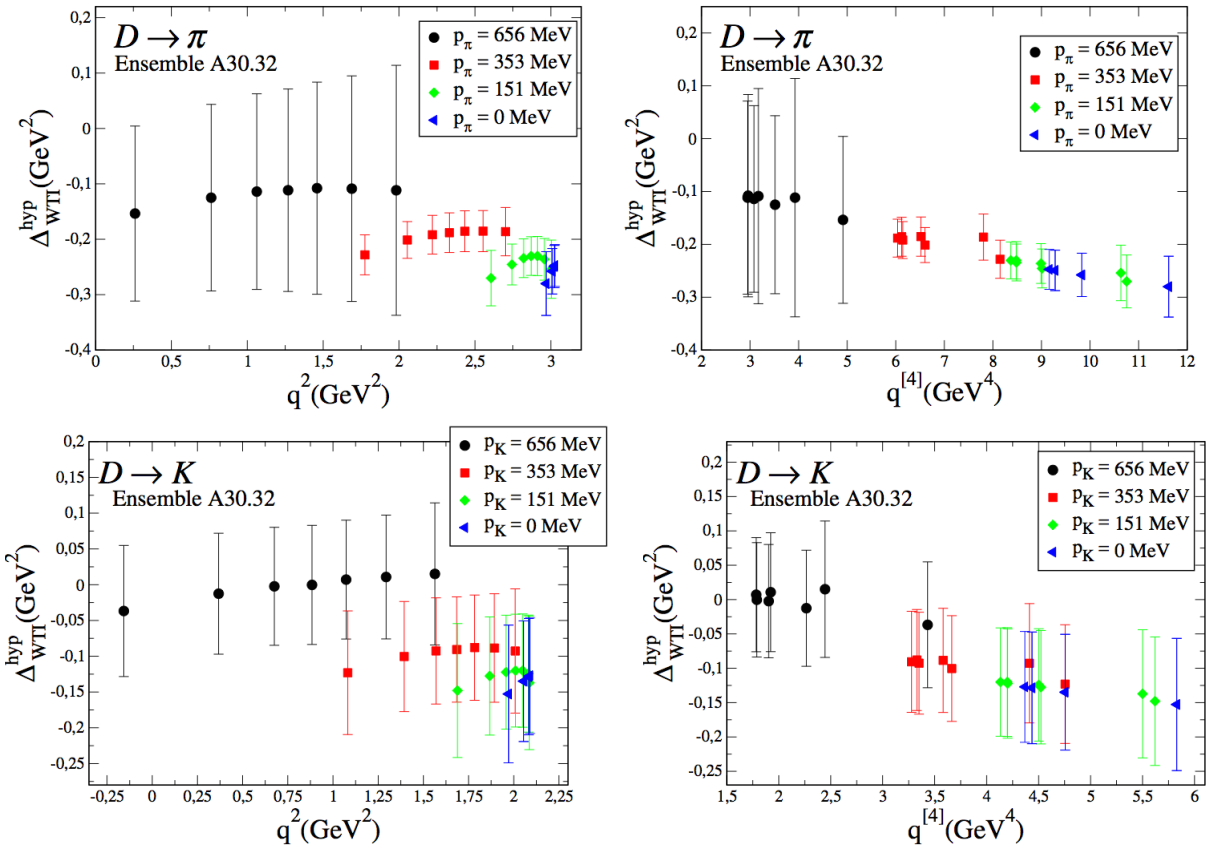

Figure 3.5: *Results for $\Delta^{\rm hyp}_{WTI}$ (see Eq. (3.42)) versus q^2 (left panels) and $q^{[4]}$ (right panels) for the $D \to \pi$ (upper panels) and $D \to K$ (lower panels) transitions in the case of the gauge ensemble A30.32.*

is small, it is different form zero and cannot depend on the Lorentz-invariant q^2 only. Instead lattice data suggest a simple, approximate linear, dependence on the hypercubic invariant $q^{[4]}$ (see right panels in Fig. 3.5). This implies a quite simplified structure for $\Delta^{\rm hyp}_{WTI}$ in Eq. (3.43) and consequently for $\langle S\rangle^{\rm hyp}$ in Eq. (3.41), namely:

$$\begin{cases} \widetilde{H}_i + H_i = 0 \quad \text{for} \quad i = 2,3,4 \\ \widetilde{H}_5 = 0 \\ \widetilde{H}_1 + H_1 = H_S \neq 0 \ . \end{cases} \tag{3.44}$$

In other words one has

$$\Delta^{\rm hyp}_{WTI} = a^2 q^{[4]} H_S \, , \tag{3.45}$$

which implies

$$\langle S\rangle_{\rm hyp} = \frac{a^2}{\mu_c - \mu_q} q^{[4]} \ H_S - \frac{1}{\mu_c - \mu_q} q^E_\mu \ \langle \widehat{V}^E_\mu \rangle_{\rm hyp} \ . \tag{3.46}$$

For the hypercubic form factor H_S we adopt the simple Ansatz

$$H_S = d^S_0 + d^S_1 m_\ell \tag{3.47}$$

with $d^S_{0,1}$ being free parameters.

The structure of the hypercubic artefacts is thus given by Eqs. (3.35) and (3.46) in terms of the five form factors H_i ($i = 1,2,3,4,S$). These quantities cannot be determined in the present work by analyzing the matrix elements of vector and scalar currents separately for each gauge ensemble. A simultaneous, global fit of all the data (more than one thousand lattice points corresponding to the time and spatial components of the vector and scalar matrix elements related to the 15 ETMC gauge ensembles of Tab. 3.1) has to be performed by considering the dependencies on q^2, m_ℓ and a^2 of the form factors $f_{+,0}$ as well as the q^2 and m_ℓ dependencies of the five hypercubic form factors H_i ($i = 1,2,3,4,S$).

3.4.3 Global fit

For the form factors $f_{+,0}(q^2, a^2)$ we have adopted the modified z-expansion of Ref. [73], viz.

$$f_+^{D\to\pi(K)}(q^2,a^2) = \frac{f^{D\to\pi(K)}(0,a^2) + c_+^{D\to\pi(K)}(a^2)\,(z-z_0)\left(1+\frac{z+z_0}{2}\right)}{\mathcal{P}_+^{D\to\pi(K)}(q^2)} \ , \tag{3.48}$$

$$f_0^{D\to\pi(K)}(q^2,a^2) = \frac{f^{D\to\pi(K)}(0,a^2) + c_0^{D\to\pi(K)}(a^2)\,(z-z_0)\left(1+\frac{z+z_0}{2}\right)}{\mathcal{P}_0^{D\to\pi(K)}(q^2)} \ , \tag{3.49}$$

where we assume for the coefficients $c_{+(0)}^{D\to\pi(K)}(a^2)$ a simple linear dependence on a^2 and $z_0 \equiv z(q^2=0)$, so that the condition $f_+(0,a^2) = f_0(0,a^2) = f(0,a^2)$ is explicitly fulfilled at finite lattice spacing. In the r.h.s. of Eqs. (3.48-3.49) the terms at second order in the

z-variable are constrained by the analyticity requirements described in Ref. [73]. As for the functions $\mathcal{P}_{+,0}$, in the case of $D \to \pi$ transition we adopt the single-pole expressions

$$\mathcal{P}_+^{D\to\pi}(q^2) = 1 - \frac{q^2}{M_V^2} \ , \tag{3.50}$$

$$\mathcal{P}_0^{D\to\pi}(q^2) = 1 - K_{FSE}^0(L)\,\frac{q^2}{M_S^2} \ , \tag{3.51}$$

while for the $D \to K$ channel we use

$$\mathcal{P}_+^{D\to K}(q^2) = 1 - \frac{q^2}{M_{D_s^*}^2}\left(1 + P_+ a^2\right) \ , \tag{3.52}$$

$$\mathcal{P}_0^{D\to K}(q^2) = 1 \ . \tag{3.53}$$

In the case of the $D \to \pi$ pole factors (3.50) and (3.51) the quantities M_V and M_S represent the vector and scalar pole masses, respectively. They are treated as free parameters in the fitting procedure. In the case of the $D \to K$ decays the data are fitted equally well even excluding the pole term in the scalar form factor and therefore we choose $\mathcal{P}_0^{D\to K}(q^2) = 1$. Conversely the physical vector meson D_s^* has a mass below the cut threshold $\sqrt{t_+} = (M_{D_s} + M_K)$. Consequently the pole factor (3.52), including a simple discretization effect proportional to a^2, is introduced to guarantee the applicability of the z-expansion.

In Eq. (3.50) the quantity $K_{FSE}^0(L)$ takes into account the FSE observed in Fig. 3.3 by adopting the following phenomenological form

$$K_{FSE}^0(L) = 1 + C_{FSE}^0\ \xi_\ell\ \frac{e^{-M_\pi L}}{M_\pi L} \ , \tag{3.54}$$

where C_{FSE}^0 is a free parameter and $\xi_\ell = 2Bm_\ell/(16\pi^2 f^2)$, with B and f being the SU(2) low-energy constants entering the LO chiral Lagrangian and determined in Ref. [50]. For the vector form factor at zero 4-momentum transfer, $f^{D\to\pi(K)}(0, a^2)$, we use the following Ansatz

$$f^{D\to\pi(K)}(0, a^2) = F_+\left[1 + A^{\pi(K)}\,\xi_\ell \log \xi_\ell + b_1\,\xi_\ell + b_2\,\xi_\ell^2 + D\,a^2\right] \ , \tag{3.55}$$

where the coefficients F_+, b_1, b_2 and D are treated as free parameters in the fitting procedure, while $A^{\pi(K)}$ is the chiral-log coefficient predicted by the hard pion SU(2) Chiral Perturbation Theory (ChPT) [74], given by

$$A^\pi = -\frac{3}{4}\left(1 + 3\widehat{g}^2\right) \ , \qquad A^K = +\frac{1}{2} \ , \tag{3.56}$$

where for the coupling constant $\widehat{g}$ we adopt the value $\widehat{g} = 0.61$ [26].

Using the ingredients described above we have performed the global, combined fit of all the data for the matrix elements $\langle \widehat{V}_0 \rangle$, $\langle \widehat{V}_{sp} \rangle$ and $\langle S \rangle$, which amount to a total of 1110 data points for both the $D \to \pi$ and $D \to K$ transitions. The total number of free parameters is 24 (19) in the case of $D \to \pi(K)$ channel, namely:

- in Eq. (3.55) 3 parameters for $D \to \pi$ (F_+, b_1 and D) and 4 parameters for $D \to K$ (F_+, b_1, b_2 and D);
- in Eq. (3.48) 2 parameters for $c_+^{D\to\pi(K)}$ (i.e., $c_+ = c_+^0 + c_+^1 a^2$);
- in Eq. (3.49) 2 parameters for $c_0^{D\to\pi(K)}$ (i.e., $c_0 = c_0^0 + c_0^1 a^2$);
- 1 parameter (M_V) in Eq. (3.50) for $D \to \pi$ and 1 parameter (P_+) in Eq. (3.52) for $D \to K$;
- 2 parameters in Eqs. (3.51) and (3.54) (M_S and C_{FSE}^0) only for $D \to \pi$,;
- 2 parameters in Eq. (3.47) for the hypercubic form factor H_S;
- in Eq. (3.36) 3 parameters for each of the four hypercubic form factors H_1, H_2, H_3 and H_4 for $D \to \pi$ and 2 parameters (i.e., $d_2^i = 0$) for $D \to K$.

The quality of the fit is quite good obtaining $\chi^2/\text{d.o.f.} \simeq 1.2$ for both the $D \to \pi$ and $D \to K$ transitions. We have tried to include extra terms in Eqs. (3.48-3.49) either proportional to z^2 (including the analiticity requirement of Ref. [73] through an appropriate term proportional to z^3) or proportional to the light-quark mass m_ℓ in the coefficients $c_{+,0}^{D\to\pi(K)}$. Since the differences in the results for both the hypercubic corrections and the form factors $f_{+,0}$ are negligible with respect to the other errors and the values of the new parameters turn out to be consistent with 0, such extended fits are not used for estimating systematic uncertainties.

From the global combined fit we obtain both the momentum dependence of the Lorentz-invariant form factors $f_{+,0}$ and the one of the five hypercubic form factors H_i ($i = 1, 2, 3, 4, S$). The dependence in q^2 of $f_{+,0}$, extrapolated to the physical pion mass and to the continuum and infinite volume limits, will be discussed and compared to the experimental data in Sec. 3.5. Here we compute the hypercubic form factors H_i coming from the global fit in order to check the quality of the subtraction of the hypercubic effects for each gauge ensemble, i.e. at finite lattice spacing and volume and for the unphysical pion masses given in Tab. 3.1. In Fig. 3.6 we show the same form factors given in Fig. 3.2 after the hypercubic contributions determined by the global fit have been subtracted from the matrix elements $\langle \widehat{V}_\mu \rangle$ and $\langle S \rangle$ using Eqs. (3.33) and (3.39). It can be seen that the hypercubic effects are properly removed and both the scalar and the vector form factors depend now only on the 4−momentum transfer q^2 within the statistical uncertainties.

In the limiting case where the parent and the child mesons are the same, Eq. (3.35) reduces to a simpler expression, namely

$$\langle D(p')|\widehat{V}_\mu^E|D(p)\rangle_{\text{hyp}} = a^2 \left[\left(q_\mu^E\right)^2 P_\mu^E H_2 + \left(P_\mu^E\right)^3 H_4 \right] , \tag{3.57}$$

because only even terms under the exchange of the initial and final PS mesons survive. In Sec. 3.3 we have noted that within the statistical uncertainties there is no evidence of hypercubic effects when the initial and final meson have the same masses (see Fig. 3.4). This might be an indication that the hypercubic form factors H_2 and H_4 can be neglected.

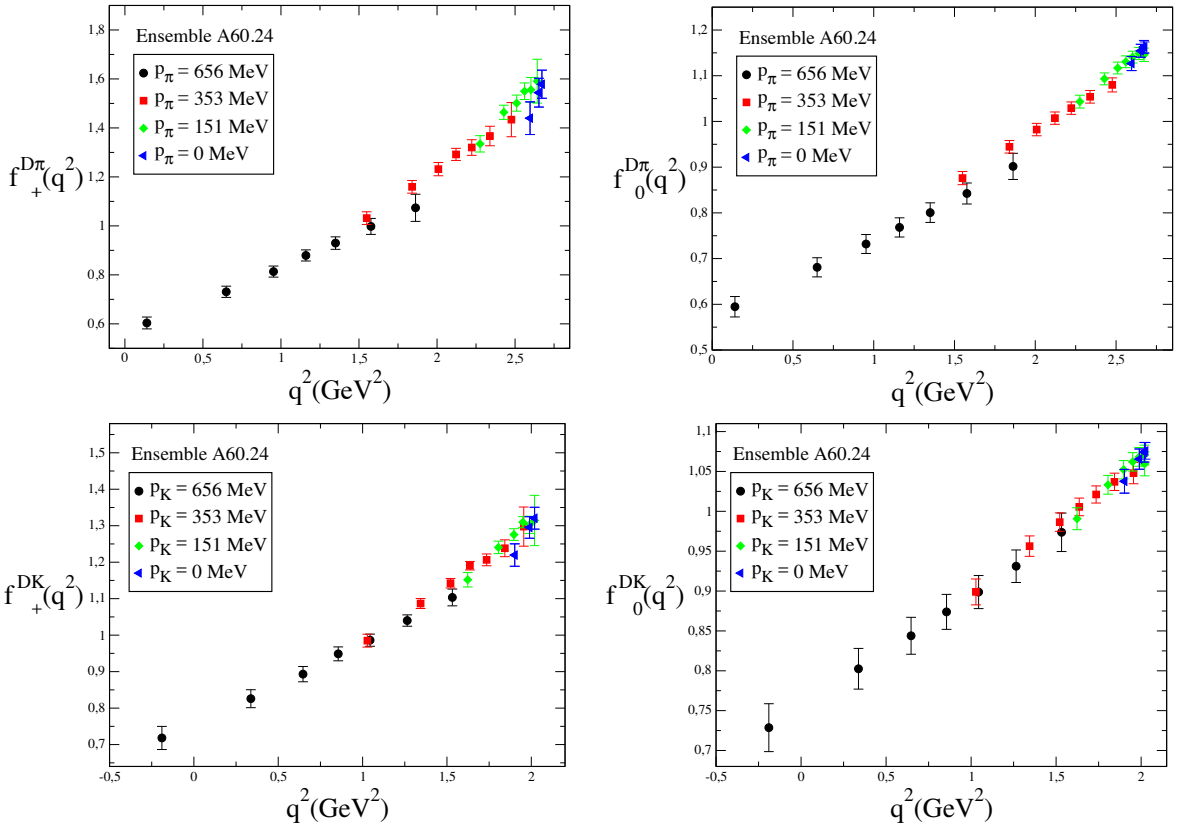

Figure 3.6: *The same as in Fig. 3.2, but after correcting for the hypercubic effects determined in the global fitting procedure using Eqs. (3.33) and (3.39). Different markers and colors distinguish different values of the child meson momentum.*

Thus, we have repeated the global fitting procedure assuming $H_2 = H_4 = 0$, which reduces the number of free parameters to 18 and 15 for the $D \to \pi$ and $D \to K$ transitions, respectively. The differences in the results for both the hypercubic corrections and the form factors $f_{+,0}$, obtained including ($H_2 \neq H_4 \neq 0$) or excluding ($H_2 = H_4 = 0$) the two hypercubic form factors H_2 and H_4 are found to be negligible within the current statistical uncertainties. Therefore, in what follows we adopt the fitting procedure in which we assume $H_2 = H_4 = 0$ as our reference fit for estimating uncertainties due to various sources of systematic errors as well as for obtaining results for the form factors $f_{+,0}^{D\to\pi(K)}(q^2)$.

We stress again that an important feature of our analysis with respect to previous studies of the semileptonic $D \to \pi(K)$ form factors is the use of a plenty of kinematical conditions corresponding to parent and child mesons either moving or at rest. Using only a limited number of kinematical conditions, for instance the Breit-frame in which $\vec{p_D} = -\vec{p}_{\pi(K)}$ or the $D-$meson at rest, the presence of the hypercubic effects may not be manifest. This point is illustrated in Fig. 3.7, which shows the subset of our data for the scalar $D \to \pi$ (left panel) and $D \to K$ (right panel) form factor f_0 corresponding only to the D-meson at rest both before and after the subtraction of the hypercubic effects

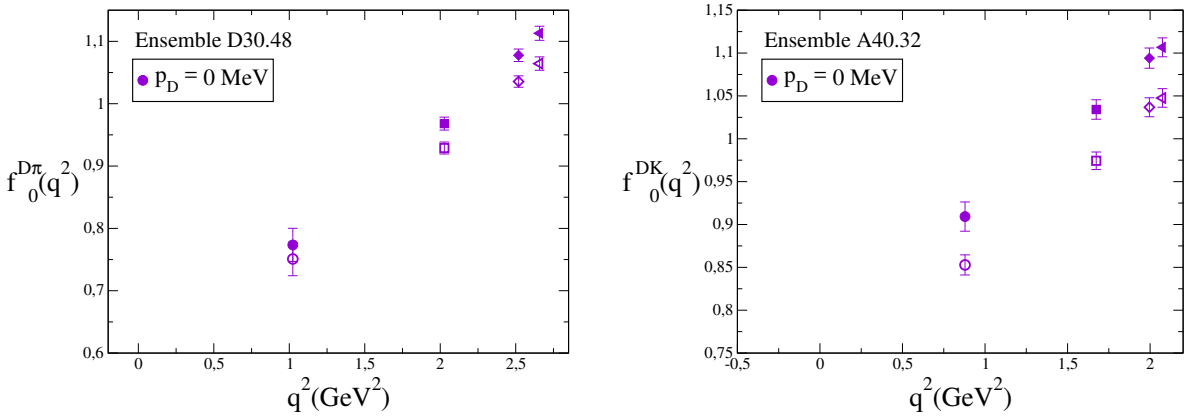

Figure 3.7: *Left panel: the scalar form factor $f_0^{D\pi}(q^2)$ corresponding to the kinematical conditions with the $D-$meson at rest for the gauge ensemble D30.48. Hollow and filled points represent, respectively, the data before and after the removal of the hypercubic effects determined in the global fitting procedure. Right panel: the same as in the left panel, but for $f_0^{DK}(q^2)$ in the case of ensemble A40.32*

determined in the global fitting procedure. Lorentz-symmetry breaking is not manifest in the limited set of data points with $\vec{p}_D = 0$, but it is not negligible. This holds for the scalar form factor f_0, while in the case of the vector form factor f_+ we find that Lorentz-symmetry breaking effects are less pronounced in the subset of data corresponding to the D-meson at rest. We stress that the differences between the data with and without hypercubic effects are a $\mathcal{O}(a^2)$ effect proportional to hypercubic invariants. Thus, any analysis of the data without the subtraction of hypercubic effects, based directly on parameterizations like Eqs. (3.48-3.49), where only discretization effects unrelated to hypercubic invariants are considered, is in principle inadequate and may lead to different results in the continuum limit.

3.5 Global fit results

The momentum dependencies of the physical Lorentz-invariant vector and scalar form factors, extrapolated to the physical pion mass and to the continuum and infinite volume limits, are shown in Fig. 3.8 for both the $D \to \pi$ and $D \to K$ transitions. Our results exhibit a remarkable precision in the full range of values of q^2 covered by the experiments (i.e., $0 \leq q^2 \leq q^2_{\rm max} = (M_D - M_{\pi(K)})^2 \simeq 3.0(1.9)$ GeV^2). Our results for the vector form factors $f_+^{D\pi}(q^2)$ and $f_+^{DK}(q^2)$ can be compared with the corresponding values determined by BELLE, BABAR, CLEO and BESIII collaborations in Refs. [6, 7, 8, 9, 10], where the partial decay rates have been measured (see also Refs. [75, 76] for a summary of the experimental results). The agreement is good except at high values of q^2, where some deviations are visible.

In Fig. 3.9 our main results for the vector and scalar form factors are compared with those obtained by choosing only the kinematical configurations corresponding to the D-meson rest frame and by performing the extrapolations to the physical pion mass and to

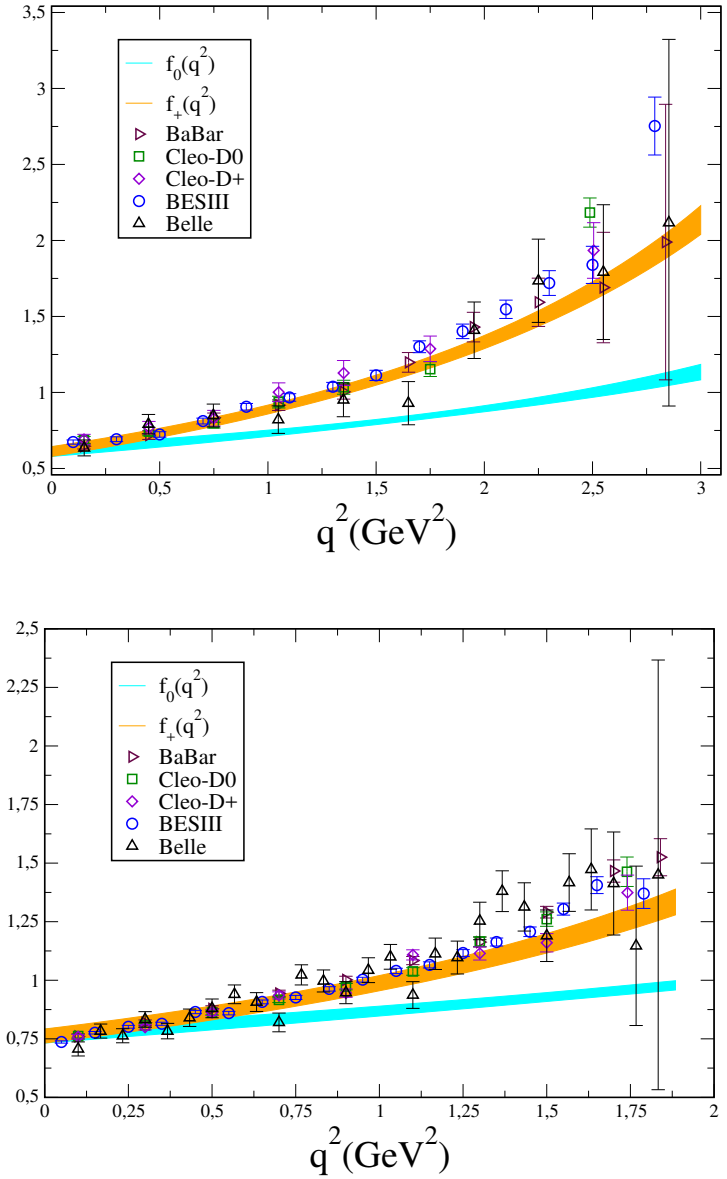

Figure 3.8: *Momentum dependencies of the Lorentz-invariant form factors $f_+(q^2)$ (orange bands) and $f_0(q^2)$ (cyan bands), extrapolated to the physical pion mass and to the continuum and infinite volume limits, for the $D \to \pi$ (left panel) and $D \to K$ (right panel) transitions, including their total uncertainties. For comparison, the values of $f_+^{D\pi(K)}(q^2)$ determined by BELLE, BABAR, CLEO and BESIII collaborations in Refs. [6, 7, 8, 9, 10] are shown. The bands correspond to the total (statistical + systematic) uncertainty at one standard-deviation level.*

the continuum and infinite volume limits without including the hypercubic terms (3.35) and (3.41). In other words, the continuum extrapolation is based only on the discretization terms contained in Eqs. (3.48-3.49). It can be seen that the neglect of hypercubic effects in the analysis and the use of a limited subset of data lead to some distortions of the

extrapolated form factors, which are more pronounced in the case of the scalar form factor. Such distortions are found to be comparable with present global uncertainties within one standard-deviation. They may become more relevant as the precision of the data will be increased in the future.

In Tab. 3.5 we provide a set of synthetic data points for the vector and scalar $D \to \pi$ form factors, $f_+^{D\pi}(q^2)$ and $f_0^{D\pi}(q^2)$, with the corresponding total uncertainties, calculated at eight selected values of q^2 between 0 and $q^2_{\rm max} = (M_D - M_\pi)^2$. The errors in Tab. 3.5 take into account the uncertainties induced by:

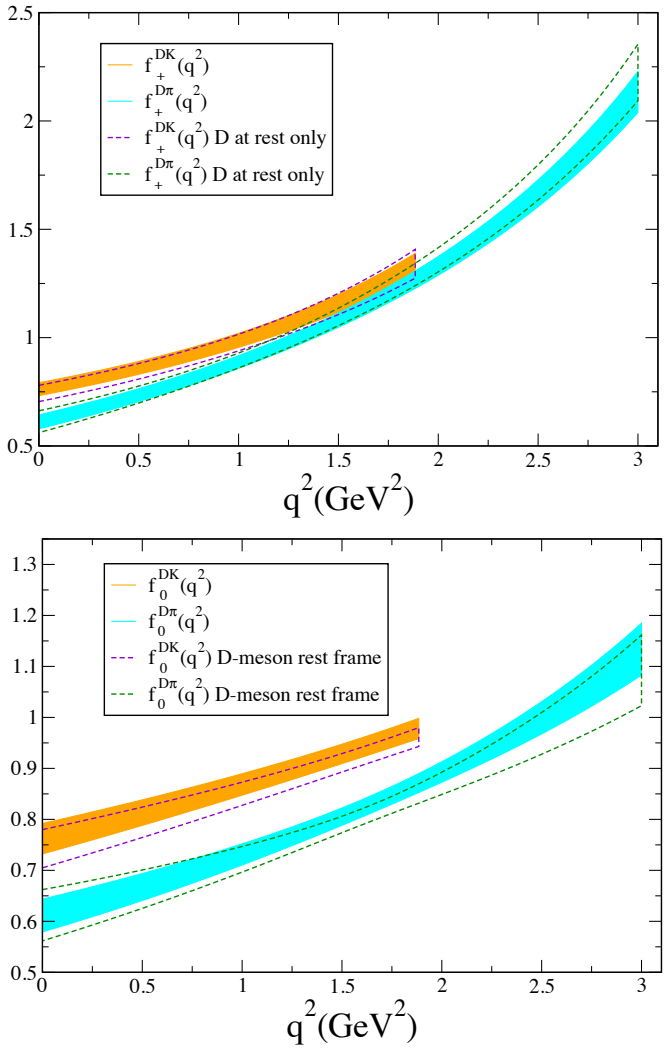

Figure 3.9: *Comparison of the vector and scalar form factors, extrapolated to the physical pion mass and to the continuum and infinite volume limits, obtained either by choosing all the kinematical configurations and including the hypercubic terms (3.35) and (3.41) in the analysis (solid lines) or by limiting to the kinematical configurations corresponding to the D-meson rest frame without considering the subtraction of hypercubic effects (dashed lines). The bands correspond to the total uncertainty at one standard-deviation level.*

q^2 (GeV^2)	$f_+(q^2)$	$f_0(q^2)$
0.0	0.612 (35) (4) (7) (1) [35]	0.612 (35) (4) (7) (1) [35]
0.4286	0.715 (31) (4) (6) (1) [32]	0.659 (29) (4) (5) (1) [30]
0.8571	0.840 (29) (3) (6) (1) [30]	0.713 (24) (3) (3) (1) [24]
1.2857	0.991 (29) (4) (6) (1) [30]	0.773 (18) (4) (2) (1) [19]
1.7143	1.179 (34) (10) (3) (1) [35]	0.842 (15) (4) (5) (1) [17]
2.1429	1.415 (43) (15) (8) (1) [47]	0.922 (19) (5) (8) (1) [21]
2.5714	1.721 (60) (21) (16) (1) [66]	1.017 (29) (7) (13) (1) [32]
3.0000	2.130 (86) (31) (27) (3) [96]	1.134 (45) (10) (18) (1) [49]

Table 3.5: *Synthetic data points for the transition $D \to \pi$ representing our results for the vector and scalar form factors extrapolated to the physical pion point and to the continuum and infinite volume limits for eight selected values of q^2 in the range between $q^2 = 0$ and $q^2 = q^2_{max} = (M_D - M_\pi)^2 \simeq 3.0$ GeV^2. The errors correspond to the uncertainties related to (statistical + fitting procedure + input parameters), chiral extrapolation, FSEs and discretization effects, respectively (see text). The errors in squared brackets correspond to the combination in quadrature of the statistical and all systematic errors.*

- the statistical noise and the fitting procedure;
- the errors in the determinations of the input parameters, namely the values of the average u/d quark mass m_{ud} the value of the charm quark mass m_c, the lattice spacing a and the $SU(2)$ ChPT LECs f and B_0, determined in Ref. [50];
- the chiral extrapolation, evaluated combining the results obtained using the SU(2) ChPT fit on all our lattice data and a fit with $b_2 = 0$ in Eq. (3.55) applied only to the data with $M_\pi < 390$ MeV[7];
- the FSE, evaluated by comparing the results obtained with and without the FSE factor (3.54);
- the discretization effects, calculated by comparing our main results with those obtained including in Eqs. (3.48-3.49) extra terms proportional to $(a\Lambda_{\rm QCD})^4$. Using a value for Λ_{QCD} equal to $\simeq 0.35$ GeV, we expect that the values of the coefficients of the extra terms are in a natural range of order $\mathcal{O}(1)$. Therefore, we adopt for the coefficients of the extra terms a (conservative) prior distribution equal to 0 ± 3.

Similarly, in Tab. 3.6 we provide a set of synthetic data points for the vector and scalar $D \to K$ form factors, $f_+^{DK}(q^2)$ and $f_0^{DK}(q^2)$, with the corresponding total uncertainties for eight selected values of q^2 between 0 and $q^2_{\rm max} = (M_D - M_K)^2$. Note that, at variance with the case of the $D \to \pi$ transition, the uncertainty related to FSE is not considered, because the data for the $D \to K$ transition do not show any visible volume effect. In

[7] In this case the total number of data values reduces to 814, since the results for the gauge ensembles A80.24, A100.24, B85.24 and B75.32 (see Tab. 3.1) are excluded from the analysis.

q^2 (GeV^2)	$f_+(q^2)$	$f_0(q^2)$
0.0	0.765 (29) (11) (1) [31]	0.765 (29) (11) (1) [31]
0.2692	0.815 (28) (12) (1) [31]	0.792 (26) (10) (1) [28]
0.5385	0.872 (28) (13) (1) [31]	0.820 (23) (10) (1) [25]
0.8077	0.937 (28) (15) (1) [32]	0.849 (21) (9) (1) [23]
1.0769	1.013 (29) (17) (1) [34]	0.879 (19) (9) (1) [21]
1.3461	1.102 (32) (21) (1) [38]	0.911 (17) (9) (1) [19]
1.6154	1.208 (36) (26) (1) [44]	0.944 (17) (8) (1) [19]
1.8846	1.336 (43) (32) (1) [54]	0.979 (17) (8) (1) [19]

Table 3.6: *Synthetic data points for the $D \to K$ transition representing our results for the vector and scalar form factors extrapolated to the physical pion point and in the continuum and infinite volume limits for eight selected values of q^2 in the range between $q^2 = 0$ and $q^2 = q^2_{max} = (M_D - M_K)^2 \simeq 1.88$ GeV^2. The errors correspond to the uncertainties related to (statistical + fitting procedure + input parameters), chiral extrapolation and discretization effects, respectively (see text). The errors in squared brackets correspond to the combination in quadrature of the statistical and all systematic errors.*

order to allow a direct employment of synthetic data points contained in Tabs. 3.5 and 3.6 without using our bootstrap samples, we have calculated the corresponding covariance matrices, which are available upon request. Furthermore, we provide in the Appendix, for the form factors $f_{+,0}^{D\to\pi(K)}$, the values of the parameters of the z-expansions of our global fit after the extrapolations to the physical pion point and to the continuum and infinite volume limits, including covariance matrices.

From Tab. 3.5 and 3.6 our results at zero 4-momentum transfer are

$$f_+^{D\to\pi}(0) = 0.612\ (35) \qquad , \qquad f_+^{D\to K}(0) = 0.765\ (31)\ , \tag{3.58}$$

which are consistent within the errors with the FLAG [5] averages $f_+^{D\to\pi}(0) = 0.666\ (29)$, based on the result of Ref. [24], and $f_+^{D\to K}(0) = 0.747\ (19)$ from Ref. [25]. Using experimental values

$$|V_{cd}| f_+^{D\pi}(0) = 0.1426\ (19) \quad , \qquad |V_{cs}| f_+^{DK}(0) = 0.7226\ (34)\ , \tag{3.59}$$

given by HFAV in Ref. [15], we can get for the CKM matrix elements $|V_{cd}|$ and $|V_{cs}|$ the results:

$$|V_{cd}| = 0.2330\ (133)_{\rm lat}\ (31)_{\rm exp} = 0.2330\ (137)\ , \tag{3.60}$$

$$|V_{cs}| = 0.945\ (38)_{\rm lat}\ (4)_{\rm exp} = 0.945\ (38)\ , \tag{3.61}$$

where the errors are from the lattice calculation and from the experiments respectively, showing that the dominant error is the theoretical one. Our results (3.60,3.61) can be compared with the determinations of $|V_{cd}|$ and $|V_{cs}|$ based on the D and D_s leptonic decay

constants, $f_D = 207.4(3.8)$ MeV and $f_{D_s} = 247.2(4.1)$ MeV, obtained in Ref. [51] using the same ETMC gauge configurations. Using the experimental values of $f_D|V_{cd}| = 46.06(1.11)$ MeV and $f_{D_s}|V_{cs}| = 250.66(4.48)$ MeV from Ref. [77] one gets

$$|V_{cd}| = 0.2221\ (41)_{\rm lat}\ (54)_{\rm exp} = 0.2221\ (68)\ , \tag{3.62}$$

$$|V_{cs}| = 1.014\ (17)_{\rm lat}\ (18)_{\rm exp} = 1.014\ (25)\ , \tag{3.63}$$

where again the errors are from the lattice calculation and from the experiments, respectively. At variance with the semileptonic case, the theoretical uncertainties of $|V_{cd}|$ and $|V_{cs}|$, obtained from the leptonic decays, are comparable to (or even smaller than) the experimental ones.

An alternative way to extract the CKM matrix elements $|V_{cd}|$ and $|V_{cs}|$ is to combine directly the momentum dependence of the semileptonic form factors obtained from lattice QCD simulations with the experimental q^2-bins of the differential $D \to \pi(K)\ell\nu_\ell$ decay rates. The application of such a strategy (see Ref. [19]) is presented in the next Section. Using $|V_{cb}| = 0.0360(9)$ from Ref. [26] we can perform the check of the unitarity of the second row of the CKM matrix. We find

$$|V_{cd}|^2 + |V_{cs}|^2 + |V_{cb}|^2 = 0.949\ (78) \qquad \text{from semileptonic decays}\ , \tag{3.64}$$

$$|V_{cd}|^2 + |V_{cs}|^2 + |V_{cb}|^2 = 1.079\ (54) \qquad \text{from leptonic decays}\ , \tag{3.65}$$

which test the second-row unitarity at the level of several percent for both semileptonic and leptonic modes.

3.6 Extraction of $|V_{cd(s)}|$ using momentum dependence of $f_+^{D\to\pi(K)}$

The starting point is the partial decay rate provided by each experiment for various bins of values of q^2 (i.e., $q_i^2 \pm \Delta q_i^2/2$ for $i = 1,\ ...,\ N_{bins}$). By integrating Eq. (1.68) in each experimental bin one has

$$\begin{aligned}\left[\Delta\Gamma(q_i^2)\right]^{\rm EXP} &\equiv \int_{\Delta q_i^2} dq^2 \frac{d\Gamma(D\to P\ell\nu)}{dq^2} = \\ &= \frac{G_F^2\,|V_{cx}|^2}{24\pi^3}\int_{\Delta q_i^2} dq^2\,|\vec{p}_P|^3\left|f_+^{DP}(q^2)\right|^2 ,\end{aligned} \tag{3.66}$$

where the r.h.s. contains the phase-space integral over the vector form factor, viz.

$$I(q_i^2) \equiv \int_{\Delta q_i^2} dq^2\,|\vec{p}_P|^3\left|f_+^{DP}(q^2)\right|^2\ . \tag{3.67}$$

Using the results of the global fit for the vector form factors $f_+^{D\pi(K)}(q^2)$, we can combine the theoretical predictions for $[I(q_i^2)]^{\rm LAT}$ of Eq. (3.67) with experimental measurements

of the partial decay rate (3.66) and get a determination of $|V_{cd(s)}|$ for each experimental q^2-bin:

$$\left|V_{cx}(q_i^2)\right|^2 = \frac{24\pi^3}{G_F^2}\frac{[\Delta\Gamma(q_i^2)]^{\rm EXP}}{[I(q_i^2)]^{\rm LAT}} \ . \tag{3.68}$$

The values of $[\Delta\Gamma(q_i^2)]^{\rm EXP}$ measured by BABAR [7, 8], CLEO [9] and BESIII [10] collaborations are collected in Tabs. 3.7 and 3.8 for the $D \to \pi$ and $D \to K$ semileptonic decays respectively. In the case of the BELLE experiment [6] the only available data are the values of $|V_{cd}|f_+^{D\pi}(q_i^2)$ and $|V_{cs}|f_+^{DK}(q_i^2)$, which can be used to extract $|V_{cd(s)}|$ adopting the lattice determinations of $f_+^{D\pi(K)}(q^2)$ at the center of each q^2-bin. This strategy is less consistent with respect to the one used for all the other experiments, since BELLE data for $|V_{cd(s)}|f_+^{D\pi(K)}(q_i^2)$ come from a variety of shapes adopted for the vector form factors. The values reported by BELLE are listed in Tabs. 3.9 and 3.10 for $D \to \pi$ and $D \to K$ semileptonic decays respectively.

Combining the BABAR, CLEO and BESIII data from Tabs. 3.7-3.8 with the theoretical results for $[I(q_i^2)]^{\rm LAT}$ and the BELLE data from Tabs. 3.9-3.10 with the theoretical values for $f_+^{DP}(q_i^2)$, we get a determination of the CKM matrix element $|V_{cd}|$ and $|V_{cs}|$ for each experimental bin. The results are shown in Fig. 3.10 for both $|V_{cd}|$ and $|V_{cs}|$. The data are strongly correlated since, among the various q^2-bins, theoretical values of $[I(q_i^2)]^{\rm LAT}$ as well as the values of $[\Delta\Gamma(q_i^2)]^{\rm EXP}$ coming from the same experiment are correlated. Thus, on the one hand side, in order to take into account the correlations of the experimental data we have calculated a global covariance matrix obtained by combining the separate covariance matrices given by BABAR, CLEO and BESIII collaborations in Refs. [7, 8, 9, 10]. No covariance matrix is provided for the BELLE data on $|V_{cd(s)}|f_+^{D\to\pi(K)}(q_i^2)$ in Ref. [6]. We treated them as uncorrelated. On the other hand side, the correlations among the lattice values of $[I(q_i^2)]^{\rm LAT}$ have been taken into account using the bootstrap samplings. It turns out that in our analysis the correlations are largely dominated by lattice data.

The determinations of $|V_{cd}|$ and $|V_{cs}|$ for the various q^2-bins exhibit an approximate constant behavior, except for $|V_{cs}|$ in the high-q^2 region, where some deviations are visible. The results of the constant fit, including all q^2-bins, for the CKM matrix elements $|V_{cd}|$ and $|V_{cs}|$ are:

$$|V_{cd}| = 0.2345\ (83) \qquad , \qquad |V_{cs}| = 0.978\ (35)\,. \tag{3.69}$$

In order to check the stability of these results we have also performed a series of constant fits including only the data below each given value of q^2. The orange bands in Fig. 3.10 show the results of these fits for $|V_{cd}|$ and $|V_{cs}|$ as a function of q^2. It can be seen that the variations of $|V_{cd}|$ and $|V_{cs}|$ are well within the uncertainties.
Results (3.69) can be compared with

$$|V_{cd}| = 0.2330\ (137) \qquad , \qquad |V_{cs}| = 0.945\ (38)\ , \tag{3.70}$$

reported in Eqs. (3.60,3.61), obtained using the values of the vector form factor at $q^2 = 0$ and the experimental results for $|V_{cd}|f_+^{D\to\pi}(0)$ and $|V_{cs}|f_+^{D\to K}(0)$ provided by HFAG [15]. It turns out that the uncertainty of $|V_{cd}|$ in Eq. (3.69) is smaller by $\approx 40\%$ with respect to the corresponding uncertainty in Eq. (3.70), while for $|V_{cs}|$ such a reduction is marginal. This

Experiment	q^2 (GeV^2)	$[\Delta\Gamma(q^2)]^{\rm EXP}\cdot 10^{16}$ (GeV)
BABAR	(0.00, 0.30)	8.09 ± 0.46
	(0.30, 0.60)	7.51 ± 0.59
	(0.60, 0.90)	7.31 ± 0.53
	(0.90, 1.20)	6.15 ± 0.46
	(1.20, 1.50)	4.88 ± 0.46
	(1.50, 1.80)	4.28 ± 0.46
	(1.80, 2.10)	3.39 ± 0.46
	(2.10, 2.40)	1.98 ± 0.40
	(2.40, 2.70)	0.77 ± 0.33
	(2.70, 2.98)	0.14 ± 0.13
CLEO D^0	(0.00, 0.30)	9.16 ± 0.66
	(0.30, 0.60)	8.04 ± 0.59
	(0.60, 0.90)	6.72 ± 0.53
	(0.90, 1.20)	6.46 ± 0.53
	(1.20, 1.50)	5.21 ± 0.46
	(1.50, 2.00)	5.54 ± 0.46
	(2.00, 2.98)	5.27 ± 0.46
CLEO D^+	(0.00, 0.30)	4.68 ± 0.46
	(0.30, 0.60)	4.35 ± 0.46
	(0.60, 0.90)	3.69 ± 0.46
	(0.90, 1.20)	3.76 ± 0.46
	(1.20, 1.50)	3.16 ± 0.46
	(1.50, 2.00)	3.56 ± 0.46
	(2.00, 3.01)	2.44 ± 0.46
BESIII	(0.00, 0.20)	6.14 ± 0.25
	(0.20, 0.40)	5.38 ± 0.24
	(0.40, 0.60)	4.81 ± 0.24
	(0.60, 0.80)	4.89 ± 0.23
	(0.80, 1.00)	4.83 ± 0.23
	(1.00, 1.20)	4.28 ± 0.22
	(1.20, 1.40)	3.74 ± 0.20
	(1.40, 1.60)	3.17 ± 0.19
	(1.60, 1.80)	3.08 ± 0.18
	(1.80, 2.00)	2.42 ± 0.16
	(2.00, 2.20)	1.86 ± 0.14
	(2.20, 2.40)	1.32 ± 0.13
	(2.40, 2.60)	0.75 ± 0.10
	(2.60, 2.98)	0.62 ± 0.09

Table 3.7: *Values of the partial decay rates* $[\Delta\Gamma(q^2)]^{\rm EXP}$ *for the* $D\to\pi$ *transition in the* q^2*-bins measured by BABAR [7], CLEO [9] and BESIII [10] collaborations. CLEO data are separately given for the* $D^0\to\pi^-\ell\nu$ *and* $D^+\to\pi^0\ell\nu$ *channels.*

Experiment	q^2 (GeV^2)	$[\Delta\Gamma(q^2)]^{\rm EXP}\cdot 10^{15}$ (GeV)
BABAR	(0.00, 0.20)	11.69 ± 0.34
	(0.20, 0.40)	10.72 ± 0.32
	(0.40, 0.60)	9.50 ± 0.27
	(0.60, 0.80)	8.16 ± 0.24
	(0.80, 1.00)	6.53 ± 0.20
	(1.00, 1.20)	5.09 ± 0.16
	(1.20, 1.40)	3.51 ± 0.13
	(1.40, 1.60)	2.14 ± 0.08
	(1.60, 1.80)	0.85 ± 0.06
	(1.80, 1.88)	0.041 ± 0.004
CLEO D^0	(0.00, 0.20)	11.74 ± 0.28
	(0.20, 0.40)	10.43 ± 0.26
	(0.40, 0.60)	9.17 ± 0.23
	(0.60, 0.80)	7.70 ± 0.21
	(0.80, 1.00)	6.17 ± 0.19
	(1.00, 1.20)	4.67 ± 0.16
	(1.20, 1.40)	3.52 ± 0.13
	(1.40, 1.60)	2.04 ± 0.10
	(1.60, 1.88)	0.84 ± 0.08
CLEO D^+	(0.00, 0.20)	11.72 ± 0.43
	(0.20, 0.40)	10.29 ± 0.39
	(0.40, 0.60)	9.24 ± 0.36
	(0.60, 0.80)	8.09 ± 0.32
	(0.80, 1.00)	5.88 ± 0.27
	(1.00, 1.20)	5.38 ± 0.24
	(1.20, 1.40)	3.27 ± 0.18
	(1.40, 1.60)	1.76 ± 0.12
	(1.60, 1.88)	0.78 ± 0.09
BESIII	(0.00, 0.10)	5.807 ± 0.076
	(0.10, 0.20)	5.762 ± 0.081
	(0.20, 0.30)	5.466 ± 0.082
	(0.30, 0.40)	4.987 ± 0.080
	(0.40, 0.50)	4.933 ± 0.079
	(0.50, 0.60)	4.248 ± 0.074
	(0.60, 0.70)	4.086 ± 0.072
	(0.70, 0.80)	3.637 ± 0.069
	(0.80, 0.90)	3.313 ± 0.065
	(0.90, 1.00)	2.982 ± 0.062
	(1.00, 1.10)	2.618 ± 0.057
	(1.10, 1.20)	2.192 ± 0.053
	(1.20, 1.30)	1.864 ± 0.049
	(1.30, 1.40)	1.508 ± 0.044
	(1.40, 1.50)	1.145 ± 0.039
	(1.50, 1.60)	0.866 ± 0.034
	(1.60, 1.70)	0.565 ± 0.029
	(1.70, 1.88)	0.250 ± 0.023

Table 3.8: *Values of the partial decay rates* $[\Delta\Gamma(q^2)]^{\rm EXP}$ *for the* $D\to K$ *transition in the* q^2*-bins measured by BABAR [8], CLEO [9] and BESIII [10]. CLEO data are separately given for the* $D^0\to K^-\ell\nu$ *and* $D^+\to K^0\ell\nu$ *channels.*

Experiment	q_i^2 (GeV^2)	$\lvert V_{cd}\rvert f_+^{D\pi}(q_i^2)$
BELLE	0.15	0.145 ± 0.012
	0.45	0.181 ± 0.015
	0.75	0.194 ± 0.017
	1.05	0.188 ± 0.020
	1.35	0.219 ± 0.024
	1.65	0.213 ± 0.033
	1.95	0.325 ± 0.043
	2.25	0.400 ± 0.062
	2.55	0.413 ± 0.101
	2.85	0.490 ± 0.282

Table 3.9: *Values of $|V_{cd}|f_+^{D\pi}(q_i^2)$ from the BELLE collaboration [6], collected in Ref. [75].*

Experiment	q_i^2 (GeV^2)	$\lvert V_{cd}\rvert f_+^{DK}(q_i^2)$
BELLE	0.10	0.688 ± 0.029
	0.17	0.762 ± 0.029
	0.23	0.743 ± 0.029
	0.30	0.811 ± 0.032
	0.37	0.762 ± 0.032
	0.43	0.817 ± 0.036
	0.50	0.856 ± 0.039
	0.57	0.915 ± 0.039
	0.63	0.882 ± 0.039
	0.70	0.798 ± 0.039
	0.77	0.996 ± 0.042
	0.83	0.970 ± 0.045
	0.90	0.921 ± 0.045
	0.97	1.015 ± 0.052
	1.03	1.070 ± 0.052
	1.10	0.911 ± 0.055
	1.17	1.083 ± 0.065
	1.23	1.067 ± 0.068
	1.30	1.219 ± 0.078
	1.37	1.343 ± 0.084
	1.43	1.278 ± 0.101
	1.50	1.158 ± 0.107
	1.57	1.378 ± 0.120
	1.63	1.433 ± 0.169
	1.70	1.375 ± 0.214
	1.77	1.116 ± 0.331
	1.83	1.411 ± 0.892

Table 3.10: *Values of $|V_{cs}|f_+^{DK}(q_i^2)$ from the BELLE collaboration [6], collected in Ref. [76].*

is largely due to the higher degree of the correlations among the theoretical values of the vector form factor $f_+(q^2)$ in the various q^2-bins in the case of the $D \to K$ transition with respect to the $D \to \pi$ one. Moreover, the central value of $|V_{cs}|$ in Eq. (3.69) is larger than the corresponding one in Eq. (3.70) by approximately one standard deviation. We stress that the same theoretical input from LQCD is used for describing the shape of the vector form factor $f_+^{D\pi(K)}(q^2)$ in all the experimental data, obtaining in this way a consistent SM analysis. The impact of the above consistency might become more significant as the precision of LQCD calculations of the semileptonic form factors will be improved in the future. Thus, the theoretical information on $f_+^{D\pi(K)}(q^2)$ in the full q^2-range allows not only to guarantee a consistent extraction of $|V_{cd}|$ and $|V_{cs}|$ within the SM, but also to get a more precise determination of $|V_{cd}|$.

Within present uncertainties our semileptonic results (3.69) are consistent with the determinations of Eqs. (3.62,3.63) obtained from experimental D and D_s leptonic decay rates [77], adopting the ETMC results [51] for the decay constants f_D and f_{D_s}. In Fig. 3.11 the above results from leptonic and semileptonic $D-$meson decays are reported as ellipses

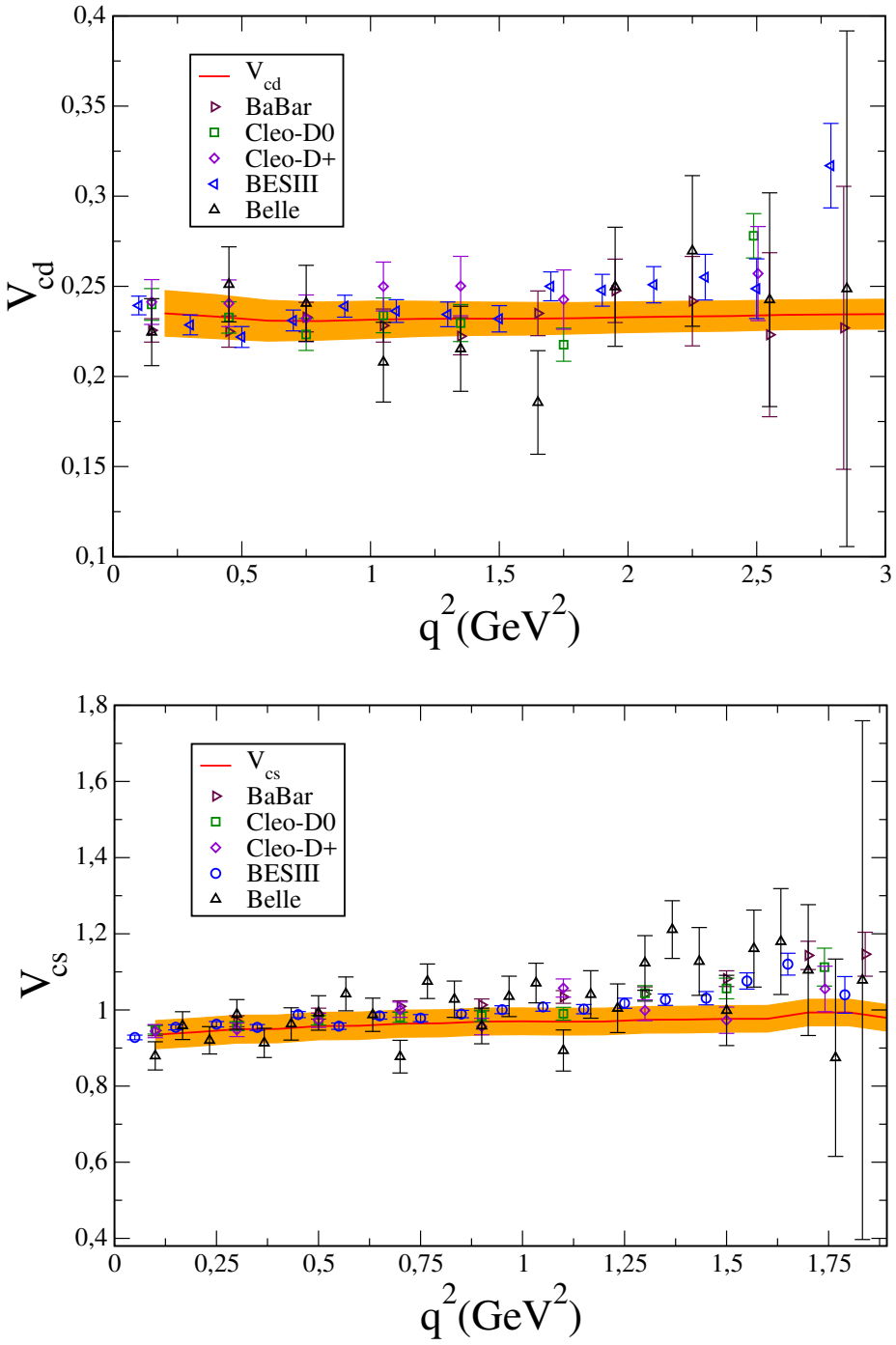

Figure 3.10: *Values of the CKM matrix elements $|V_{cd}|$ (upper panel) and $|V_{cs}|$ (lower panel) obtained by combining the theoretical predictions for the phase-space integrals $[I(q_i^2)]^{\rm LAT}$, based on the vector form factor $f_+^{DP}(q^2)$ evaluated on the lattice in Ref. [18], with the experimental data of the $D\to\pi$ and $D\to K$ semileptonic differential decay rates $[\Delta\Gamma(q_i^2)]^{\rm EXP}$, measured by BELLE [6], BABAR [7, 8], CLEO [9] and BESIII [10] collaborations. The solid lines and the bands are described in the text.*

in the ($|V_{cd}|$, $|V_{cs}|$) plane corresponding to a 68% probability contour. The ellipses corresponding also to the leptonic and semileptonic FLAG averages [5] for $|V_{cd}|$ and $|V_{cs}|$ are shown as well as the constraint imposed by the second-row unitarity, indicated by a dotted line.

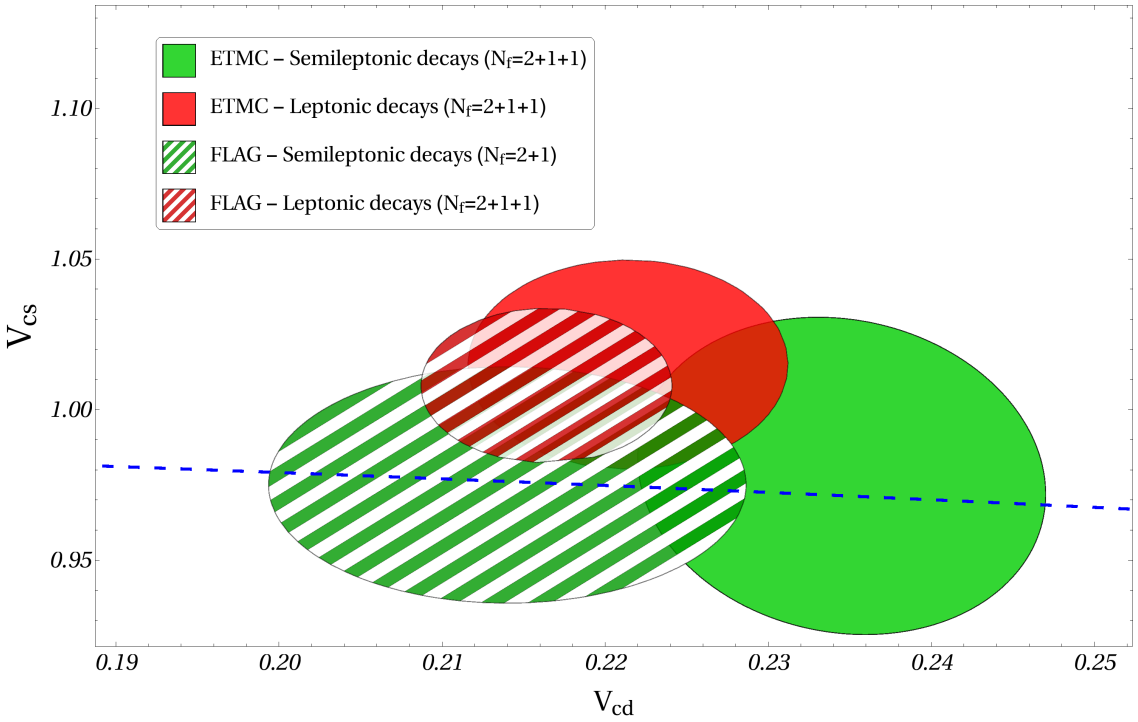

Figure 3.11: *Results for $|V_{cd}|$ and $|V_{cs}|$ obtained from leptonic and semileptonic D- and D_s-meson decays, represented respectively by green and red ellipses corresponding to a 68% probability contour. The solid ellipses are the results of Ref. [51] and of this work, obtained with $N_f = 2 + 1 + 1$ dynamical quarks. The striped ellipses correspond to the latest FLAG results [5], which for the semileptonic decays are based on the LQCD results obtained in Refs. [24, 25] with $N_f = 2 + 1$ dynamical quarks. The dashed line indicates the correlation between $|V_{cd}|$ and $|V_{cs}|$ that follows from the CKM unitarity.*

Using $|V_{cb}| = 0.0360(9)$ from Ref. [26] and our semileptonic results (3.69) we can test the unitarity of the second row of the CKM matrix, obtaining

$$|V_{cd}|^2 + |V_{cs}|^2 + |V_{cb}|^2 = 1.013\ (68)\ , \tag{3.71}$$

which can be compared with the corresponding result $|V_{cd}|^2 + |V_{cs}|^2 + |V_{cb}|^2 = 0.949\ (78)$ of Eq. (3.64).

Conclusions

In this thesis we have presented the first lattice $N_f = 2+1+1$ determination of the vector and scalar form factors of the $D \to \pi\ell\nu$ and $D \to K\ell\nu$ semileptonic decays, which are relevant for the extraction of the CKM matrix elements $|V_{cd}|$ and $|V_{cs}|$ from experimental data. Our analysis, reported in Ref. [18], is based on the gauge configurations produced by ETMC with $N_f = 2+1+1$ flavors of dynamical quarks at three different values of the lattice spacing with pion masses as small as 210 MeV. Quark momenta are injected on the lattice using non-periodic boundary conditions. The matrix elements of both vector and scalar currents are determined for a plenty of kinematical conditions in which parent and child mesons are either moving or at rest.

Lorentz symmetry breaking due to hypercubic effects is clearly observed in the data and included in the decomposition of the current matrix elements in terms of additional form factors. We found evidence that hypercubic artefacts may be governed by the difference between the parent and the child meson masses. This represents a very important issue, which warrants further investigations, since it might become particularly relevant in the case of the determination of the form factors governing semileptonic B-meson decays into lighter mesons. We remark that the values of the quark momentum were not chosen having in mind the investigation of hypercubic effects in semileptonic form factors. In particular, the use of spatially symmetric quark momenta is not ideal for such a purpose. We have planned to perform new simulations removing the above constraint and optimizing the choice of the twisted BCs. Nevertheless, we stress that the main structure of the hypercubic effects on the matrix elements of the vector and scalar currents has been understood.

After the extrapolations to the physical pion mass and to the continuum limit we determine the vector and scalar form factors in the whole kinematical region from $q^2 = 0$ up to $q^2_{\rm max} = (M_D - M_{\pi(K)})^2$, obtaining a good overall agreement with experiments. Some deviations are visible at high values of q^2 for both $D \to \pi\ell\nu$ and $D \to K\ell\nu$ decays. Combining the momentum dependence of the semileptonic vector form factors $f_+^{D\to\pi}(q^2)$ and $f_+^{D\to K}(q^2)$ with the differential rates measured for the semileptonic $D \to \pi\ell\nu$ and $D \to K\ell\nu$ decays, we get a determination of the CKM matrix elements $|V_{cd}|$ and $|V_{cs}|$ fully consistent with the SM. Furthermore, we have found that this new method for the extraction of $|V_{cd}|$ and $|V_{cs}|$ induce a reduction of the uncertanty, which is $\approx 40\%$ in our determination of $|V_{cd}|$. At zero 4-momentum transfer we get

$$f_+^{D\to\pi}(0) = 0.612\ (35)\ , \tag{3.72}$$

$$f_+^{D\to K}(0) = 0.765\ (31)\ , \tag{3.73}$$

and using experimental values provided by the BABAR, CLEO, BESIII and BELLE collaborations in Refs. [6, 7, 8, 9, 10] for the decay rates of the $D \to \pi(K)\ell\nu$ decays, together with our determination of the momentum dependence of the vector form factors $f_+^{D\to\pi(K)}(q^2)$, we determine

$$|V_{cd}| = 0.2345\ (83)\ , \tag{3.74}$$

$$|V_{cs}| = 0.978\ (35)\ . \tag{3.75}$$

Including also the determination of $|V_{cb}|$ from B-meson decays [26], the test of the second-row of the CKM matrix is verified at the percent level of precision:

$$|V_{cd}|^2 + |V_{cs}|^2 + |V_{cb}|^2 = 1.013\ (68)\ . \tag{3.76}$$

Appendix: The z-expansion of the physical vector and scalar form factors

After the extrapolations to the physical pion point and to the continuum and infinite volume limits, the z-expansions of the vector and scalar form factors, adopted in this work, are written in the case of the $D \to \pi$ transition as

$$f_+^{D\to\pi}(q^2) = \frac{f^{D\to\pi}(0) + c_+^{D\to\pi}(z - z_0)\left(1 + \frac{z+z_0}{2}\right)}{1 - P_V\ q^2}\ , \tag{3.77}$$

$$f_0^{D\to\pi}(q^2) = \frac{f^{D\to\pi}(0) + c_0^{D\to\pi}(z - z_0)\left(1 + \frac{z+z_0}{2}\right)}{1 - P_S\ q^2}\ . \tag{3.78}$$

The values of the five parameters $f^{D\to\pi}(0)$, $c_+^{D\to\pi}$, P_V, $c_0^{D\to\pi}$ and P_S are collected in Tab. 3.11, with the corresponding covariance matrix given in Tab. 3.12.

$f^{D\to\pi}(0)$	$c_+^{D\to\pi}$	P_V (GeV^{-2})	$c_0^{D\to\pi}$	P_S (GeV^{-2})
0.6117 (354)	−1.985 (347)	0.1314 (127)	−1.188 (256)	0.0342 (122)

Table 3.11: *Values of the parameters appearing in the z-expansions of the vector and scalar form factors (3.77-3.78) in the case of the $D \to \pi$ transition.*

	$f^{D\to\pi}(0)$	$c_+^{D\to\pi}$	P_V	$c_0^{D\to\pi}$	P_S
$f^{D\to\pi}(0)$	$1.25642 \cdot 10^{-3}$	$7.18296 \cdot 10^{-3}$	$6.77051 \cdot 10^{-3}$	$3.66997 \cdot 10^{-5}$	$2.87257 \cdot 10^{-5}$
$c_+^{D\to\pi}$	$7.18296 \cdot 10^{-3}$	$6.56690 \cdot 10^{-2}$	$6.30124 \cdot 10^{-2}$	$1.73569 \cdot 10^{-3}$	$8.43689 \cdot 10^{-4}$
P_V	$6.77051 \cdot 10^{-3}$	$6.30124 \cdot 10^{-2}$	$1.20371 \cdot 10^{-1}$	$2.24220 \cdot 10^{-3}$	$3.25631 \cdot 10^{-3}$
$c_0^{D\to\pi}$	$3.66997 \cdot 10^{-5}$	$1.73569 \cdot 10^{-3}$	$2.24220 \cdot 10^{-3}$	$1.48010 \cdot 10^{-4}$	$9.60595 \cdot 10^{-5}$
P_S	$2.87257 \cdot 10^{-5}$	$8.43689 \cdot 10^{-4}$	$3.25631 \cdot 10^{-3}$	$9.60595 \cdot 10^{-5}$	$1.60179 \cdot 10^{-4}$

Table 3.12: *Covariance matrix corresponding to the z-expansions of the vector and scalar form factors (3.77-3.78) in the case of the $D \to \pi$ transition.*

Analogously in the case of the $D \to K$ transition the z-expansions of the vector and

scalar form factors read as

$$f_+^{D\to K}(q^2) = \frac{f^{D\to K}(0) + c_+^{D\to K}(z-z_0)\left(1+\frac{z+z_0}{2}\right)}{1-q^2/M_{D_s^*}^2}\,, \tag{3.79}$$

$$f_0^{D\to K}(q^2) = f^{D\to K}(0) + c_0^{D\to K}(z-z_0)\left(1+\frac{z+z_0}{2}\right)\,, \tag{3.80}$$

where the values of the three parameters ${}^{D\to K}(0)$, $c_+^{D\to K}$ and $c_0^{D\to K}$ are collected in Table 3.13, with the corresponding covariance matrix given in Tab. 3.14.

$f^{D\to K}(0)$	$c_+^{D\to K}$	$c_0^{D\to K}$
0.7647 (308)	−0.066 (333)	−2.084 (283)

Table 3.13: *Values of the parameters appearing in the z-expansions of the vector and scalar form factors (3.79-3.80) in the case of the $D \to K$ transition.*

	$f^{D\to K}(0)$	$c_+^{D\to K}$	$c_0^{D\to K}$
$f^{D\to K}(0)$	$9.50493 \cdot 10^{-4}$	$6.92027 \cdot 10^{-3}$	$5.66397 \cdot 10^{-3}$
$c_+^{D\to K}$	$6.92027 \cdot 10^{-3}$	$7.99358 \cdot 10^{-2}$	$7.55735 \cdot 10^{-2}$
$c_0^{D\to K}$	$5.66397 \cdot 10^{-3}$	$7.55735 \cdot 10^{-2}$	$1.10925 \cdot 10^{-1}$

Table 3.14: *Covariance matrix corresponding to the z-expansions of the vector and scalar form factors (3.79-3.80) in the case of the $D \to K$ transition.*

Bibliography

[1] S. Chatrchyan et al. [CMS Coll.], *Observation of a new boson at a mass of 125 GeV with the CMS experiment at the LHC*, *Phys. Lett.* **B716** (2012) 30–61, [arXiv:1207.7235 [hep-ex]].

[2] G. Aad et al. [ATLAS Coll.], *Observation of a new particle in the search for the Standard Model Higgs boson with the ATLAS detector at the LHC*, *Phys. Lett.* **B716** (2012) 1–29, [arXiv:1207.7214 [hep-ex]].

[3] N. Cabibbo, *Unitary Symmetry and Leptonic Decays*, *Phys. Rev. Lett.* **10** (1963) 531–533.

[4] M. Kobayashi and T. Maskawa, *CP Violation in the Renormalizable Theory of Weak Interaction*, *Prog. Theor. Phys.* **49** (1973) 652–657.

[5] S. Aoki et al. [Flavour Lattice Averaging Group (FLAG)], *Review of lattice results concerning low-energy particle physics*, *Eur. Phys. J.* **C77** (2017) 112, [arXiv:1607.00299 [hep-lat]].

[6] L. Widhalm et al. [Belle Coll.], *Measurement of $D^0 \to \pi\ell\nu\,(K\ell\nu)$ Form Factors and Absolute Branching Fractions*, *Phys. Rev. Lett.* **97** (2006) 061804, [arXiv:hep-ex/0604049 [hep-ex]].

[7] J. P. Lees et al. [BaBar Coll.], *Measurement of the $D^0 \to \pi^- e^+ \nu_e$ differential decay branching fraction as a function of q^2 and study of form factor parameterizations*, *Phys. Rev.* **D91** (2015) 052022, [arXiv:1412.5502 [hep-ex]].

[8] B. Aubert et al. [BaBar Coll.], *Measurement of the hadronic form factor in $D^0 \to K^- e^+ \nu_e$ decays*, *Phys. Rev.* **D76** (2007) 052005, [arXiv:0704.0020 [hep-ex]].

[9] D. Besson et al. [CLEO Coll.], *Improved measurements of D meson semileptonic decays to π and K mesons*, *Phys. Rev.* **D80** (2009) 032005, [arXiv:0906.2983 [hep-ex]].

[10] M. Ablikim et al. [BESIII Coll.], *Study of Dynamics of $D^0 \to K^- e^+ \nu_e$ and $D^0 \to \pi^- e^+ \nu_e$ Decays*, *Phys. Rev.* **D92** (2015) 072012, [arXiv:1508.07560 [hep-ex]].

[11] T. Becher and R. J. Hill, *Comment on form-factor shape and extraction of $|V_{ub}|$ from $B \to \pi\ell\nu$*, *Phys. Lett.* **B633** (2006) 61–69, [arXiv:hep-ph/0509090 [hep-ph]].

[12] D. Becirevic and A. B. Kaidalov, *Comment on the heavy $\to$ light form-factors*, *Phys. Lett.* **B478** (2000) 417–423, [arXiv:hep-ph/9904490 [hep-ph]].

[13] C. G. Boyd and M. J. Savage, *Analyticity, Shapes of Semileptonic Form-Factors, and $\bar{B} \to \pi\ell\bar{\nu}$*, *Phys. Rev.* **D56** (1997) 303–311, [arXiv:hep-ph/9702300 [hep-ph]].

[14] D. Scora and N. Isgur, *Semileptonic meson decays in the quark model: An update*, *Phys. Rev.* **D52** (1995) 2783–2812, [arXiv:hep-ph/9503486 [hep-ph]].

[15] Y. Amhis et al. [Heavy Flavor Averaging Group (HFLAV)], *Averages of b-hadron, c-hadron, and τ-lepton properties as of summer 2016*, arXiv:1612.07233 [hep-ex].

[16] R. Baron et al. [ETM Coll.], *Light hadrons from lattice QCD with light (u,d), strange and charm dynamical quarks*, *JHEP* **06** (2010) 111, [arXiv:1004.5284 [hep-lat]].

[17] R. Baron et al. [ETM Coll.], *Light hadrons from Nf=2+1+1 dynamical twisted mass fermions*, *PoS* **LATTICE2010** (2010) 123, [arXiv:1101.0518 [hep-lat]].

[18] V. Lubicz, L. Riggio, G. Salerno, S. Simula and C. Tarantino [ETM Coll.], *Scalar and vector form factors of $D \to \pi(K)\ell\nu$ decays with $N_f = 2 + 1 + 1$ twisted fermions*, *Phys. Rev.* **D96** (2017) 054514, [arXiv:1706.03017 [hep-lat]].

[19] L. Riggio, G. Salerno and S. Simula, *Extraction of $|V_{cd}|$ and $|V_{cs}|$ from experimental decay rates using lattice QCD $D \to \pi(K)\ell\nu$ form factors*, arXiv:1706.03657 [hep-lat].

[20] N. Carrasco, P. Lami, V. Lubicz, E. Picca, L. Riggio, S. Simula et al. [ETM Coll.], *Scalar and vector form factors of $D \to \pi\ell\nu$ and $D \to K\ell\nu$ decays with $N_f = 2 + 1 + 1$ Twisted femions*, *PoS* **LATTICE2015** (2016) 261, [arXiv:1511.04877 [hep-lat]].

[21] V. Lubicz, L. Riggio, G. Salerno, S. Simula and C. Tarantino [ETM Coll.], *Hypercubic Effects in semileptonic $D \to \pi$ decays on the lattice*, *PoS* **LATTICE2016** (2016) 280, [arXiv:1611.00022 [hep-lat]].

[22] P. F. Bedaque, *Aharonov-Bohm effect and nucleon-nucleon phase shifts on the lattice*, *Phys. Lett.* **B593** (2004) 82–88, [arXiv:nucl-th/0402051 [nucl-th]].

[23] G. M. de Divitiis, R. Petronzio and N. Tantalo, *On the discretization of physical momenta in lattice QCD*, *Phys. Lett.* **B595** (2004) 408–413, [arXiv:hep-lat/0405002 [hep-lat]].

[24] H. Na, C. T. H. Davies, E. Follana, J. Koponen, G. P. Lepage and J. Shigemitsu [HPQCD Coll.], *$D \to \pi \ell \nu$ Semileptonic Decays, $|V_{cd}|$ and 2^{nd} Row Unitarity from Lattice QCD*, *Phys. Rev.* **D84** (2011) 114505, [arXiv:1109.1501 [hep-lat]].

[25] H. Na, C. T. H. Davies, E. Follana, G. P. Lepage and J. Shigemitsu [HPQCD Coll.], *$D \to K \ell \nu$ semileptonic decay scalar form factor and $|V_{cs}|$ from Lattice QCD*, *Phys. Rev.* **D82** (2010) 114506, [arXiv:1008.4562 [hep-lat]].

[26] C. Patrignani et al. [Particle Data Group (PDG)], *Review of Particle Physics*, *Chin. Phys.* **C40** (2016) 100001.

[27] P. W. Higgs, *Broken Symmetries and the Masses of Gauge Bosons*, *Phys. Rev. Lett.* **13** (1964) 508–509.

[28] F. Englert and R. Brout, *Broken Symmetry and the Mass of Gauge Vector Mesons*, *Phys. Rev. Lett.* **13** (1964) 321–323.

[29] L. Wolfenstein, *Parametrization of the Kobayashi-Maskawa Matrix*, *Phys. Rev. Lett.* **51** (1983) 1945.

[30] C. Jarlskog, *Commutator of the Quark Mass Matrices in the Standard Electroweak Model and a Measure of Maximal CP Violation*, *Phys. Rev. Lett.* **55** (1985) 1039.

[31] M. Bona et al. [UTfit Coll.], *The Unitarity Triangle Fit in the Standard Model and Hadronic Parameters from Lattice QCD: A Reappraisal after the Measurements of Δm_s and BR($B \to \tau \nu_\tau$)*, *JHEP* **10** (2006) 081, [arXiv:hep-ph/0606167 [hep-ph]].

[32] K. G. Wilson, *Confinement of Quarks*, *Phys. Rev.* **D10** (1974) 2445–2459.

[33] H. B. Nielsen and M. Ninomiya, *No Go Theorem for Regularizing Chiral Fermions*, *Phys. Lett.* **105B** (1981) 219–223.

[34] K. Symanzik, *Continuum Limit and Improved Action in Lattice Theories: (1). Principles and ϕ^4 Theory*, *Nucl. Phys.* **B226** (1983) 187–204.

[35] K. Symanzik, *Continuum Limit and Improved Action in Lattice Theories: (2). $O(N)$ Nonlinear Sigma Model in Perturbation Theory*, *Nucl. Phys.* **B226** (1983) 205–227.

[36] R. Frezzotti, P. A. Grassi, S. Sint and P. Weisz [Alpha Coll.], *Lattice QCD with a chirally twisted mass term*, *JHEP* **08** (2001) 058, [arXiv:hep-lat/0101001 [hep-lat]].

[37] R. Frezzotti and G. C. Rossi, *Twisted mass lattice QCD with mass non-degenerate quarks*, *Nucl. Phys. Proc. Suppl.* **128** (2004) 193–202, [arXiv:hep-lat/0311008 [hep-lat]].

[38] R. Frezzotti and G. C. Rossi, *Chirally improving Wilson fermions 1. O(a) improvement*, *JHEP* **08** (2004) 007, [arXiv:hep-lat/0306014 [hep-lat]].

[39] R. Frezzotti and G. C. Rossi, *Chirally improving Wilson fermions 2. Four-quark operators*, *JHEP* **10** (2004) 070, [arXiv:hep-lat/0407002 [hep-lat]].

[40] B. Sheikholeslami and R. Wohlert, *Improved Continuum Limit Lattice Action for QCD with Wilson Fermions*, *Nucl. Phys.* **B259** (1985) 572.

[41] P. Weisz, *Continuum Limit Improved Lattice Action for Pure Yang-Mills Theory. 1.*, *Nucl. Phys.* **B212** (1983) 1–17.

[42] P. Weisz and R. Wohlert, *Continuum Limit Improved Lattice Action for Pure Yang-Mills Theory. 2.*, *Nucl. Phys.* **B236** (1984) 397.

[43] M. Luscher and P. Weisz, *Efficient Numerical Techniques for Perturbative Lattice Gauge Theory Computations*, *Nucl. Phys.* **B266** (1986) 309.

[44] Y. Iwasaki, *Renormalization Group Analysis of Lattice Theories and Improved Lattice Action: Two-Dimensional Nonlinear O(N) Sigma Model*, *Nucl. Phys.* **B258** (1985) 141–156.

[45] R. Frezzotti, P. A. Grassi, S. Sint and P. Weisz, *A Local formulation of lattice QCD without unphysical fermion zero modes*, *Nucl. Phys. Proc. Suppl.* **83** (2000) 941–946, [arXiv:hep-lat/9909003 [hep-lat]].

[46] G. Martinelli, C. Pittori, C. T. Sachrajda, M. Testa and A. Vladikas, *A General method for nonperturbative renormalization of lattice operators*, *Nucl. Phys.* **B445** (1995) 81–108, [arXiv:hep-lat/9411010 [hep-lat]].

[47] P. Young, *Jackknife and bootstrap resampling methods in statistical analysis to correct for bias*, *Statistical Science* **11** (1996) 189–228.

[48] S. Gusken, *A Study of smearing techniques for hadron correlation functions*, *Nucl. Phys. Proc. Suppl.* **17** (1990) 361–364.

[49] C. Best, M. Gockeler, R. Horsley, E.-M. Ilgenfritz, H. Perlt, P. E. L. Rakow et al., *Pion and rho structure functions from lattice QCD*, *Phys. Rev.* **D56** (1997) 2743–2754, [arXiv:hep-lat/9703014 [hep-lat]].

[50] N. Carrasco et al. [ETM Coll.], *Up, down, strange and charm quark masses with N_f = 2+1+1 twisted mass lattice QCD*, *Nucl. Phys.* **B887** (2014) 19–68, [arXiv:1403.4504 [hep-lat]].

[51] N. Carrasco et al. [ETM Coll.], *Leptonic decay constants f_K, f_D, and f_{D_s} with $N_f = 2 + 1 + 1$ twisted-mass lattice QCD*, *Phys. Rev.* **D91** (2015) 054507, [arXiv:1411.7908 [hep-lat]].

[52] V. Lubicz, A. Melis and S. Simula [ETM Coll.], *Masses and decay constants of $D^*_{(s)}$ and $B^*_{(s)}$ mesons with $N_f = 2 + 1 + 1$ twisted mass fermions*, *Phys. Rev.* **D96** (2017) 034524, [arXiv:1707.04529 [hep-lat]].

[53] N. Carrasco, P. Lami, V. Lubicz, L. Riggio, S. Simula and C. Tarantino [ETM Coll.], *$K \to \pi$ semileptonic form factors with $N_f = 2 + 1 + 1$ twisted mass fermions*, *Phys. Rev.* **D93** (2016) 114512, [arXiv:1602.04113 [hep-lat]].

[54] R. Baron et al. [ETM Coll.], *Computing K and D meson masses with $N_f = 2 + 1 + 1$ twisted mass lattice QCD*, *Comput. Phys. Commun.* **182** (2011) 299–316, [arXiv:1005.2042 [hep-lat]].

[55] K. Osterwalder and E. Seiler, *Gauge Field Theories on the Lattice*, *Annals Phys.* **110** (1978) 440.

[56] C. McNeile and C. Michael [UKQCD Coll.], *Decay width of light quark hybrid meson from the lattice*, *Phys. Rev.* **D73** (2006) 074506, [arXiv:hep-lat/0603007 [hep-lat]].

[57] R. Frezzotti, V. Lubicz and S. Simula [ETM Coll.], *Electromagnetic form factor of the pion from twisted-mass lattice QCD at $N_f = 2$*, *Phys. Rev.* **D79** (2009) 074506, [arXiv:0812.4042 [hep-lat]].

[58] M. Albanese et al. [APE Coll.], *Glueball Masses and String Tension in Lattice QCD*, *Phys. Lett.* **B192** (1987) , 163–169.

[59] R. Sommer, *A New way to set the energy scale in lattice gauge theories and its applications to the static force and α_s in SU(2) Yang-Mills theory*, *Nucl. Phys.* **B411** (1994) 839–854, [arXiv:hep-lat/9310022 [hep-lat]].

[60] M. Constantinou et al. [ETM Coll.], *Non-perturbative renormalization of quark bilinear operators with $N_f = 2$ (tmQCD) Wilson fermions and the tree-level improved gauge action*, *JHEP* **08** (2010) 068, [arXiv:1004.1115 [hep-lat]].

[61] D. Guadagnoli, F. Mescia and S. Simula, *Lattice study of semileptonic form-factors with twisted boundary conditions*, *Phys. Rev.* **D73** (2006) 114504, [arXiv:hep-lat/0512020 [hep-lat]].

[62] C. T. Sachrajda and G. Villadoro, *Twisted boundary conditions in lattice simulations*, *Phys. Lett.* **B609** (2005) 73–85, [arXiv:hep-lat/0411033 [hep-lat]].

[63] P. F. Bedaque and J. W. Chen, *Twisted valence quarks and hadron interactions on the lattice*, *Phys. Lett.* **B616** (2005) 208–214, [arXiv:hep-lat/0412023 [hep-lat]].

[64] D. Becirevic, P. Boucaud, J. P. Leroy, J. Micheli, O. Pene, J. Rodriguez-Quintero et al., *Asymptotic behavior of the gluon propagator from lattice QCD*, *Phys. Rev.* **D60** (1999) 094509, [arXiv:hep-ph/9903364 [hep-ph]].

[65] F. de Soto and C. Roiesnel, *On the reduction of hypercubic lattice artifacts*, *JHEP* **09** (2007) 007, [arXiv:0705.3523 [hep-lat]].

[66] C. Aubin et al. [Fermilab Lattice, HPQCD, MILC Coll.], *Semileptonic decays of D mesons in three-flavor lattice QCD*, *Phys. Rev. Lett.* **94** (2005) 011601, [arXiv:hep-ph/0408306 [hep-ph]].

[67] S. Di Vita, B. Haas, V. Lubicz, F. Mescia, S. Simula and C. Tarantino [ETM Coll.], *Form factors of the $D \to \pi$ and $D \to K$ semileptonic decays with $N_f = 2$ twisted mass lattice QCD*, *PoS* **LATTICE2010** (2010) 301, [arXiv:1104.0869 [hep-lat]].

[68] T. Kaneko, B. Fahy, H. Fukaya and S. Hashimoto [JLQCD Coll.], *D meson semileptonic decays in lattice QCD with Moebius domain-wall quarks*, *PoS* **LATTICE2016** (2017) 297, [arXiv:1701.00942 [hep-lat]].

[69] T. Primer et al. [Fermilab Lattice, MILC Coll.], *D meson semileptonic form factors with HISQ valence and sea quarks*, *PoS* **LATTICE2016** (2017) , 305.

[70] C. Bernard, J. Bijnens, E. Gmiz and J. Relefors, *Twisted finite-volume corrections to K_{l3} decays with partially-quenched and rooted-staggered quarks*, *JHEP* **03** (2017) 120, [arXiv:1702.03416 [hep-lat]].

[71] C. G. Boyd, B. Grinstein and R. F. Lebed, *Model independent extraction of $|V_{cb}|$ using dispersion relations*, *Phys. Lett.* **B353** (1995) 306–312, [arXiv:hep-ph/9504235 [hep-ph]].

[72] M. C. Arnesen, B. Grinstein, I. Z. Rothstein and I. W. Stewart, *A Precision model independent determination of $|V_{ub}|$ from $B \to \pi e \nu$*, *Phys. Rev. Lett.* **95** (2005) 071802, [arXiv:hep-ph/0504209 [hep-ph]].

[73] C. Bourrely, I. Caprini and L. Lellouch, *Model-independent description of $B \to \pi \ell \nu$ decays and a determination of $|V_{ub}|$*, *Phys. Rev.* **D79** (2009) 013008, [arXiv:0807.2722 [hep-ph]].

[74] J. Bijnens and I. Jemos, *Vector formfactors in Hard Pion Chiral Perturbation Theory*, *Nucl. Phys.* **B846** (2011) 145–166, [arXiv:1011.6531 [hep-ph]].

[75] G. Rong, Y. Fang, H. L. Ma and J. Y. Zhao, *Determination of $f_+^\pi(0)$ or Extraction of $|V_{cd}|$ from Semileptonic D Decays*, *Phys. Lett.* **B743** (2015) 315–324, [arXiv:1410.3232 [hep-ex]].

[76] Y. Fang, G. Rong, H. L. Ma and J. Y. Zhao, *Determination of $f_+^K(0)$ and extraction of $|V_{cs}|$ from semileptonic D decays*, *Eur. Phys. J.* **C75** (2015) 10, [arXiv:1409.8049 [hep-ex]].

[77] J. L. Rosner, S. Stone and R. S. Van de Water, *Leptonic Decays of Charged Pseudoscalar Mesons - 2015*, *Submitted to: Particle Data Book* (2015) [arXiv:1509.02220 [hep-ph]].